Department of Construction Sciences
Solid Mechanics

ISRN LUTFD2/TFHF-21/5244-SE(1-50)

Impact of wood fibers on the mechanical performance of biocomposite materials

Master's Dissertation by

José María Moreno Iváñez de Lara

Supervisors:
Stephen Hall, Div. Solid Mechanics
Luis Valencia, Biofiber Tech
Linnea Kilegran, Biofiber Tech.

Examiner:
Matti Ristinmaa, Div. Solid Mechanics

Printed by Media-Tryck AB, Lund, Sweden
For information, address:
Division of Solid Mechanics, Lund University, Box 118, SE-221 00 Lund, Sweden
Webpage: www.solid.lth.se

Abstract

Plastics are amazing materials with outstanding properties that make them very useful and cheap for a wide range of uses. However, their pollution to the environment has become one of the main problems to solve in this century.

In this Master Thesis biocomposites from Biofiber Tech are studied. This material is a composite material formed by treated wood fibers and a polymeric matrix. The influence of the fibers in the matrix on the material properties is defined by many factors such as their orientation, distribution and adhesion capabilities with the matrix.

To study different surface treatments that Biofiber Tech. has developed, Lund University received two different shipments of samples. On the first one, a microstructure inspection was performed with X-ray tomography and three different phases were characterized apart from the matrix: fibers, voids and fiber aggregates. The volume fraction, spatial and size distribution and orientation of these phases were quantified and related to the material structure and properties.

For the second shipment of samples received, the study was focused more on the fracture mechanisms by carrying out premortem and post-mortem X-ray tomographies on tensile tested samples, observing the fractures in relation tu the structure of the material and distinguishing if the failure was caused by matrix, fiber or adhesive fracture.

Acknowledgements

I would like to thank Stephen Hall for all the help he has given me during the whole Master Thesis, with all the knowledge and the good atmosphere you bring to the table all the work has been easier to develop. To Sara Johansson for borrowing me some of her time and skills with the testing in the lab and the data analysis with the structure tensor code. Not to forget Luis and Linnea from Biofiber Tech. who have always supported me with their time and taught me a lot of interesting stuff from biocomposites, as well as for providing the samples that made possible this project.

To my new Erasmus friends, international and not so international. Charlotte, Sergio, Douglas and Ombeline, thank you for all the good times together that helped me take a break from the work and keep enjoying my Erasmus experience to the fullest. Equally huge thanks to my new Spanish friends that acted as emotional support in the stressful times which we suffered together, specially to Amparo, Salva, Iván, Baldo, Eric, Marina and Pilar, I wish to meet you guys again in Misko University.

Finally and most importantly, to my family, you raised me, taught me and always supported me in my decisions, without you all of this would have been impossible, thank you for making this Erasmus experience possible, in which I have grown so much as a person. There are no words to express my gratefulness for everything you have done for me.

Contents

List of Figures **vii**

1. Introduction **1**
- 1.1 Motivation . . . 2
- 1.2 Scope of the thesis . . . 2

2. Theoretical background **3**
- 2.1 Composite materials . . . 3
- 2.2 Polymers . . . 4
- 2.3 Wood . . . 8
- 2.4 Injection moulding . . . 9
- 2.5 Biofiber . . . 11
- 2.6 X-rays . . . 12
- 2.7 Mechanical testing . . . 16

3. Methodology **19**
- 3.1 Samples . . . 19
- 3.2 X-ray tomographies . . . 21
- 3.3 Tensile testing . . . 24

4. Segmentation **26**
- 4.1 Porosity segmentation . . . 27
- 4.2 Aggregation segmentation . . . 29
- 4.3 Fiber segmentation . . . 30

5. Results **31**
- 5.1 First shipment . . . 31
- 5.2 Second shipment . . . 39

6. Conclusion **48**
- 6.1 Future work . . . 49

Bibliography **51**

A. Mechanical testing results from first shipment's samples **53**

B. Phase Segmentation analysis of the first shipment samples **61**

C. First shipment tomography results **93**
D. Phase Segmentation analysis of the second shipment samples **113**
E. Fracture volume analysis **136**

List of Figures

2.1 Schematic representations of (a) continuous and aligned, (b) discontinuous and aligned, and (c) discontinuous and randomly oriented fiber reinforced composites [4] 4
2.2 Fiber composite fracture: (b) Interface failure, (c) Fiber failure 5
2.3 Tacticity of polymer chains [20] 5
2.4 Example of a semicrystaline polymer microstructure [23] 6
2.5 Polypropylene monomer of propylene 6
2.6 Typical mechanical responses of polymers: creep (left), depending on the material (middle) and thermal dependence (right) [20] 7
2.7 Polymer braking mechanisms: Stress-strain curve with macroscopic behaviour (left) and microscopic behaviour of the polymer chains (right) [20] 7
2.8 Cellulose chemical structure [2] 9
2.9 Injection moulding machine labeled [8] 10
2.10 Injection moulding defects [18] 11
2.11 X-ray photons interaction with matter [22] 13
2.12 Operation principle of a tomography: Image acquisition (left) and reconstruction of the slice (right) [22] 14
2.13 Image magnification concept with a cone beam geometry [13] 15
2.14 Drawing of a normalized dogbone [9] 16
2.15 Example of an stress-strain curve with the characteristic parameters pointed out 18

3.1 First shipment samples 20
3.2 Second shipment samples 20
3.3 Identification of the different phases found in the premortem tomography of a biocomposite 22
3.4 First sample cross section 11μm resolution tomography overlapped with the 4μm resolution one (inside the circle) taken 22
3.5 Left: Paint-sprayed samples for DIC. Right: misaligned sample at loading machine 25

4.1 Porosity fraction depending on the threshold used for the analysis . . 28
4.2 Porosity fraction (continuous line) and Number of pores (dashed line) depending on the radius used for the DE-filter 29
4.3 Aggregate fraction depending on the threshold used for the analysis . 30

5.1 First row: Original picture of the tomographies (11 μm res). Second row: Segmentation of the first shipment of samples. Aggregates (green), fibers (light blue), voids (orange) and matrix (dark blue). 31
5.2 First shipment's samples void picture, colored depending on its orientations 32
5.3 Heat map views of the porosity projection views found in 119-F (a) with the histogram of the location of these voids (b) 33
5.4 Void measurements on the fist shipment's samples 34
5.5 Volume picture of the aggregates segmentation 34
5.6 Histogram of the aggregates angle orientation from C18-P 35
5.7 Heat map views of the aggregates presence found in C18-P 35
5.8 Aggregates measurements on the fist shipment's samples 36
5.9 Heat map top views of the fibers distribution in the first shipment samples 36
5.10 Histogram of the fibers angle orientation from C18-P 37
5.11 Histogram of the fibers yaw rotation for the first shipment samples . . 37
5.12 First shipment's stress strain plot 38
5.13 First shipment samples' Mechanical properties 39
5.14 Premortem tomographies of the second shipment samples. Original picture (Top row) and segmented one (bottom). Aggregates (green), fibers (light blue), voids (orange) and matrix (dark blue) 40
5.15 Porosity distribution heat map from Fib-30 and F92-20. Premortem and postmortem segmentation 40
5.16 Segmented tomography of the Fib-30 fracture. Aggregates (green), fibers (light blue), voids (orange) and matrix (dark blue) 41
5.17 Segmented tomography of the F92-40 fracture. Aggregates (green), fibers (light blue), voids (orange) and matrix (dark blue) 42
5.18 Segmented tomography of the F92-20 fracture. Aggregates (green), fibers (light blue), voids (orange) and matrix (dark blue) 43
5.19 Segmented tomography of the Ref-40 fracture. Aggregates (green), fibers (light blue), voids (orange) and matrix (dark blue) 44
5.20 Segmented tomography of the Six-40 fracture. Aggregates (green), fibers (light blue), voids (orange) and matrix (dark blue) 44
5.21 Segmented top views of the fracture areas from the tomography of each sample. Aggregates (green), fibers (light blue), voids (orange) and matrix (dark blue) 45
5.22 Strain Stress curve obtained for the second shipment samples 46
5.23 Properties obtained from the the second shipment samples Strain Stress curves (Ref-40 did not yield) 47

1

Introduction

Plastics are a material used daily by everyone, from kitchenware to electronics, clothing, transport and toys, they can be found everywhere. It is a wonderful material with a wide range of properties to choose depending on its final desired use, while keeping a cheap cost and an ease to produce and mould into different shapes. Nevertheless, this wonderful material may have one disadvantage, it may be destroying our planet.

In the second half of the 19th century, new synthetic materials were invented, but it is not until the 20th century when Leo Baekeland, considered the father of the plastic industry, invented the fully synthetic plastic known as bakelite, which could be mass-produced serially. Its amazing properties, as a thermosetting polymer (heat-resistant, nonconductive, resistant to scratches, easy to be moulded, durable), made a game changer in the industry, pushing new polymers to be created and produced [16].

Already at the end of the 20th century, plastics were discovered to be also pollutants. Their durability made them able to be found everywhere, from the Mount Everest to the bottom of the sea. According to the trade association PlasticsEurope, around 9 million tonnes of plastic are thrown into the oceans annually [15]. The effects have been noticed in many ways, such as on the famous Great Pacific Garbage Patch (GPGP), an island of just plastic waste with a surface area of 1.6 million km^2 (twice as the state of Texas) and created by the plastic waste carried by the natural currents of the world [21]. Whether mistaken for food by animals, becoming a trap for them or simply causing visual pollution in the environment, plastic pollution has become a real problem.

People are nowadays more concerned about the pollution problem and, far from being fixed, it is starting to be controlled by the appearance of new substitutes such as bio-based or recycled plastics, paper utensils and public awareness to reduce such use of plastic.

Among the mitigations is Biofiber Tech. a Swedish start-up located in Stockholm that develops what is called a biocomposite. This material combines polymers, biopolymers or recycled polymers with wood fibers to act as a new substitute for polymers with mechanical properties that other materials cannot compete.

In collaboration with Biofiber Tech. this Master Thesis addresses the search and characterization of those mechanical properties of the so called Biofiber material that the company is developing, with different variants of the fibers that are in research. To do so, a complete volume analysis on each kind of sample has been made, using X-ray tomography and analysing both porosity and fiber distribution, orientation, and aggregation along the sample and relating these properties to its mechanical behaviour and comparing them with pre-mortem and post-mortem tomographies.

1.1 Motivation

It is clear that polymers are essential to our lives, they are in almost every piece of technology that we hold. However, their impact on nature and wildlife is becoming more evident every year, which consequently influences us not only empathetically but also physically. Furthermore, polymers come from nonrenewable fossil sources, which means that the material has a limited time of being produced.

Biofiber Tech. is a company that has a new and different approach to produce biocomposites, polymers with fibers that reduce the content of plastic in the material, could improve mechanical properties, increase the biodegradability of the material and decrease the carbon footprint considerably in its production (as the fibers are taken from sustainable forests).

Research on the material properties and fracture mechanisms of such complex materials could be of high use to improve the production methods and guide future research on how to improve the material properties.

1.2 Scope of the thesis

This Master Thesis consists of the study of the impact of wood fibers, which went through different surface treatments, on the mechanical properties of a biocomposite material that is composed of fibers and a polymeric matrix. Biofiber Tech. provided different samples for analysis.

The analysis will consist on phase characterization and cause of the fracture based on x-ray tomography imaging performed on the samples before and after they are tensile tested. As said before, the samples were provided by Biofiber Tech., but the tensile testing and image acquisition was performed at Lund Tekniska Högskola (LTH). All data processing and handling has been done with Matlab-2020B®from MathWorks, although some data visualization has also been done with ParaView 5.4.1.

2

Theoretical background

In this chapter the theoretical knowledge used in this Master Thesis is explained, both related to the properties of the material type used and the techniques used to analyze it.

2.1 Composite materials

In the last years, composite materials have increased their presence in the industry, the reason is because they combine the properties of different materials to achieve a better one. A composite is composed by mixing two or more components with different properties: one in a major phase, called matrix, and a minor one, called filler.

The properties of the final material will not only depend on the components used, but also on the quantities, shape of the filler and interaction of the components with each other. The kind of materials dealt with in this project are the ones known as fiber-reinforced composites, more specifically on WFRP composite, which stands for Wood Fiber Reinforced Polymer or WPC as wood-polymer composites.

Fiber-reinforced composites are usually high stiffness and strength materials with a relatively low density. To achieve this, a strong and ductile matrix (usually used thermoplastics) is used. Different functions that the matrix fulfills in the material:

- distribute the load along the fibers;
- prevent crack propagation: so if a fiber breaks because a defect or otherwise, the crack would not spread across the whole sample, as it would do with a block material of the filler;
- prevent chemical and abrasive degradation of the fibers: similarly to the cracks the toughness of the matrix allows fibers to be more fragile than if they would be by themselves, as they are protected from the exterior by it;

- maintain fiber orientation: the one that was designed for the material.

The matrix properties are very important so the strong and rigid fibers are protected and can bear most of the load. The length of the fibers and their orientation is very important for the properties of the material: Aligned fibers give the material anisotropic properties, bearing higher loads on the longitudinal axes, as the fibers act as cables, but much lower properties in the transverse one, as the matrix will be the one holding the load. On the other side, random orientation or other combinations of this alignment would give more isotropic properties (Figure 2.1), with properties between the two others.

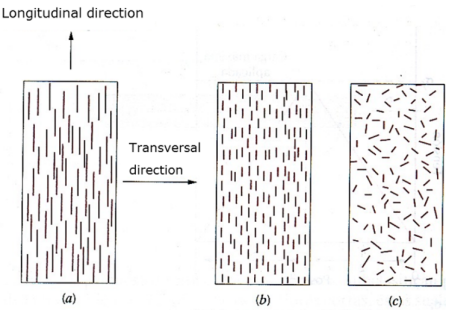

Figure 2.1 Schematic representations of (a) continuous and aligned, (b) discontinuous and aligned, and (c) discontinuous and randomly oriented fiber reinforced composites [4]

Furthermore, length of the fibers is of big importance, as it has been found that high aspect ratio fibers achieve higher fracture stresses than those materials with shorter and thicker fibers [12]. Although one advantage of long fibers is that if they break, the matrix keeps holding them together and they start to act as shorter fibers.

Because of the above outlined reasons, fiber reinforced composite materials require strong interactions between the constituents. This interactions might be either chemical or physical, but the better the interaction is, the better the load will be distributed to the fibers uniformly, and the harder it is for the cracks to propagate along the matrix. In Figure 2.2 it can be seen the different fractures that may be found in a composite material, if the bounding between the fiber and the matrix fails the composite may not profit fully from the toughness of the fibers.

2.2 Polymers

Polymers are organic compounds of high molecular weight formed by many repetitive smaller units called monomers that bond together by a covalent bond. By classifying them in terms of their properties, three main different groups of polymers can

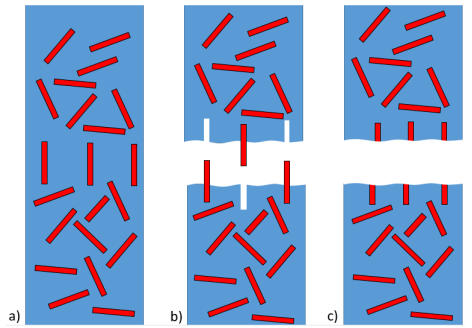

Figure 2.2 Fiber composite fracture: (b) Interface failure, (c) Fiber failure

be defined: thermosets, thermoplastics and elastomers. The last one being the one with the most different properties, it can be found in elastic materials such as rubber bands, whose polymers are slightly cross-linked and this gives them the ability to stretch highly and afterwards recover the initial properties.

Thermosets are very crosslinked between each other, which leads to high rigidity and inability to melt at high temperatures. On the other hand, thermoplastics, which are the most common plastics in use, present either linear or branched molecules, and they can be melted even after processing, which allows the material to be processed easily (no chemical reactions involved) and be recycled in most cases.

Another classification of the polymers could be based on the crystal structure. These can either present no crystallinity at all (as the thermosets and elastomers do) or some crystallinity that is reflected on the properties of the material (some thermoplastic materials). The volume covered by crystalline structures influences the mechanical properties of the final material: a higher crystallinity usually means higher strength, Young modulus and others. The degree of crystallinity may depend on different factors such as the composition of the monomers (Higher molecular weight increase the probability), the tacticity (when pendant groups of the monomers are in the same side it is more probable to form crystals, Figure 2.3), the cooling rate when processing the material (slower, more probable) or other factors such as the presence of impurities or the presence of plastifyers.

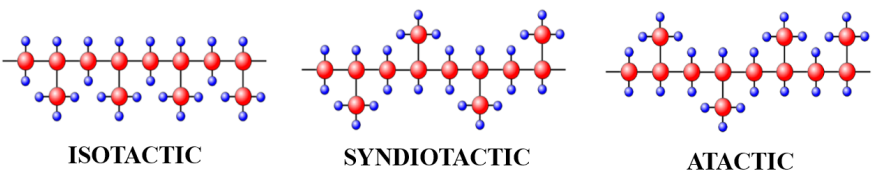

Figure 2.3 Tacticity of polymer chains [20]

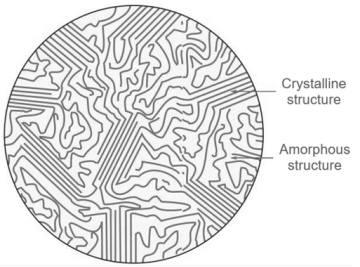

Figure 2.4 Example of a semicrystaline polymer microstructure [23]

Polypropylene

The polymer used in all of the samples analyzed in this project was polypropylene. This is one of the most produced plastics in the world nowadays, mainly used in packaging for consumer products, but used in all kind of other sectors such as the automotive industry (inner decoration), textile industry and domestic industry (plastic buckets, chairs...).

Polypropylene is thermoplastic formed from a propylene monomer (Figure 2.5) that usually arranges in isotactic structures and that shows crystallinity degree up to 60% (Figure 2.4) [11]. It is a material characteristic for its low density ($\approx$ 0.9 g/cm3), good impact strength, fatigue resistance, chemical resistance, good electrical insulation, ease to be processed, recyclability (as it is a thermoplastic) and relatively cheap price. On the other hand, the material is highly flammable and is susceptible high UV degradation.

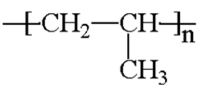

Figure 2.5 Polypropylene monomer of propylene

Mechanical breaking mechanisms

As explained before, polymers are long chains of monomers and their mechanical properties are widely influenced by the level of cross-linking and the degree of crystallinity that these present. However, the properties depend also highly on the temperature and the strain-rate conditions. Polymers are considered viscoelastic materials, which mean two things: that at high temperatures they will behave more like a rubber and that under a constant load they may experience creep (which is a gradual increase in elongation with time).

Even when a tensile test is applied under normal conditions, the shape of the stress-strain curve may differ a lot depending on the material used. In Figure 2.6, it

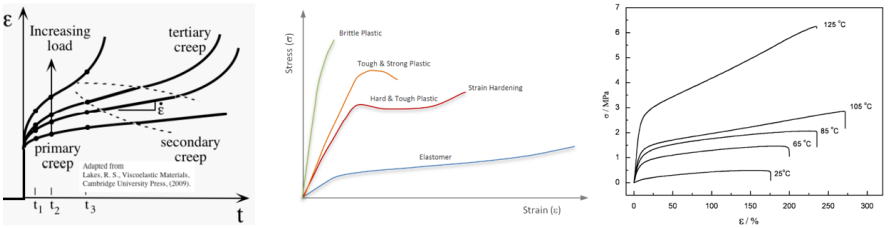

Figure 2.6 Typical mechanical responses of polymers: creep (left), depending on the material (middle) and thermal dependence (right) [20]

can be seen the widely different ways that polymers may behave depending on their composition. Because of this, a good way to define the properties of the polymer would be to list the yield of strength, the Young's Modulus before yield, the Tensile Strength and the toughness of the sample.

During tensile deformation, polymers present a characteristic reduction in cross-section area. This reduction is referred as "necking" and it happens at the yielding of the material (because this reduction of area reduces the stress that the material can withstand). Microscopically in semi-crystalline polymers, the deformation is mainly caused by the elongation of the amorphous chains presented in the material (elastic deformation). Once these chains are completely elongated or their movement is restricted by the entanglement between them, the crystalline structures start to deform until they break apart from each other. This breaking leads to an irreversible deformation (plastic strain) presented also in the reduction of the cross-section of the sample (necking). When the stress continues to be applied on the sample, the remaining parts of the crystalline structures (lamellae) start to align, and the chains keep unraveling until the point where the polymer chains start to break apart and the sample fails.

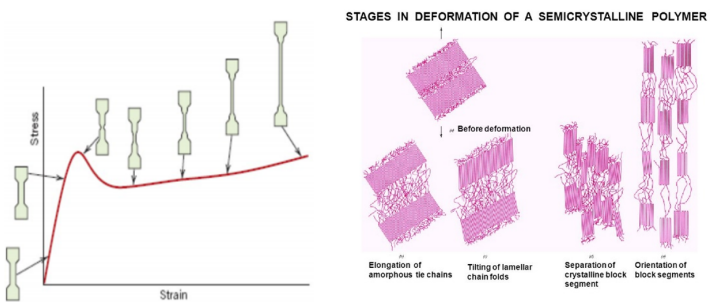

Figure 2.7 Polymer braking mechanisms: Stress-strain curve with macroscopic behaviour (left) and microscopic behaviour of the polymer chains (right) [20]

2.3 Wood

Wood has been a construction material since the beginnings of the human species. Used to build weapons and tools in the Stone Age it can be considered with the stone, the richest and most storied history material in the world of construction. From then a lot has changed and nowadays it can be found in many places, both in large scale, such as boats, shelters and even buildings (Especially with the new Swedish regulations that allow tall residential buildings to be built out of wood [3]), as in small scale, such as straws, dispensable cutlery and plates or even bottles [17], where wood is starting to be a substitute of the plastic everyday products.

Perhaps a reason of this rediscovery of wood and its reappearance in the industry has to do with the fact that could be the perfect example of an environmentally sustainable product [6]: it comes from a natural resource, it is biodegradable, sustainable and its carbon footprint is the lowest compared to any construction material. Furthermore, it is a material with outstanding specific strength (ratio between strength and density), great insulation properties (better than glass), low expansion coefficient (does not dilate or contract as steel) and highly machinable.

There are different ways to classify woods, but one of the most used is in Hardwood and Softwood depending if it comes from a rounded shape trees or conical ones. Although the name does not always coincide with the properties of the structure – some hardwood can have relatively weak properties and vice versa – softwoods are considered to be lighter and with a smaller density than the others. Because of this, hardwoods (oak, maple, walnut...) are usually used for construction of large structures such as floors, roofs and walls and softwoods (pine, beach, ash...) are usually used for building smaller things for decoration like furniture, doors and windows.

Structurally, wood could be considered a composite material composed of cellulose fibers and a lignin matrix (which is an organic polymer of high importance in the formation of the cell walls). In this Master Thesis, the samples present mainly cellulose fibers, as is the rigid part of the material that is of interest to use in other composites.

Cellulose

Cellulose is an organic compound composed by chains of a repetitive structure formed by carbon, hydrogen and oxygen atoms (Figure 2.8). Cellulose can be found not only in wood (composed around 50% of cellulose), but also is very commonly produced from cotton, which is richer in it (around 90% of cellulose). It is mainly used to produce paper and paperboard, but, as said before, it can also be used as a filler in other materials.

Lignocellulose-based fibers are the most common type of biodegradable fillers used in composite materials, not only for their reduced cost and environmentally friendly character, as already said, but also because of their physical properties. The fiber usually come from softwoods, but the properties can vary a lot depending on

their origin (several local plants and crops can also work as resources). Other properties of cellulose fibers are their low density, low energy consumption, nonabrasive nature and the possibility of including a high percentage of fibers in the matrix. On the other hand, the main problem that may present when using such fibers is the high moisture absorbance nature of the material that might reduce the capacity to adhere to the polymeric matrix.

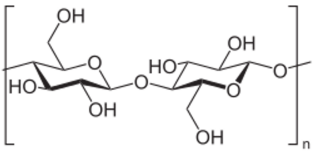

Figure 2.8 Cellulose chemical structure [2]

2.4 Injection moulding

Injection moulding is one of the most widely used methods used in polymer manufacturing, along with extrusion moulding. It is also used for producing composite materials with polymeric matrix and discontinuous fibers.

In the production of an injection moulded polymer (Figure 2.9), the raw material would come in form of plastic granulates called pellets. These are fed into a hopper that leads them to a heating cylinder. Then the pellets melt and the polymer is forced into by a rotating screw (sometimes a hydraulic piston) to an extruder that is positioned in the nozzle of a mould (which usually is around 90°C for thermoplastic manufacturing and 200°C for thermosets). The mould is filled by pressure (between 70-200 MPa) and the polymer solidifies with the desired shape of the product. Once the product is solid, the mould opens and, with the help of a series of bars that push the part out of it, the polymer piece is ejected. The mould closes and the melted polymer from the extruder fills again the mould, repeating the process.

Complex shapes with high dimensional accuracy can be achieved with this manufacturing method, with a high production rate (5-60 seconds although it can get to several minutes for thermosets). Some variants of this technique allow to inject-mould different materials into one only shape (co-injection moulding) or to form shapes that involve two parts that should not be touching each other such as hinge joints (overmoulding).

Defects usually presented in injection moulding

As said, injection moulding has many capabilities and advantages of use, however because some temperature gradients on the material, there can be identified three main regions that present different properties [1], as outlined below.

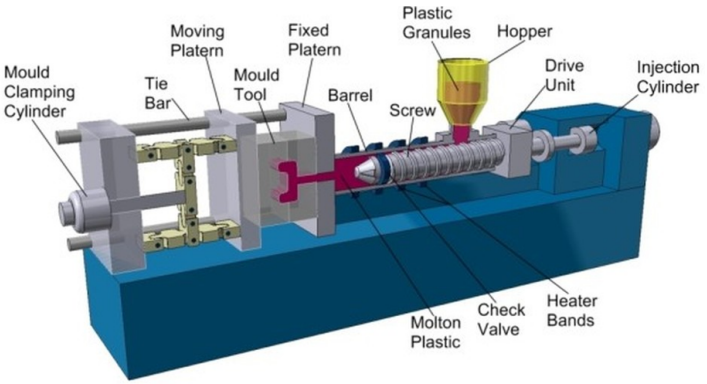

Figure 2.9 Injection moulding machine labeled [8]

- An outer part called skin or surface that is indirect contact with the mould. This solidifies almost immediately because of the big difference in temperature between the melt and the mould, which leads to the alignment of polymers with the flow direction;

- A phase in between the outer and the inner part defined as the shear zone where the material experiments shear forces caused by the flow of the material. This phase leads to strong orientation and a higher crystallinity degree and can sometimes substitute the bulk layer depending on the thickness of the sample;

- An inner part called core or bulk layer that refers to the last part to be filled, where the thermal gradient is the smallest and takes the most time to solidify. Here, there can be found random oriented polymers with a low degree of crystallinity with isotropic properties.

The temperature gradients, followed by some uneven cooling on the mould, lead to the appearance of defects in injection moulded products. Some of these effects are (Figure 2.10), described below.

- Internal voids in the bulk of the sample caused by the shrinkage of the material when it first starts solidifying in the surface sucking material from the internal core of the volume;

- If the mould runners are too thin, the head of the melt may solidify prematurely obstructing the mould to be fully filled. This specially happens in sharp corners of the mould where the material is not able to fully adapt to the shape of the mould);

- If the mould does not close completely because of any problem with the clamping, some flash (unwanted extra material that flows outside of the mould) may appear;

- Sink marks are pretty common to be found also as a result of the solidification of the sample or in the inlet cavity to the mould or because some flow problems or because of the shrinkage of the material when solidifying.

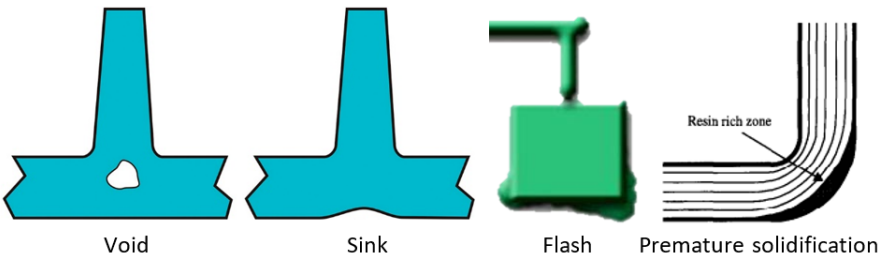

Figure 2.10 Injection moulding defects [18]

To avoid these kind of defects a proper control is needed of the injection pressure, the flow speed of the material, the temperatures used, both for the filling and for the cooling, and control on the mould design to avoid sharp corners or narrow shapes [18].

2.5 Biofiber

Biofiber is a bio-composite material produced by Biofiber Tech. in Stockholm. The material consists of a polymeric matrix and modified wood fibers as a filler. Depending on the final intended use, different thermoplastic matrices can be used: polypropylene (recycled, bio-based or regular), polyethylene (recycled, bio-based or regular) or polytactic acid (PLA).

The filler used in the matrix are wood fibers that receive a surface treatment to reduce moisture absorbance and increase the plastic compatibility and thus the interaction with the matrix. The wood fibers, which come from untreated thermomechanical pulp (TMP), are produced into a granulate that can then be mixed with the desired matrix in a compounder machine, producing the pellets that can be used in an injection moulding or compression moulding machine to manufacture products, as if it was a polymer material. The treatment that Biofiber Tech. applies to the samples are critical for the interaction between fibers and matrix, as the natural water absorbance properties of the wood used in the material restricts drastically its adhesion to polymers.

Bio-composite materials, like the one produced at Biofiber Tech. have many advantages against other materials. The first and most obvious being the reduced carbon footprint when manufacturing them. They have similar properties than plastics, but if they end up in the landfill have a significantly smaller impact in the environment.

2.6 X-rays

X-rays are electromagnetic radiation widely used in the world of mechanics and medicine to visualize inner parts of materials/body that would not be able to be seen with many other methods.

The basic working principle used when doing a radiography is that X-rays pass more easily through low density mater and are absorbed or scattered by denser mater. Therefore, if an x-ray beam is directed to a sample the picture taken by a detector on the other side of the sample, will be of the denser parts of the sample, omitting the less dense ones.

Energy

We refer to X-rays, as the electromagnetic radiation with a wavelength in the range of [0.01, 10] nm, with a photon energy between 124eV - 124keV. The energy that X-rays have can be analyzed with the Broglie relationship between waves and particles (Equation 2.1) combined with the energy wavelength relation (Equation 2.2) It can thus be seen how the photon energy is inversely proportional to its wavelength($\downarrow\lambda$=$\uparrow$E) which means that if harder mater is to be studied, smaller wavelengths, with higher energy, would be required.

$$\lambda = \frac{h}{p} \tag{2.1}$$

$$E^2 = (m * c^2)^2 + (p * c)^2 \rightarrow E_{photon} = pc \tag{2.2}$$

Taking into account that photons do not have mass, where h is Plank's constant, p is the momentum of the "Particle", c is the speed of light in a vacuum.

Interaction with matter

As has already been said, X-ray radiation interacts less with less dense matter, but depending on the dense mater and on the energy of the beam, the photon interaction can be different.

Although there are five different main types of interaction only Compton scattering, photoelectric absorption and coherent scattering are significant for the energy interval normally used in material studies (absorption and diffraction processes). To calculate the number of photons that are transmitted through an object, the Beer-Lambert attenuation law can be used.

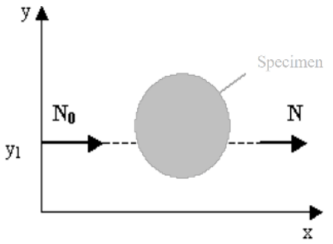

Figure 2.11 X-ray photons interaction with matter [22]

$$N(y_i) = N_0 * exp\left(-\int \mu(x, y_i)dx\right) \tag{2.3}$$

$$\mu = \rho\left[a * \frac{Z^m}{E^n * A} + b * \frac{Z}{A}\right] \tag{2.4}$$

Where N_0 is the number of incident photons, N the transmitted number of photons, μ the linear attenuation coefficient (with the photoelectric absorption and incoherent scattering component respectively), E the X-ray energy, Z and A the atomic number and weight and m, n, a and b constants.With this relation, it can be seen how low energy X-rays have greater sensitivity. Also, for low energies (E<30KeV) photoelectric absorption is predominant in the system, and otherwise Compton scattering.

Detection

There are different sorts of detectors for X-ray beams, but basically they all measure the photon flux, spatial distribution, spectrum or other properties of X-rays. This radiation can be measured by different principles such as: the ionization of gas, conversion to visible light (scintillator), or production of electron-hole pairs in a semiconductor (The number of these is proportional to the energy applied to the semiconductor). Also, the detector can either measure each x-ray photon independently (Photon-counting detector) or measure the total amount of energy captured in a region of the detector (integrating detector).

Generation

Although X-ray radiation can be found in nature, if wanted to be produced, there are two main ways to do it: by change of orbit of electron coming from electronic shell or by accelerating electrons.

The characteristics of an X-ray beam are the Energy (eV) and Brilliance $\left(\frac{photon}{sec * mm^2 * mrad^2}\right)$. The first one takes into account the capacity to go through matter and the second one depends on the intensity, convergence and size of the beam. A

higher brilliance allows to focus on very small specimens, to use a monochromatic beam with a small resolution in energy, to use properties of coherence and a shorter scanning time. The two main instruments to produce an X-Ray beam are an X-ray tube and a synchrotron each of them with its own advantages.

In this work a laboratory x-ray tomograph equipment has been used, which uses an X-ray tube. This generator accelerates a number of electrons with a high voltage to collide them with a metal target. The change of trajectory of the electrons caused by this collision derives in the production of X-rays. In this instrument the continuous spectrum of the generated beam depends of the generating voltage and current. If the voltage is increased, the X-ray energy and, thus, penetration capacity increases. On the other hand, if the current intensity is increased, the flux of electrons is increased, increasing the number of electrons that get to the detector, and reducing the darkness of the image (the same result would happen, if the exposure time was increased).

Tomography

X-ray tomography is a non-destructive full-field experimental method that allows the visualization of the composition and internal structure of bulk objects. Creating a tomographic image requires an X-ray source, a 2D radiation detector, and a method to make the sample rotate (to change the view analyzed with the x-ray detector). The transmission tomography is formed from a series of X-ray attenuation images (radiography) recorded for different angles of rotation of the sample that can be translated into a set of slices of the sample which follow a reconstruction to give a 3D image volume that reveals different materials, as described in Figure 2.12.

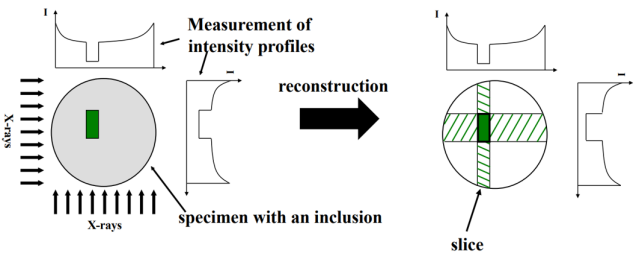

Figure 2.12 Operation principle of a tomography: Image acquisition (left) and reconstruction of the slice (right) [22]

With the set of radiographies from different angles, and focusing in only one line dimension of every radiography, the image of the cross-section of the sample at that height can be created (one of the approaches to achieve this is the back-projection). Note that the center of rotation has to be set correctly in order to end up with a focused image. Each slice will then represent a finite thickness of the object with

a defined voxel resolution (extension in 3D of a pixel) that can vary from around 100µm for an X-ray tube source, to around 5µm for a synchrotron one.

Quality dependence The quality of the tomograph will depend on many factors, the most importance one listed here:

- Specimen: Ideally should be cylindrical and avoid sharp edges to avoid problems with the reconstruction of the image
- Beam geometry: The X-ray beam can follow a cone beam geometry (particular from X-ray tubes) or a parallel beam (Synchrotron). For the first, the cross-section of the beam increases with the distance to its source. This provides the possibility to make a geometrical magnification on the sample by approaching the source to the sample or moving the detector away although it is more difficult to achieve a good slice reconstruction (Figure 2.13). On the other hand, in a synchrotron the beam is filtered to achieve small coherent beams, increasing the resolution of the final picture, to a point where this is limited by the detector.

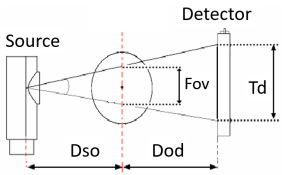

Figure 2.13 Image magnification concept with a cone beam geometry [13]

- Detector: principal element of the measurement, scintillators are the most common one. Depending on the software, each pixel detector could be combined to loose resolution but increase the contrast of the image, as more photons get to each pixel (Bin).
- Acquisition time: It controls the exposure time of the sample in each picture, it has the same effect as increasing the current of the source, as more photons are absorbed.
- Voltage and Power: As explained in Section 2.6, voltage controls the penetration of the beam, and current the number of photons per unit of area of the sample.
- Angle step: a smaller angle step the smoother will be the final reconstruction (the more pictures will be taken).
- Reconstruction algorithm: filters for blurring and artefacts, adaptations to polychromacy and divergence.

2.7 Mechanical testing

Mechanical testing on materials has been used since the beginning of engineering to analyze, under controlled conditions, the properties of materials and structures and extract useful data to estimate the performance in the real world or even the sole purpose of understanding the sample.

What could be considered the most used testing mechanism, is tensile testing, which consists of progressively loading a sample in the longitudinal direction until its failure while recording both the force applied to the sample and the deformation experienced by it. As simple as this test may be, there are a lot of different ways to do it and a lot of parameters to control if it is to be done properly. For this kind of test on polymeric materials (which is our case) there is an International Standard that can be found: the ISO 527:2019EN – Plastics: Determination of tensile properties, with 5 different parts.

The sample analyzed is a standardized aspect ratio piece that can be found on ISO 527-2:2012 usually referred as dogbone. The dogbone is a prism shape with a reduction in width (not in thickness) in its middle to act as a stress concentrator (Figure 2.14).

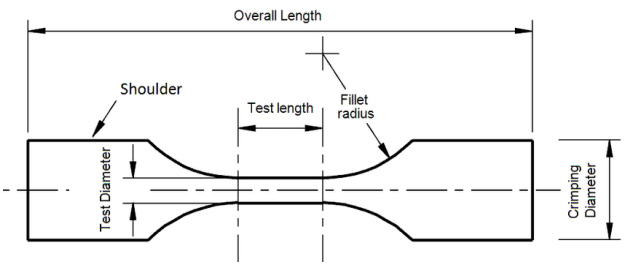

Figure 2.14 Drawing of a normalized dogbone [9]

Data acquisition

As said before, while subjecting a sample to a gradually increasing force, two parameters should be recorded: the load and the deformation applied to the sample. This can be done by different methods, but usually the proper loading machine is able to do so.

The loading machine is composed of two clamps that hold the sample: one static, which is usually the bottom one, and one moving part that that applies the force to the sample. Depending on the action part that moves the upper clamp, the loading machine could either be electro-mechanic, hydraulic or pneumatic. The most typical one is the electro-mechanic, which uses an electric motor to turn two screws that controls the position of the upper clamp. With this mechanism the machine controls the deformation rate that is applied to the sample (which should be

constant). Other methods to measure deformation may include extensometers (they are intrusive, so not ideal), optic lasers or cameras.

To measure the load it could be used what is called a strain gauge, which is an electrical variable resistor whose resistance varies with the deformation of the material it is attached to. Attaching this to a material whose properties are well known, can enable the measurement of the load applied to the material. Another way to measure the load involves measuring the power usage from the machinery to perform the deformation, or the pressure in the hydraulic system for the hydraulic loading machine.

Data analysis

Although the force and displacement are the values recorded in the experiment, to make the results more useful and allow them to be extrapolated to different situations, there are parameters engineers use from the initial sample measurements and the data acquired by the experiment.

The engineering stress (Equation 2.5) and engineering strain (Equation 2.6) are the tension that the sample holds and the deformation that the sample presents with respect to its initial length.

$$\sigma_{engineer} = F/A_0 \tag{2.5}$$

$$\varepsilon_{engineer} = \frac{\Delta l}{l_0} \tag{2.6}$$

However, when deforming a sample, its cross section does change, so the stress and strain calculated are not the real ones. The real values obtained for this parameters with respect instantaneous lengths are called true stress (Equation 2.7) and true strain (Equation 2.8). If the sample does not suffer a considerable necking (this is, a visible reduction in the cross section where the stress concentrates most caused by an uneven deformation on all the sample) there can be done an approximation.

$$\sigma = F/A_f \approx \sigma_e * (1 + \varepsilon_e) \tag{2.7}$$

$$\sigma_{true} = \ln \frac{A_0}{A_f} \approx \ln (1 + \varepsilon_e) \tag{2.8}$$

With these parameters the characteristic Stress-Strain curve can be plotted for the material. From this curve, other considerable parameters can be taken, such as: Toughness, Yield of Strength, Ultimate Tensile Strength (UTS) (which, for our case, will be the same as fracture stress), fracture strain and Young Modulus (Figure 2.15).

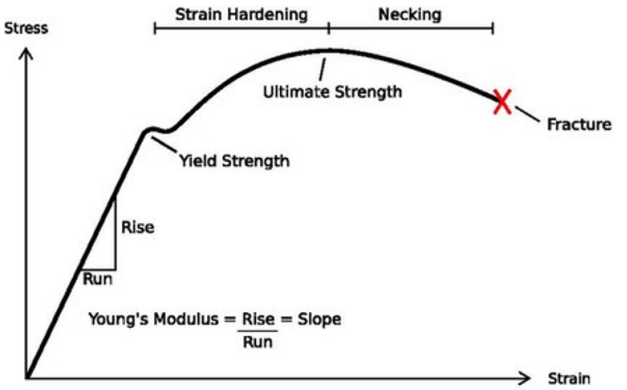

Figure 2.15 Example of an stress-strain curve with the characteristic parameters pointed out

3

Methodology

To analyse the influence of wood fibers in the biocomposite material, an experimental procedure was followed, where the same steps in the same order were applied to every sample, so the comparison between them was reliable.

3.1 Samples

Two different batches of samples from Biofiber Tech. were analysed during the master thesis, most of them composed of approximately of 40%wt of fibers and 60%wt PP (Polypropylene).

First Shipment

The first set of samples that were received from the company was composed by eight kinds of samples (Figure 3.1), each type with either a different fiber surface treatment or with a different manufacturing procedure.

The label used to name them explains the surface treatment that was applied to it and the letter that follows indicates how the material was formed in the compounder, either if the wood was introduced into the hopper in the form of fibers (F) or in pellets (P). A brief description of the manufacturing difference between the samples follows:

- **119:** It is the reference fiber, without any chemical treatment.
- **120, 121 and 123:** Different chemical treatments. Single compounding.
- **125:** Another chemical treatment was applied. The sample went through the compounder twice before going into the injection moulding machine so the fibers should be mixed more uniformly distributed along the matrix.
- **A14:** As 119, it is a reference fiber of another wood batch.
- **C18:** Fibers from the same batch as A14 with an applied chemical treatment.

Fibers 119, 120, 121, 123 and 125 are of the same batch, hence they are comparable between each other (This will be called Type 1). The same happens between A14 and C18, which will be called Type 2. More parameters can be found in Annex A.

Figure 3.1 First shipment samples

For this batch of samples, the analysis was less intensive than for the second batch. The analysis only covered the tensile test and a pre-mortem tomography, because the effort was to be focused on the second shipment that had a new surface treatment applied to them that was of more interest to Biofiber Tech.

Second shipment

The second shipment of samples was composed of four different kind of samples plus a reference one (Figure 3.2). For this batch the analysis was performed before and after the tensile testing.

Figure 3.2 Second shipment samples

Depending on the chemical treatment, each sample received an internal name, in this document, the number that follows indicates the percentage of fibers in the

material. Again, the composites present a PP matrix, this time with 3% of a coupling agent. On the other hand, there are some differences between the samples worth mentioning:

- **Ref-40:** It is the reference fiber.
- **Fib-30:** Presents a new surface treatment of the fiber.
- **Six-40:** Chemically treated similar to F92 fibers but with an stronger concentration.
- **F92-20 and F92-40:** Fibers treated with a different chemical treatment than the previous ones mentioned

For the second shipment of samples, the steps followed for every sample were the following:

1. Pre-mortem X-ray tomography
2. DIC Tensile test[1]
3. Post-mortem X-ray tomography
4. Data analysis

3.2 X-ray tomographies

Only one tomography was performed for each kind of sample, as it was thought that if they performed similarly in the tensile tests, these would have similar structures. Depending on the shipment of samples, a different set of parameters was used for the tomography, but in the same shipment all variables were the same, so the analysis performed later allowed comparison between samples.

In the images, it can be found three main phases represented with three main different brightness. The darkest one corresponds to the voids inside the sample, the second one brighter which can be found would correspond to the matrix, and a third bright one which are found to be the cellulose fibers (Figure 3.3).

First shipment

As said before, for this shipment only pre-mortem tomographies were performed, and not for every sample but only for 119-F, 121-F, 125-F and C18-P. As this set of samples were of a bigger size, two different tomographies were performed: one with a lower resolution (11μm) to have a whole cross-section view of the sample

[1] Unfortunately, although the DIC images were taken, it was not possible to analyze them due to the timeframe of the project.

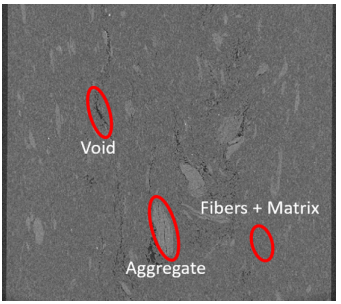

Figure 3.3 Identification of the different phases found in the premortem tomography of a biocomposite

inner structure, used for the porosity and aggregations analysis, and another one with a higher resolution (4μm) focused on the centre of the sample to achieve a better segmentation of the fibers to analyse its orientation (see Figure 3.4).

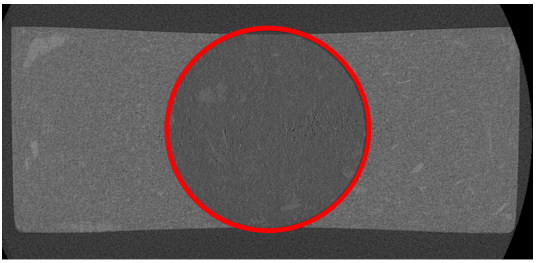

Figure 3.4 First sample cross section 11μm resolution tomography overlapped with the 4μm resolution one (inside the circle) taken

The parameters used for this tomography can be found on Table 3.1.

Tomograph	Voxel size	Number of images	Voltage	Power	Exposure time
Zeiss Xradia Versa XRM520	4.009 μm	1601 over 360º	60 kV	4.98 W	2.1 s
Zeiss Xradia Versa XRM520	11.007 μm	1601 over 360º	60 kV	4.98 W	1.5 s

Table 3.1 Scan parameters of the tomographies for the first shipment samples

Second shipment

In this case, the cross-sections of the samples received were small enough to make a high resolution tomography of the samples. For this case, a new tomograph that

allowed to take different shots of the sample and mount them on each other to achieve a bigger picture was used. Moreover, the new tomograph also allowed to scan the samples in packs of three, for that reason it was scanned a total of nine samples (three of the Fib-30, two of the Ref-40, two of the F92-40 and one of each of the other types of samples).

These samples were scanned both the premortem and postmortem . To identify which tomography belonged to which sample, first the fracture location and paint pattern of the broken sample from the DIC picture was used to identify the postmortem tomographies and then the premortem volume picture was identified by connecting the samples with similar microstructures. In the volume pictures, the same phases found in the first shipment are identified in the second shipment.

The scan parameters can be found in the following table:

Tomograph	Voxel size	Number of images	Voltage	Exposure time
RXSolutions EasyTom150	7 μm	1440 over 360º	60 kV	0.8 s

Table 3.2 Scan parameters of the tomographies for the second shipment samples

Internal structure analysis

The tomography imaging was used to characterize the internal structure of the sample and to do so the phases of the sample shown in Figure 3.3 were segmented. For the porosity, parameters like the void volume fraction or the number and size of pores were calculated, in addition to parameters that were thought to be of interest like the median pore size and the size of the biggest void plus a histogram of the pore angle to the vertical (by calculating the structure tensor of the volume [7]).

Visual images that would give an idea of the spatial distribution of the porosity were also plotted, like a heat map of the projections of the sample, a histogram of the location where the porosity appeared, or an RGB image that indicated the preferred orientation for each pore voxel depending on the colour it was shown.

A similar analysis was made for the aggregates found in the sample, with the difference that the orientation of these accumulations was made using the "regionprops3" function from Matlab, which gave the roll, pitch and yaw of the aggregates, and from which the aggregate shapes were found to be mostly planar or fiber-like. This change was made because the structure tensor code is focused for fiber-alike shapes as it gives an orientation of every voxel individually, and planes have two main directions.

For the fibers, the analysis made was much simpler, as the segmentation was not as precise as the others, and the fibers could not be independently isolated. Because of this reason, the structure tensor code was a better option for the orientation analysis. On the other hand, the resolution of the tomography meant that the images were very heavy, meaning that it was not possible with Matlab to analyse the full

stack at once, so some analysis like the RGB orientation image was not possible to get.

Tomographies can also be analysed visually to give a qualitative explanation on how the sample failed and how the fiber interaction with the matrix influenced the mechanical properties calculated.

3.3 Tensile testing

For the first set of samples, although no tensile tests were performed in the LTH laboratory, data from previous tensile tests were provided by Biofiber. These data could be processed and the results from the data analysis can be found in this report and in Annex A, but there were no data provided from the analysis on how the tests were performed or at which speed.

For the tensile testing performed in Lund University, at least one sample from each kind was tested, so data from each type could be gathered. The load in the test was done with a constant loading rate:

$$Loading\ rate = L = 2\ mm/min$$

The loading machine recorded the force applied and the time when the measurement was made, so the elongation has to be calculated with the loading rate. As said before, the new samples from the second shipment were smaller than the first ones and when tightening the samples in the loading machine, the clamps come closer together as the same time as they are tight, which led to some buckling of the sample (Figure 3.5, Right). This was not of much importance as after the test started to record some data, the stretching of the sample ended up with the clamps being aligned with the sample again, but it has to be taken into account when calculating the Young's Modulus or other parameters which take into account the initial stage of the curve. Furthermore, as all samples present the same problem, the comparison between them was still be reliable. It was found out afterwards that this could have been solved by preloading the machine until the bending was eliminated on the sample.

Mechanical properties

The mechanical testing was used to draw the stress-strain curve to find the characteristic mechanical properties of the material. From there, found values such as the Ultimate strength (Equation 3.1), ultimate strain (Equation 3.2), yield of strength (σ_y), Young's Modulus (E) and the Toughness (U_T) could be determined.

$$\sigma_f = \frac{F_{fracture}}{A_0} \tag{3.1}$$

$$\varepsilon_f = \frac{\Delta l_f}{l_0} \tag{3.2}$$

Figure 3.5 Left: Paint-sprayed samples for DIC. Right: misaligned sample at loading machine

To get the final curve, the mean between the different samples tested was made, omitting the samples whose recorded data outstood the rest of its kind. As no significant necking could be observed, it is hard to determine the yield of strength (σ_y) of the material. To do so, it was first calculated the Young's Modulus (E) by the method established in Section 10.3.3. of the ISO 527-1:2012, where the Young's Modulus is calculated as the slope of the least-squares regression up to a strain of 0.25%. Then, the yield of Strength (σ_y) was determined by the method in which the yield happens where the strain-stress curve crosses a line whose slope equals to the Young's Modulus, and it crosses the x-axis at 0.2% of strain. This value is used as an indicator of how quickly the slope decreases, or how quickly the creep begins. Finally, the toughness of the sample (U_T) was calculated as the amount of energy that can be absorbed by a unit of volume before its fracture. The trapezoidal integral of the line was used to achieve it.

4

Segmentation

After the tomographies were performed, the images were segmented using Matlab-2020B®looking to separate each of the phases presented in the biocomposite material, in particular porous, fibers and aggregates of fibers (Figure 3.3). To do so, the same procedure procedure was followed, always keeping in mind that all samples should go through the same segmentation procedure so the results obtained are comparable. More detailed information on how the segmentation procedure was developed in Annexes B and D.

The segmentation parameters were obtained always after cropping the tomography images to get rid of the surroundings of the sample. the segmentation procedure is described below:

1. **First shipment samples**

    - **Porosity:** The medium resolution volume picture is binarized with a threshold value (0.33); pixels with a brightness below this colour will be considered white and the rest black. To the resulting image a progressive D-E filter[1] of radius 2 is applied and afterwards all groups of pixels smaller than 8 voxels (cube of side 2) are eliminated.
    - **Aggregations:** The medium resolution volume picture goes through an E-D filter[2] of radius 3, then subjected to a non-local mean filter with a smoothing degree of 0.03. Once the picture is smoothed it is binarized with a threshold value (0.38), and the formations smaller than 1000 voxels (a cube of side 10) are filtered out.
    - **Fibers:** The high resolution volume picture is binarized with a threshold value (0.1955), afterwards, the aggregate mask obtained previously is rescaled to match the high resolution tomography size and the aggregates located in this one are subtracted to isolate the fibers.

[1] Filter where the image is subjected to a Dilatation followed by an Erosion (Matlab filters), both with a sphere of radius “x”.

[2] Filter where the image is subjected to an Erosion followed by a Dilatation (Matlab filters), both with a sphere of radius “x”.

2. **Second shipment samples**

    - **Porosity:** The $7\mu m$ resolution tomography is binarized with a threshold value (0.25), pixels with a brightness below this colour will be considered white and the rest black. To the resulting image a progressive D-E filter of radius 2 is applied and afterwards all groups of pixels smaller than 8 voxels (cube of side 2) are eliminated.
    - **Aggregations** A progressive E-D filter[3] of radius 3 is applied and another variable is created from the image, which is the result of applying a non-local mean filter with a smoothing degree of 0.03 to the E-D image. Then both images are binarized with a threshold value (0.2775) and combined with an AND filter (only elements presented in both pictures will be stored). Finally, groups segmented smaller than $0.0013mm^3$ are masked out (same volume size as before)
    - **Fibers** Similarly as done to the samples from the first shipment, the tomography picture is binarized with a threshold value (0.2925), and then the aggregates are masked out with the previous segmentation performed to keep only the individual fibers.
    - **Post-mortem tomographies:** These were segmented with the same parameters as the pre-mortem ones, as the parameters used in the image acquisition were exactly the same in the tomograph. However, the fracture regions were omitted due to both the difficulties to align the samples precisely in the tomograph or in the image. The fracture is segmented and analyzed in parallel to not take the fracture space in the void characterization.

4.1 Porosity segmentation

To get to the procedure used to achieve the mask, the 3D volume filters that Matlab presents were explored. After some trial and error, it was found that the porosity in the sample was presented in so small aggregations that any filter done previously to the binarization of the mask resulted in the smoothing or disappearance of many small voids (this is because regular filters smooth the picture to get rid of the noise of the picture but, as said, the voids are so small that this are taken as if they were noise).

For this reason, it was decided to binarize first the picture. The binarization consisted in thresholding the pixels either to 0 or 1. Those pixels below a brightness value where considered potential voids and highlighted, and the rest of them were masked out. To choose this threshold value, the volume fraction of the voids masked out in the binarization was plotted versus the searched value.

[3] Filter where the images goes multiple times through an E-D filter while increasing the filtering radius from 1 to the final defined value.

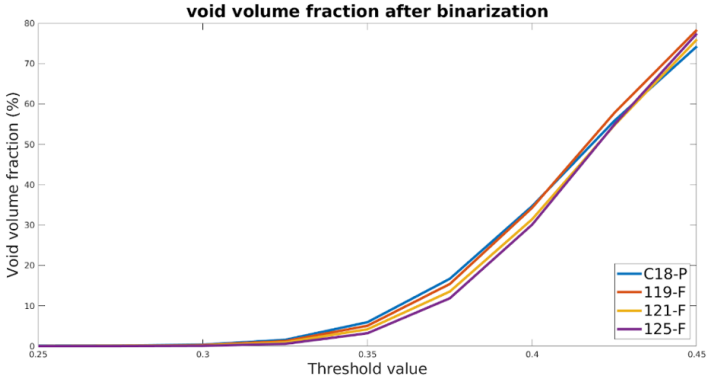

Figure 4.1 Porosity fraction depending on the threshold used for the analysis

Taking as an example the first shipment plot (Figure 4.1) it can be seen how the curve is relatively flat until the value gets around 0.3-0.35. This increase of slope is caused as the matrix phase starts to be implemented in the mask, increasing drastically the fraction of the mask. With this information and always checking visually the segmentation, the value to be used is found.

Once the mask is done, there can be found many small unconnected voids that will be filtered out (to get rid of the noise), so they will not be taken into account, or big voids that are next to each other but not united, so in the results analysis these would be considered as separate voids, that in reality they may be connected. To solve this, a series of D-E filters are used, where those voids that are isolated will not increase in size, but those that are next to each other will. To see the influence of this filter and the radius that could be used for our analysis, it is again plotted the void fraction and the number of voids against the radius of the filter used (in Figure 4.2 there can be seen the example of the first shipment).

It can be found how when the radius is increased, the number of voids is decreased (because these are being connected), but the void fraction increases (because the pixels between the connected areas are highlighted). In the example shown in Figure 4.2, the chosen value was 2 voxels, as the void fraction was not considerably modified, but it could be seen how the voids were being connected.

Finally, to get rid of the noise segmented as voids, those under a certain size are taken out. The value used for this filter was always an integer value to the cube, so, for example, to take out voids of a size equivalent to a cube of side 2, 3, or 4 (8, 27, 64 voids connected), always considering the 26 possible ways to be connected.

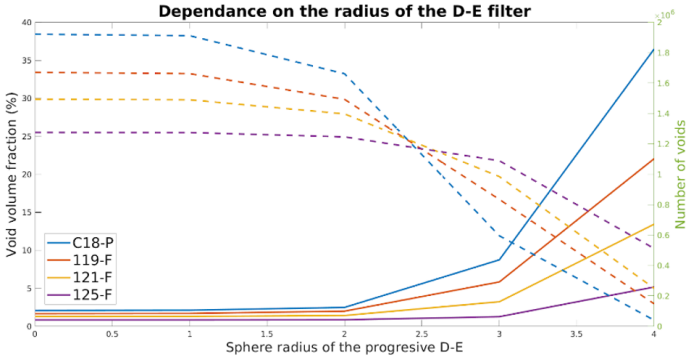

Figure 4.2 Porosity fraction (continuous line) and Number of pores (dashed line) depending on the radius used for the DE-filter

4.2 Aggregation segmentation

An aggregation was considered for every group of fibers that were connected and was bigger than a cube of volume 0.0013 mm³ (10x10x10 voxels with a resolution of 11 µm). To segment them, a different approximation to the porosity segmentation was followed, as in this case it is wanted to smooth the whole picture so the big bright (fiber) groups of voxels are brightened out, and the isolated voxels are darkened.

A series of filters to blur out the fibers while enlightening the aggregations were tested. Then E-D filter was tested before binarizing the picture: as the image is first eroded, this helps to get rid of the individual bright fibers, keeping the brightness of the big ones intact. It was found out that a non-local mean filter could achieve this function nicely, but Matlab did not present this kind of filter for a 3D volume picture, so it was applied to each individual slice in the xy-plane (as this is the biggest one and where the aggregations could be seen the best). All of these filters and parameters were checked visually by comparing the slices before and after the filter.

Then the image was binarized and, as with the porosity, a plot of the void fraction was plotted against the threshold value used, but this time the bright spots were turned 1. Figure 4.3 shows an example of this plot for the first shipment where there is a value where the aggregate volume fraction becomes approximately constant, which are the aggregates that should be of the same brightness because of the smoothening done to the picture.

To finish with the segmentation and, as said before, all aggregations smaller than 0.0013 mm3 were filtered out.

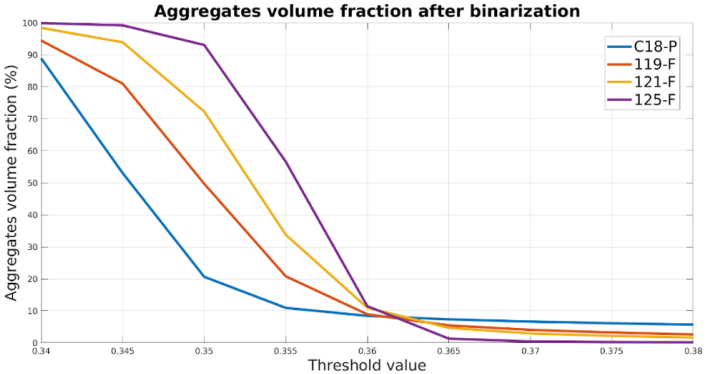

Figure 4.3 Aggregate fraction depending on the threshold used for the analysis

4.3 Fiber segmentation

By plotting the brightness histogram of the sample tomographies, it could be seen how both fibers and matrix had a similar influence on the X-rays, leading to a small difference in brightness in the resultant picture. Additionally, because of the thin shape of the fibers, any regular filter would result only in a smoothing out of the fibers such that they would disappear, as happened with the porosity segmentation. On the other hand, if D-E filters where applied, because of the fibers being so abundant, this would result in a brightening of the whole volume.

For the above reasons, the only filter that was applied was thresholding the high resolution tomographies. The threshold value applied was chosen visually, as not even the volume fraction of fibers estimated gave a considerable good result to the segmentation. Once the fibers were segmented, the aggregations were excluded from the fiber mask by using the aggregate mask obtained previously.

5

Results

5.1 First shipment

Phase analysis

As said in Section 3.2, only pre-mortem tomographies were made of the first shipment samples that were considered of most interest. Based on the results extracted from the tensile test data provided by Biofiber Tech. it was chosen to analyze the samples 119-F, 121-F, 125-F and C18-P. The first one for being the reference, the second one for achieving the best performance, the last one for being the one with the worst performance and the other one as it had an outstanding stress-strain curve compared to the other samples whose compounding was made in the form of fibers. Some more images for every sample analyzed with annotations about the discoveries can be found in Annex C.

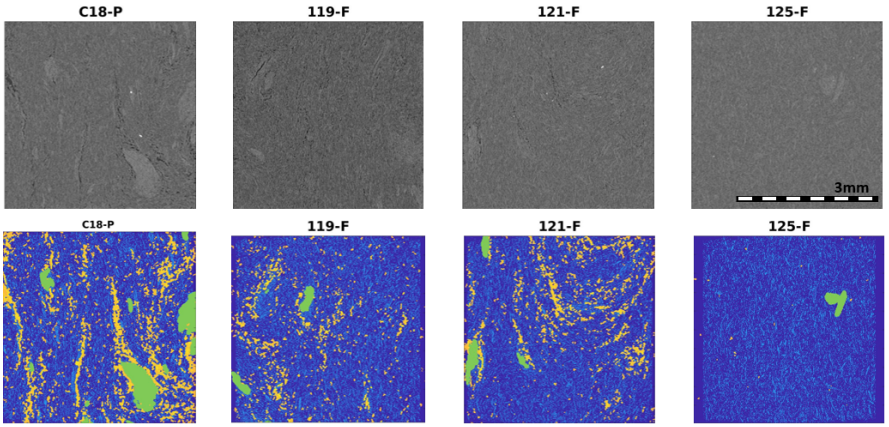

Figure 5.1 First row: Original picture of the tomographies (11 μm res). Second row: Segmentation of the first shipment of samples. Aggregates (green), fibers (light blue), voids (orange) and matrix (dark blue).

In Figure 5.1 it can be found a summary of the tomographies segmentation, this picture was made by adjusting the size of the aggregates and porosity segmentation ($11\mu m$ Tomography) to overlay the fiber segmentation to the ($4\mu m$ tomography). Here, it has to be taken into account that although the picture presented shows just a small area of the sample volume, the area encompassed by the aggregate and porosity segmentation is bigger than the one shown, as explained in Figure 3.4. In the second row it can be identified the three different phases segmented: Fibers (Light blue), Aggregates (green) and Porous (orange).

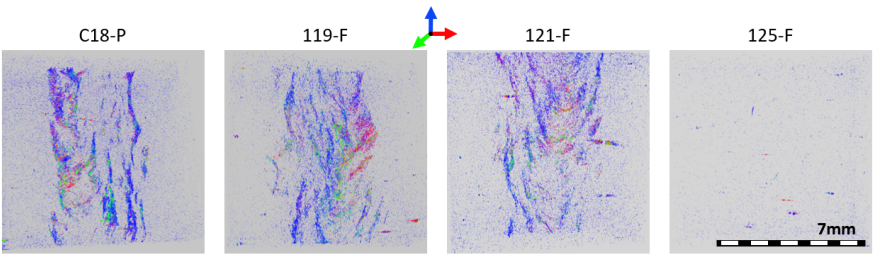

Figure 5.2 First shipment's samples void picture, colored depending on its orientations

Porosity A 3D volume picture was made by plotting the porosity segmented from the tomography (Figure 5.2). This plot was made by masking the porosity and calculating the Structure Tensor of this phase to analyze its orientation along the sample. The color of each voxel of the picture depends on the components of the orientation vector extracted from the Structure Tensor: Red component depending on the value of the x-direction (horizontal), green component depending on the value of the y-direction (depth), and blue component depending on the value of the z-direction (vertical). With this information, it is seen how the samples' voids tend to be formed with a vertical orientation, mainly caused probably by the shrinkage of the bulk material to the different surfaces of the sample when solidifying in its manufacturing. This orientation can also be found in Annex C where it is plotted a histogram about the voxel angle with the vertical axis.

Furthermore, there can be found in the samples some voids that present a U-shape along the vertical axis (in sample 121-F this shape is the most obvious one). This is considered to be caused by two reasons: The flow of the polymeric material when manufacturing, and the slipstream caused by the movement of aggregates relative to the matrix. The difference in density of the polymer along the traversal direction (due to the temperature gradient along the volume) generates differences in speed depending on its location, leading to the formation of possible wave fronts. These wave fronts originate from the separation of some polymer chains (forming polymer layers) that cause independent solidification nuclei, which make the layers

more obvious when shrinking apart. These layers may also be caused by the flow movement of different aggregates in the matrix, which forms other slipstreams.

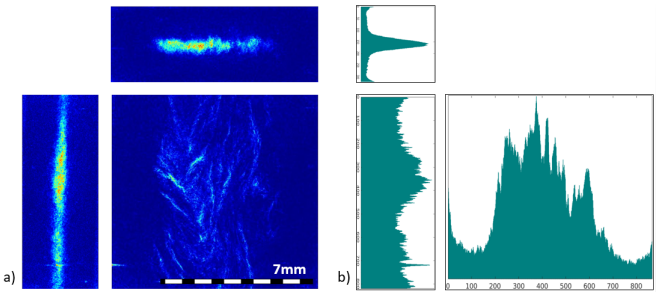

Figure 5.3 Heat map views of the porosity projection views found in 119-F (a) with the histogram of the location of these voids (b)

To analyze the distribution of the porous along the material, a heat map is plotted of the three main views alongside with a histogram of the location of its coordinates. With these plots, different information can be extracted. Starting with the fact that the porosity does not seem to change remarkably along the longitudinal axis as the tomography just shows a fraction of the whole sample (the bottom and top borders are not shown). On the other hand, the side borders are shown in the tomograph and it is seen how some voids seem to be concentrated in the bulk of the sample, because of the same reason as the vertical alignment of these voids explained previously in this same section.

Taking a deeper look at the porosity displacement, it can be found some concentration of voids in the corners of the sample, caused probably by a premature solidification of the material before reaching these corners. This is a typical problem found in injection moulding pieces, that may have been worsened by the introduction of fibers in the material, increasing its viscosity and ability to flow when melted. Although in Figure 5.3 only the results for sample 119-F are shown, in Annex C can be found the rest of the samples.

In Figure 5.4 can be found some of the quantification parameters found for the different samples whose tomographies where taken. The biggest void size was found in C18-P with a volume size of $0.6412 mm^3$. Although there is a big difference in the void fraction of each sample, as in the number of voids, the median size found on it is pretty similar to each other, meaning the presence of a big number of small voids in every sample.

Aggregates Looking at the aggregates that were segmented, it was found a great difference in quantity between the samples analyzed (Figure 5.5). Although it was defined in Chapter 4.2 that an aggregate was a continuous block of fibers bigger than $0.013 mm^3$ after an smoothing of the image, the shape that these could get was

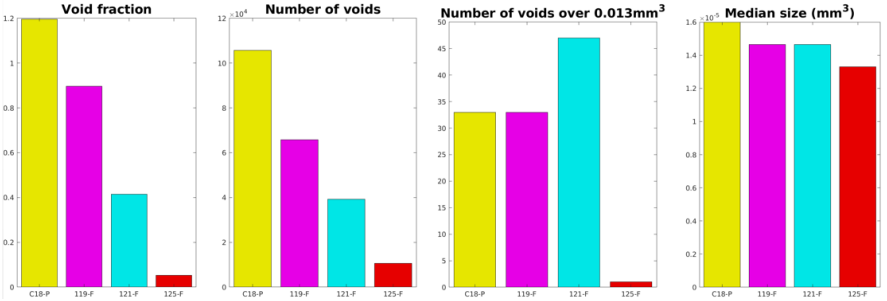

Figure 5.4 Void measurements on the fist shipment's samples

not defined (even though that the smoothing filters applied to the picture restricted the appearance of thin structures) , so this could either be presented as cylinder (or fibers), planes or spheres depending on the aspect ratio of the clumps. Determining this can be crucial to determine its orientation, as a sphere has no orientation and planes have two main orientations.

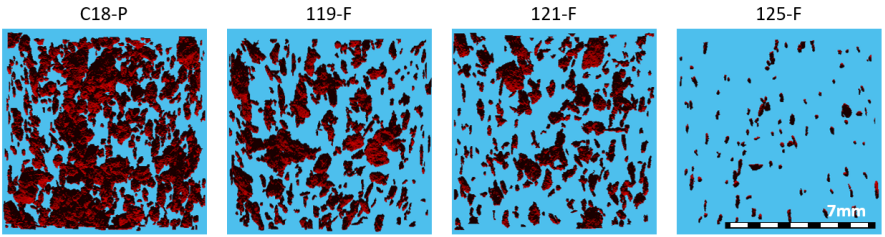

Figure 5.5 Volume picture of the aggregates segmentation

After an analysis of the main dimensions of the aggregates, it is found that these have a preference to be presented mainly in plane shapes and some fiber shapes (almost no spherical shapes where found). Because of this, it was decided to calculate orientation in terms of the roll, yaw and pitch that they presented (Figure 5.6). This rotations are understood from the starting point where the main axis of the aggregate is oriented in the x-direction (width of the dogbone) and the second main direction is in the y-direction (thickness of the dogbone). All angles are made positive to have an easier understanding, but in Annex C it can be seen how the plots are symmetrical along the system of reference.

From this plot, it is found another preferred orientation for the aggregates, which tend to orient parallel to the main sides of the sample. This can be confirmed by the heat map of the aggregates segmented (Figure 5.7). On the top view of the figure it can be seen how the aggregates tend to form ovals around the center and how these seem to be oriented in the vertical direction of the sample. All aggregates

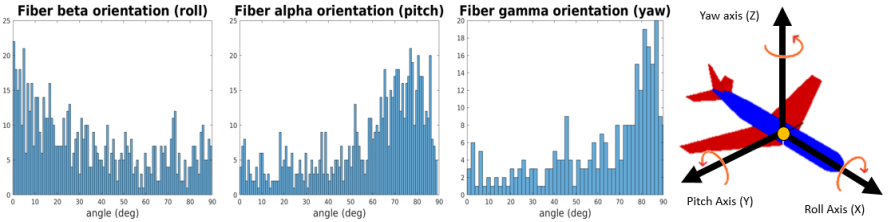

Figure 5.6 Histogram of the aggregates angle orientation from C18-P

are not aligned parallel to the main side, but they tend to be placed vertical, with its normal vector pointing to the center of the sample, resulting in the overall preference orientation commented before (as the main side is longer, there are more aggregates parallel to this one). On the spatial distribution of the samples, no pattern or specific placement was found in any of the samples but the one that they also appear in the borders of the sample (not as porous).

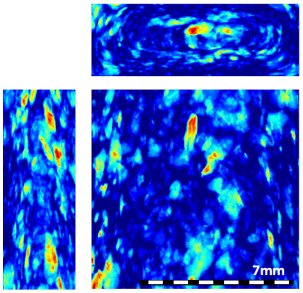

Figure 5.7 Heat map views of the aggregates presence found in C18-P

Some quantified parameters about the aggregates sizes and presence in the sample were calculated and characterized, and these can be found in Figure 5.8. The biggest aggregate size was found in C18-P with an estimated size of $1.05mm^3$. As expected from the volume view tomographies (Figure 5.5), the samples have a different presence of aggregates, being 125-F one with the least and smaller ones, caused by the good mixture achieved with the second compounding. On the other hand, it seems that the introduction of fibers in the form of pellets to the compounding lead to an evident increase in both the size and quantity of aggregates, leaving the two other samples with similar properties.

Making a comparison between Figure 5.8 and Figure 5.4, a direct relation can be found between the number of aggregates and their size with the porosity profile of the sample.

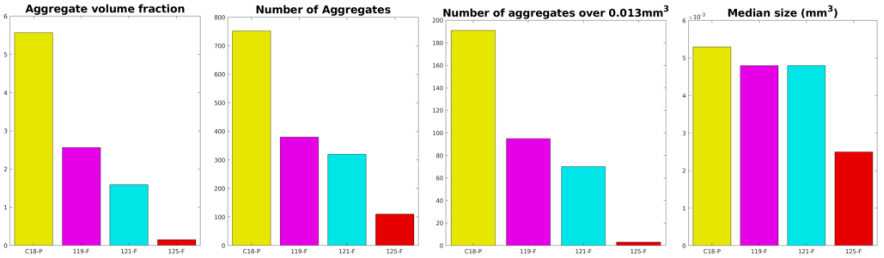

Figure 5.8 Aggregates measurements on the fist shipment's samples

Fibers The poor segmentation achieved on the fibers restricts the analysis that is able to be applied to the sample. This limitation is caused by many reasons. The first one because the tomography picture does not show the whole cross section of the sample, hiding half of the information. The second one, because the threshold chosen to apply to the binarization of the sample is too soft to segment the fibers independently, and it is too strong that some fibers are segmented thinner than what the visual exam shows as shown in Annex B. This two reasons meant that most of the quantitative analysis done in the previous phases was not reliable to calculate (fiber volume fraction, aspect ratio, size histogram...)

Finally, the third reason is because of the data size: the resolution is so high that when trying to apply some of the same analysis performed on the other pictures, Matlab crashes because of its memory use restrictions. To mitigate this last limitation, some functions like the Structure Tensor code were run on the samples by packing the data into smaller batches, however this did not solve everything.

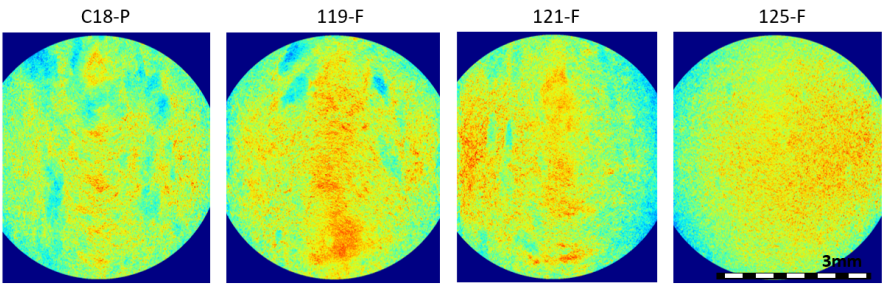

Figure 5.9 Heat map top views of the fibers distribution in the first shipment samples

On the other side, there was still some figures and analysis that could be done. One of them was the heat maps to look for any kind of distribution of the sample. Although the side views where not reliable to calculate (because of the imaged area), the top view showed different distributions between the samples (Figure 5.9).

In the figures and more evident in C18-P and 119-F, there are some light spots that show a characteristic lack of fibers, caused by the empty space left when taking away the aggregates. On the other hand, the fibber distribution depends a lot on the sample, where some samples like 119-F presents a higher concentration of fibers in the bulk and others like 121-F and 125-F seem to be displaced to one of the sides. Moreover, in 125-F there was found to be a more scattered distribution of fibers, caused probably by the better mixture achieved by the second time the mixture went through the compounder.

Taking a look at the orientation of the fibers from the Structure Tensor, it is seen how these seem to be usually aligned with the vertical axes. Unluckily, it was not possible to get an orientation based on the location of the sample such as Figure 5.2, because of the Matlab memory limitations. However, in all samples can be found the pattern shown in Figure 5.10, where the fibers are aligned with the vertical axes. This alignment might be caused for the same reason the polymer chains align in the shear zone, as explained in Section 2.4.

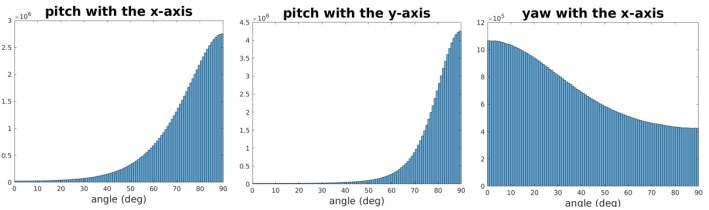

Figure 5.10 Histogram of the fibers angle orientation from C18-P

The main difference found between samples is the yaw distribution (Figure 5.11. However, as it is seen that the main direction is vertical, the yaw does not suppose a big change in the orientation of the fibers.

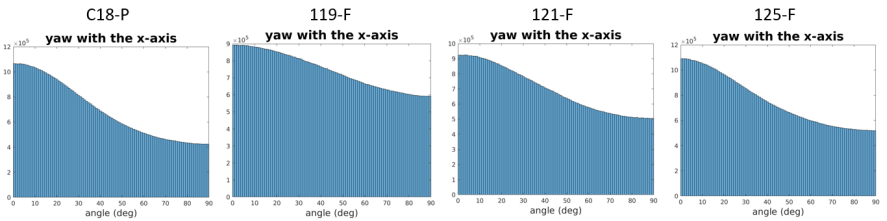

Figure 5.11 Histogram of the fibers yaw rotation for the first shipment samples

Mechanical results

When plotting the data that Biofiber Tech. provided about the tensile test in just one figure, it can be seen how every sample has a strain hardening behaviour along the

whole deformation and does not present the characteristic yielding associated with the ”necking” that most polymers have.

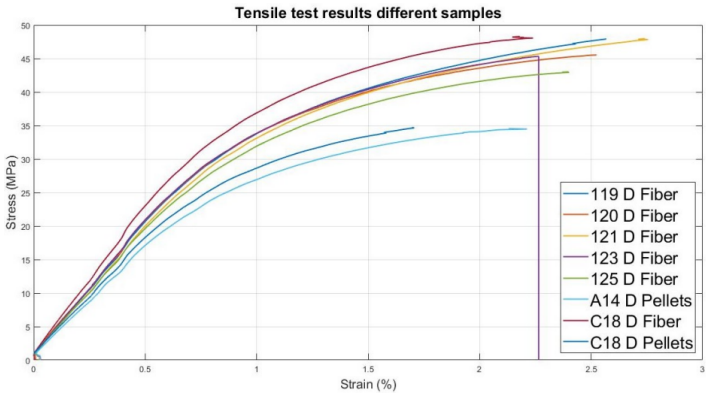

Figure 5.12 First shipment’s stress strain plot

Taking a look at Figure 5.12, the properties of all samples whose fibers where directly pressed into the compounder, seem to be higher than those where the wood was introduced in the form of pellets. However, to compare the sample properties, these were calculated as explained in Section 3.3 and were plotted in bar charts for an easier comparison.

Taking a look into Figure 5.13, is is confirmed that the properties achieved by those samples whose fibers were introduced in the form of pellets to the compounder present poorer properties. On the other side, the rest of the samples present similar Young’s modulus and similar properties to each other apart from the following ones.

Even though 125-F was the sample that presented the least porosity and the least amount of aggregates, it seems that sample 125-F tends to be weaker than the rest of them, something that could be explained because of the double compounding that was subjected to. Fibers may burn when too much energy is applied to them, which might deteriorate them. On the other hand, sample 121-F seems to have high tensile properties, being the one with the highest toughness of them, explained by a high fracture strain and a similar UTS as the rest samples.

The sample whose fibers were not treated (119-F), presented the highest values for the measured properties after 121-F: the highest yield of strength, highest fracture stress and the second highest fracture strain and toughness. This properties were very close to the ones from 121-F, but the sample with a surface treatment lasted longer, leading to an increase of the properties that take into account the plastic region of the curve.

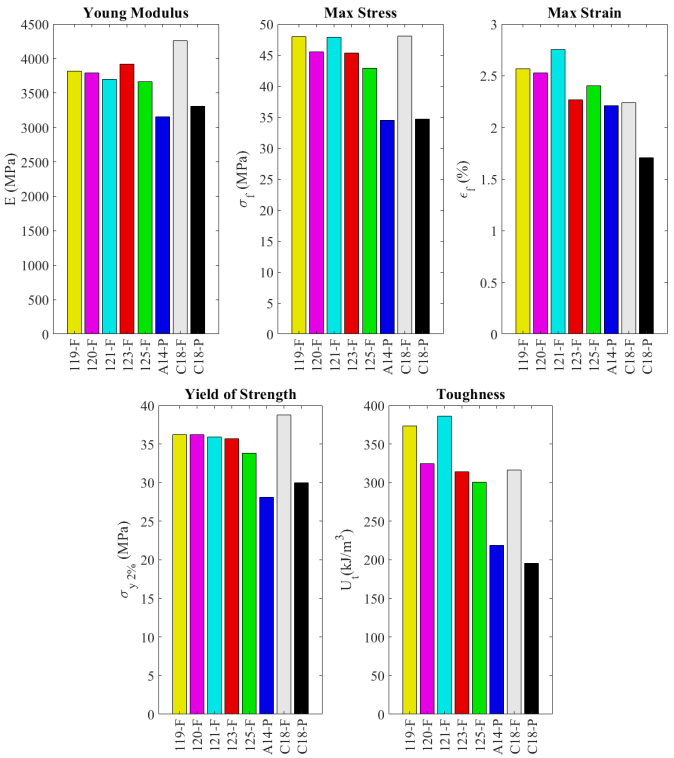

Figure 5.13 First shipment samples' Mechanical properties

5.2 Second shipment

Phase analysis

The results obtained in the segmentation can be seen in Figure 5.14, where some differences between samples can already be identified, like that the sample F92-20 presents less fibers and higher porosity, or that the Ref-40 sample already presents the characteristic void U-shapes found in the first shipment samples.

After segmentation, the results from the heat map distribution of the pores show some characteristic cyclic patterns along the longitudinal direction (Figure 5.15. This pattern was very unusual as along this direction the porosity should be relatively constant. This has been identified as an artifact on the tomographies, because the same pattern was presented on every sample 6 times (4 complete cycles and one partial on the top and bottom of the sample) coinciding with the number of tomographies that were stitched together.

This flaw in the reconstruction algorithm not only means that the quantitative

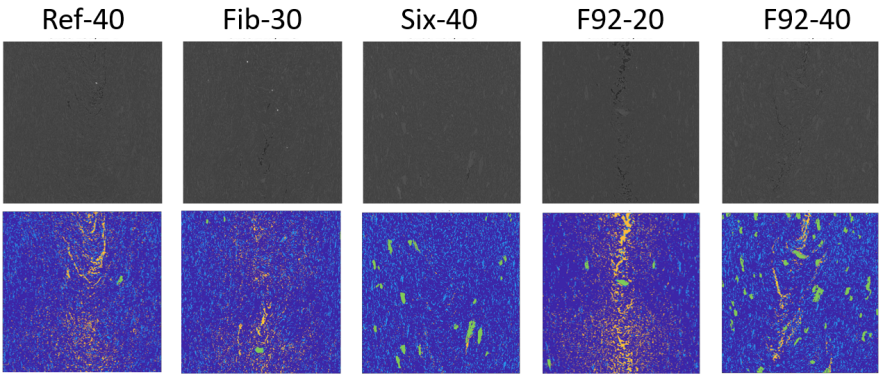

Figure 5.14 Premortem tomographies of the second shipment samples. Original picture (Top row) and segmented one (bottom). Aggregates (green), fibers (light blue), voids (orange) and matrix (dark blue)

results got from the tomography are not valid, but also that the comparison between them neither is because its effect changes with the tomography analysed. As a result, only qualitative analysis were able to be performed on these tomographies, so the analysis was focused on the breaking mechanisms that were observed in the postmortem tomographies. Further work is needed to resolve this issue.

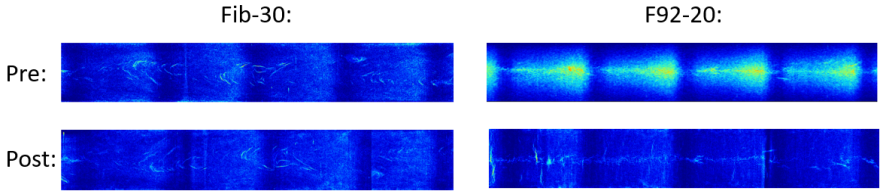

Figure 5.15 Porosity distribution heat map from Fib-30 and F92-20. Premortem and postmortem segmentation

Breaking mechanisms

Although the identified artifacts from the tomographies limits the reliability of the parameters that can be calculated such as volume fraction distribution and others, the images can still be used for many things such as to understand the breaking mechanisms of the samples.

To make the phase identification easier, the tomography image were semgented to plot each phase in a different color: dark blue for matrix, light blue for fibers, green for fiber aggregates, and orange for voids/air. This makes it easier for the eye to identify the phases, and if big structures or uncommon things are presented, they

are easier to be spotted. Furthermore, as the volume analyzed is not large along the z-axis and the analysis will just be qualitative, the change in brightness found in the previous section should not have a big influence.

Depending on the sample, different fractures were spotted, and although some patterns were found such as the enlargement of pores that acted as stress concentrators, or that the fiber alignment influenced the fracture surface area, there are different things to highlight in each sample. More information and images can be found in Annex E.

Fib-30 It can be seen how, away from the fracture, the voids are along the matrix space and they grow along the matrix, avoiding the fibers (Figure 5.16.a). It is not until when a void grows enough and surrounds a fiber, when the fiber disappears in the slice, meaning that either the fiber did not fail but the interface did as the fiber came apart, or that the matrix by itself failed and tore apart not being able to distribute well enough the force to the fibers. However, due to the small matrix presence found in the borders of the isolated fiber, it makes more sense for the failure to come from the matrix/fiber interaction.

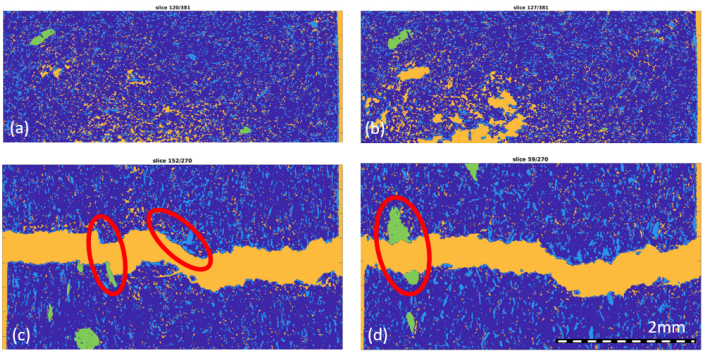

Figure 5.16 Segmented tomography of the Fib-30 fracture. Aggregates (green), fibers (light blue), voids (orange) and matrix (dark blue)

Similarly, in Figure 5.16(c), an aggregate separated from the matrix lead to a drastic change in the path of the fracture to follow the shape of the aggregate. This is a very good example of matrix/fiber adhesion failure. On the other hand, in Figure 5.16(d), another aggregate can be seen that broke apart without being detached from the matrix. As this aggregate was of a bigger size, its surface in contact with the matrix was enough to hold under the applied force.

It should be highlighted that in Figure 5.16(c) there is another change in the fracture path along the center of the sample, caused possibly by the peeling of fibers that were oriented parallel to the fracture direction; this is also observed in the other samples.

F92-40 In Figure 5.17(a) and (b), it can be found again how voids tend to grow in size along the borders of the fibers and even more on the aggregates, which is an indicator on the lack of adhesion in these regions. This makes sense as aggregates are just fibers whose surface area by volume ratio are the smallest, meaning that the load they hold is the highest and the area to attach to the material is the smallest. This also coincides with the finding that higher aspect ratio fibers increase the mechanical performance in composites.

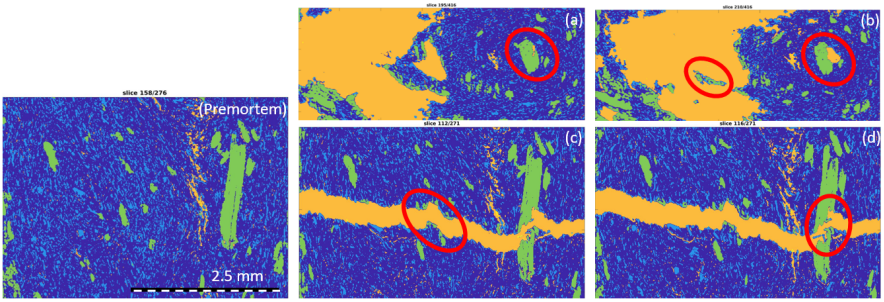

Figure 5.17 Segmented tomography of the F92-40 fracture. Aggregates (green), fibers (light blue), voids (orange) and matrix (dark blue)

Nevertheless, as seen in every picture from Figure 5.17, there are sometimes aggregates that break before the adhesion fails. In 5.17(c) and (d) a long aggregate that have broken apart can be seen; this is probably because of the considerable aspect ratio compared to other aggregates that present a more spherical shape. An individual fiber can be spotted inside the aggregate in 5.17(d) that looks like it stretched and tore in two (as there is one in the top and one in the bottom piece located at the same place in the aggregate).

Looking at the differences between the premortem sample and the postmortem in the same slice (c), there does not seem to be a big difference on the size of the pores other than the appearance of new ones. Also the slope of the protruding break that is found in the middle of the sample, corresponds to the direction that the fibers had on the same region on the premortem piece. Meaning that the fracture developed between the fibers and avoided them.

F92-20 This sample is characteristic for its reduced amount of fibers, which can be easily identified by just looking at this phase in the pictures. Fibers are not only less common to be spotted, but aggregates are not found to be as big as in other samples and more voids are seen in the middle of the sample.

In Figure 5.18 a great number of transversal cracks can be seen in the sample that are not in contact with the fractured area. These are cracks that could be reason for failure of the sample but held more than the final fracture area. The cracks show how the material broke in a more ductile way than the previous ones, which is in

accordance with with the fact that is the one with the least amount of fibers, meaning that it should behave more similarly to its matrix (polypropelene).

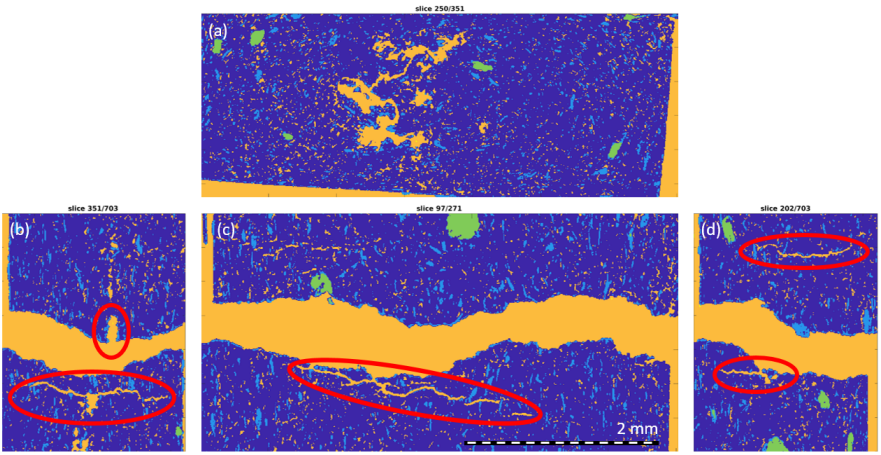

Figure 5.18 Segmented tomography of the F92-20 fracture. Aggregates (green), fibers (light blue), voids (orange) and matrix (dark blue)

In Figure 5.18(d) an aggregate of small size coloured blue whose surface area was not big enough to adhere to the matrix is seen cleanly separated from from it. Also, similar to other samples, horizontally aligned fibers act as cracks propagators, as can be seen in Figure 5.18(b) and (c).

From this sample it is also worth notting the void in contact with the surface of the fracture in Figure 5.18(b). It is probable that this void acted as a stress concentrator and was the origin of the the starting crack that grew and caused the fracture.

Ref-40 Other than some ring artefacts that were found in the tomography, in Figure 5.19 a high concentration of porosity can be observed, compared to the other samples. Also, it can be identified how the fracture surface is very similar between the top and bottom parts, meaning that the fracture can be considered more brittle than the others.

The reason for this brittleness is likely the fiber alignment in the region, because the fracture seems to be caused by matrix fiber interaction along the whole surface. In the middle region of the sample (Figure 5.18.b) a similar failure profile can be seen to the flow patterns identified in the porosity images from the tomographies performed to the first shipment samples (Figure 5.2).

Six-40 Figure 5.20(c) shows the fiber orientation following oval shapes concentric to the center of the sample similar to the ones found in the first shipment analysis (Figure 5.7). This may be a big influence on the fracture shape, as the voids appear in 5.20(d) follows a similar pattern to this ovals, probably because it is the direction

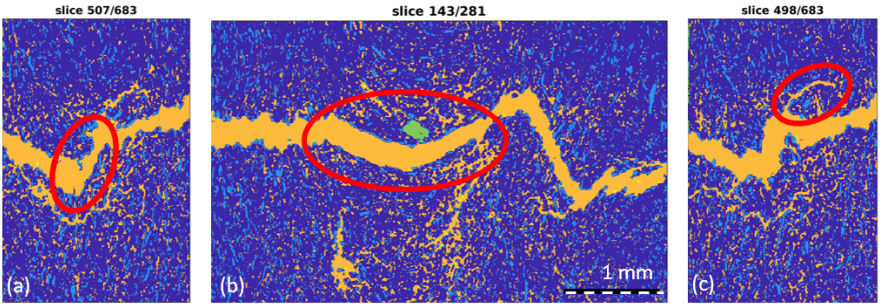

Figure 5.19 Segmented tomography of the Ref-40 fracture. Aggregates (green), fibers (light blue), voids (orange) and matrix (dark blue)

that can be followed to encounter the least number of fibers or to be tangential to the longer width of them.

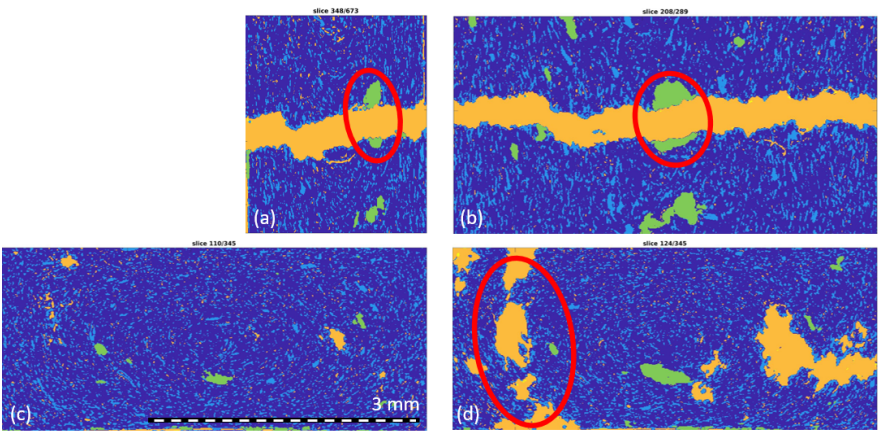

Figure 5.20 Segmented tomography of the Six-40 fracture. Aggregates (green), fibers (light blue), voids (orange) and matrix (dark blue)

A broken aggregate with a planar shape was again spotted in this sample, indicating the adhesion worked properly here. However in Figure 5.20(a) it seems that fracture happened following a similar pattern perpendicular to the fiber alignment in some places, meaning again some fiber/matrix adhesion failure.

Adhesion comparability

To compare the fiber/matrix adhesion, a visual analysis was used, where snapshots were taken to the top view of the tomography at a height where the fracture is visible but the surface of the sample pieces are near. Those fibers that failed to adhere to

the matrix and did not break will be shown as individual fibers surrounded by voids. Another similar way to check the fracture nature is to look not only at the individual fibers, but also at the border of the fracture to see if the frontier is mainly of fibers or also matrix.

As seen in some samples, such as Ref-40, there are some fibers that are horizontally aligned, and these are the weakest points, on which the fracture usually develops. However, most of the fibers are aligned with the longitudinal axis of the sample - as seen in the orientation analysis from the first shipment samples (Figure 5.10) - this will be a good indicative on which fibers adhered better to the matrix.

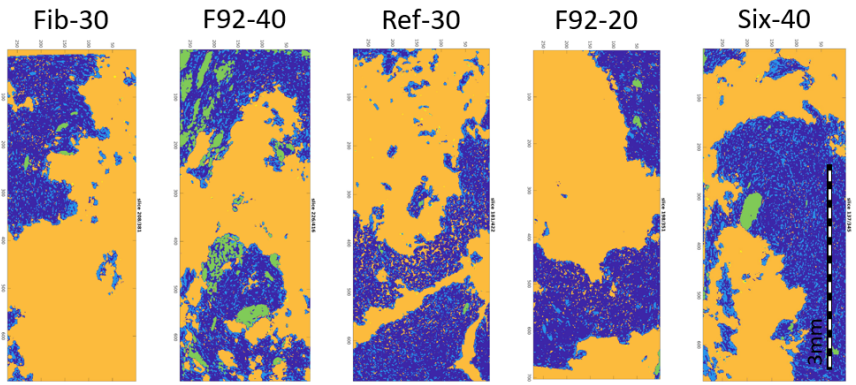

Figure 5.21 Segmented top views of the fracture areas from the tomography of each sample. Aggregates (green), fibers (light blue), voids (orange) and matrix (dark blue)

Although in every sample some isolated fibers can be found, there are some samples that present more individual fibers that failed to adhere to the matrix than others. In all the samples, the fracture border with the sample is formed mainly (almost fully) by fibers, which can indicate that there is always an adhesive failure. However sample F92-20 is the one that by eyesight appears to have the most matrix in the border, although it might be because this has around half the mass fiber fraction of the samples.

On the other hand, Six-40 is the sample that presents the biggest fiber groups in the sample, although almost no individual fibers are spotted. F92-20 is the sample with the most uniform fracture seen, which indicates a clean failure in terms of crack propagation. Although, as before, this can be explained by the small presence of fibers in the sample; F92-40 is another sample which does not present many isolated fibers in the fracture even though that is the one with the most amount of aggregates (recalling that aggregates are usually weak points for the matrix adhesion).

In Fib-30, a similar behaviour to F92-40 is found with small isolated fibers that were not able to hold sufficiently to the matrix. Finally, Ref-40 fibers presents by far

the worst adhesion to the polymeric matrix, where many fiber groups of different sizes can be spotted.

Mechanical results

As only one sample for almost every sample was tested the results should not be considered very reliable when defining the properties achieved by the surface treatment. This is a starting point of the property characterization and is mainly used to be compared and analyzed with the properties obtained from the previous tomographies analysis.

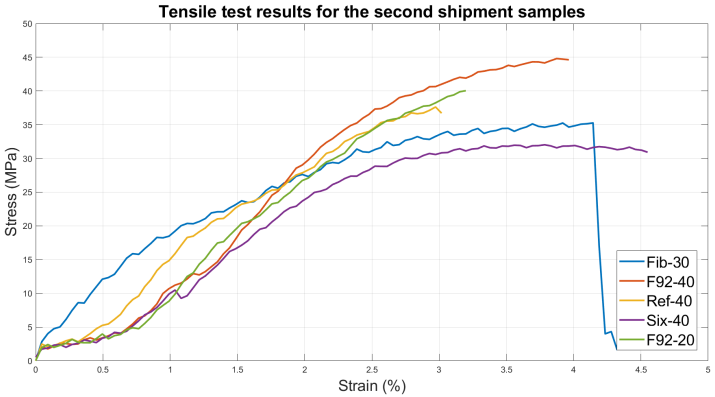

Figure 5.22 Strain Stress curve obtained for the second shipment samples

The first thing to notice in the curves is the big amount of strain developed for such a small stress. This deformation is caused by the loading machine stretching the sample when it was tilted after clamping the samples, as seen in Figure 3.5, meaning that although it is measured as deformation, this is not real deformation absorbed by the sample. It is because of this that the strain at fracture is not calculated for the properties analysis. In addition, the Young's Modulus is calculated as the tangent between [0.7, 2]% of strain for all samples except of Fib-30 which does not present the same curve shape. Similarly, for every sample except Fib-30, to calculate the yield of strength instead of starting the parallel line at 0.2%, it is started at 0.7% to be in accordance with the Young's Modulus calculation.

Furthermore, there seems to appear an oscillation in the curves from Figure 5.22, probably caused by some noise in the machine (it could also be found after the sample failed).

Every sample seems to present similar properties between each other, but by taking a deeper look into the curves and to Figure 5.23 to compare the properties extracted from the curves it can be seen how F92-40 presents the highest properties of every sample except for the toughness, for which Fib-30 has the highest value,

possibly because of the first region of the curve where the sample was not tilted before loading. Also, Fib-30 deforms a lot before failure, and in this deformation a lot of energy is absorbed by the material.

F92-20 has very similar properties to those of F92-40, but the lower amount of fibers in the first one leads to lower the maximum stress that it can hold, resulting in a very limited toughness compared to the second one and Fib-30. Six-40, although being the one with the highest strain of them all is the one that has the poorest properties out of the treated samples, mainly caused because of the limited stress it is able to handle.

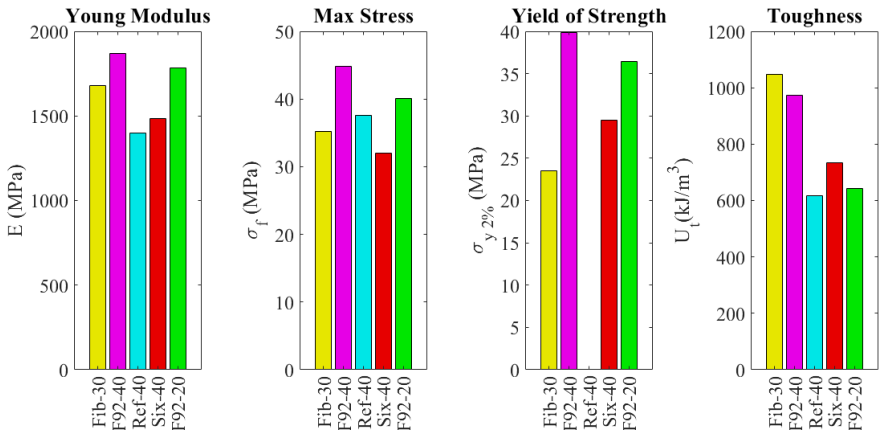

Figure 5.23 Properties obtained from the the second shipment samples Strain Stress curves (Ref-40 did not yield)

Six-40 properties are only higher over the reference fibers (Ref-40). The reference sample has a more or less similar behaviour to F92-20, maybe because the absence of a surface treatment limits the influence of fibers in the material (because of adhesion problems), and the small amount of fibers in the other one causes the same effect on the sample.

The results obtained from the tests are mainly proportional to the fiber ability to adhere to the matrix: F92-40 with the highest properties presents a clean fracture surface, in a similar way to Fib-30; Ref-30 has the poorest properties according to the tensile test performed, and the fiber/matrix interaction does not have a high influence on the fracture. F92-20 is the only sample that does not follow this statement, probably because, as said, the lack of fibers limits its influence in the material properties. By this, it can be proved that the mechanical properties of these samples can be mainly defined by the matrix/fiber interaction.

6

Conclusion

Biocomposites are interesting materials that present structures and properties with a big potential in industry as a substitute for rigid polymers. In this Master Thesis, the influence of wood fibers on the mechanical properties and fracture mechanisms of biocomposites was studied, as well as how the shape of the mould when using injection moulding can vary the different properties of the material.

For the samples tested and analyzed, it can be said that the fractures happened mainly due to fiber adhesion failure, and the sample properties achieved were directly related to how the fibers managed to attach to the matrix. In this way, the order of the performance developed by the surface treatments used on the samples tested from higher to lower is the following: F92, Fib, Six, and lastly Ref. Thus, every surface treatment applied by Biofiber Tech. to the fibers increased the mechanical performance of the material.

In a more general view of the results found in the Master Thesis, the mould shape and filling profile were seen to have a high influence on the void formation and fiber orientation. Fibers, as polymer chains, align with the flow direction, especially in the in the shear zone and the skin. By designing the shape of the mould correctly, fiber alignment could be achieved to withstand higher loads. On the other hand, it was proved that the main difficulty this material faces in terms of mechanical properties, is to achieve a matrix-fiber interaction capable to withstand high forces and be able to distribute the loads between the fibers correctly.

Because of the above conclusion, two main related factors should be taken into account when optimizing the properties of the material:

1. the fracture of the material usually occurs along the fibers oriented perpendicular to the load force, where the matrix interface fails more easily;

2. higher fiber aspect ratio seem to increase the mechanical performance of the material.

Due to the first factor, Combined with the previously mentioned fact that fibers and voids usually align with the flow direction of the material when manufacturing,

it is expected that the material will achieve lower fracture stresses when the load is applied in the transverse direction of the piece.

The reason higher fiber aspect ratios seem to increase the mechanical properties of the material was found to be that a high aspect ratio presents a higher surface to volume ratio on the fibers, increasing the surface availability for the fibers to adhere to the matrix in relation to the force that they will hold. This means that the load distribution that this interface has to handle is smaller. Consequently, aggregates should be avoided as they mainly are fibers with a very low aspect ratio. Furthermore, the remaining humidity on the cellulose can be evaporated in the manufacturing process, leading to micro-voids in its surface, as it was seen in the premortem tomographies from the first shipment samples.

6.1 Future work

As usually happens with research work, some questions are answered, but many more are asked. To continue with the work started in this Master Thesis, it is considered that the DIC data collected during the tensile test should be analyzed to observe how deformation develops along the sample and, with the help of the imaging obtained in the premortem and postmortem tomographies, see if there are any microstructure defects or components that act as main stress concentrators. DIC could be useful not only to see how the stress is distributed along the sample but also to focus the work on the tomographies on the microstructure where this stress is focused, speeding up the process of the understanding of the fracture mechanisms in this composite material. Furthermore, not only the parts where the stress concentrates the most would be of interest, but also those which present the least deformation could be examples of how the mechanical properties of the material could be increased.

To keep on with the work being developed in this Master Thesis, the tomographies performed in the second shipment could be still used to achieve quantitative data about each phase as done in to the first shipment samples. These data compared between the premortem and postmortem samples could be of high interest, as it could be seen if fibers, aggregates or porous change their orientation with the deformation. A hypothesis could be that the fibers and aggregates do not present considerable deformation, but they orient parallel to the load, as opposed to what could happen to the porosity, where new pores would appear in a perpendicular direction to the applied force.

One of the most crucial parts in the to-do list for future work is to repeat the analysis on at least three samples of each kind to ensure that the results obtained in this analysis for each fiber kind are in accordance to the trend. Three samples as the ISO recommends for the tensile test properties characterization.

Complementary to this Master Thesis, there are still a lot of things that can be performed to understand better the properties of the material. To investigate in a

deeper way the nature of the sample failure (matrix, fiber or interaction fracture), it has been thought to perform an image analysis, similar to DIC, where the fracture surface of the bottom part is aligned to the top part of it. With this alignment and a correct phase segmentation, depending if in the phases found in the top and bottom part of the segmentation the fracture nature could be calculated quantitatively.

Further investigation could be done on the sample to fully understand the fracture mechanisms. For example, different tomographies taken of the sample in-situ during tensile testing could help to see with time how the fracture is formed, or to use different destructive testing such as impact tests could unravel other fracture mechanisms. Moreover, other analysis could be performed to investigate the influence on the fiber and porosity orientation when modifying parameters in the manufacturing injection moulding such as flow speed or injection pressure.

Other imaging methods could be useful to use to segment and characterize the phase distribution and orientation, such as WAXS and SAXS. Neutron imaging could be of special interest in this material, such as the fibers used are made of wood that (although being dried) presents some water content that would present a high contrast in the imaging, making the segmentation of the fibers easier and more accurate. With this method, it could even be possible to estimate the length and aspect ratio of the fibers.

Bibliography

[1] E. Andreasson, L. Persson, H. Jacobsson, and J. Nordgren. “Integrating moldflow and abaqus in the package simulation workflow”. In: 2013.

[2] E. an Anvia division. *Microcrystalline cellulose (mcc)*. URL: https://www.excipia.eu/microcrystalline-cellulose/. (Access date: 17.06.2021).

[3] W. arkitekter. *Wood, nature smartest material*. URL: https://whitearkitekter.com/news/wood-natures-smartest-building-material/. (Access date: 15.05.2021).

[4] A. Atia. *Investigation of the Mechanical and Tribological Properties of Polypropylene Matrix Composites Produced by Injection Method*. PhD thesis. 2014. DOI: 10.13140/RG.2.1.5087.1204.

[5] Biofiber. *Fibra-q innovation*. URL: https://www.fibra-q.com/our-innovation. (Access date: 17.06.2021).

[6] U. building construction. *Wood / timber / lumber as a construction material*. URL: http://www.understandconstruction.com/wood.html. (Access date: 17.06.2021).

[7] V. A. Dahl. “Structure tensor: computation, visualization, and application” (2009). URL: http://people.compute.dtu.dk/vand/notes/ST_intro.pdf.

[8] P. designs. *Introduction to injection moulding*. URL: https://predictabledesigns.com/introduction-to-injection-molding/. (Access date: 17.06.2021).

[9] M. Fouda. *Active Control of Vibrating Structures Using Damping Effect of Shape Memory Alloy Wires*. PhD thesis. 2013. DOI: 10.13140/RG.2.2.35701.68321.

[10] Greenpeace. *Datos sobre la producción de plásticos*. URL: https://es.greenpeace.org/es/trabajamos-en/consumismo/plasticos/datos-sobre-la-produccion-de-plasticos/. (Access date: 15.05.2021).

[11] D. Hans. *Kunststoffe : Eigenschaften und Anwendungen*. Springer Berlin, 2011. ISBN: 9783642161728.

[12] K. Klein, P. Sauerbier, T. Koddenberg, and A. Krause. "Utilization of recycled material sources for wood-polypropylene composites: effect on internal composite structure, particle characteristics and physico-mechanical properties". *Fibers* **6** (2018), p. 86. DOI: 10.3390/fib6040086.

[13] E. Lage, J. J. Vaquero, S. Redondo, M. Abella, G. Gil, A. Udias, and M. Desco. "Design an development of a high performance micro-ct system for small animal imaging". In: 2006, pp. 3549–3552. DOI: 10.1109/NSSMIC.2006.353765.

[14] V. Landry and P. Blanchet. "Surface preparation of wood for application of waterborne coatings". *Forest Products Journal* **62** (2012), pp. 39–45. DOI: 10.13073/FPJ-D-10-00011.1.

[15] C. Moore. "Plastic pollution". *Encyclopedia Britannica* (2020). URL: https://www.britannica.com/science/plastic-pollution.

[16] Plasticseurope. *El plástico: una historia de más de 100 años de innovación*. URL: https://www.plasticseurope.org/es/about-plastics/what-are-plastics/history. (Access date: 15.05.2021).

[17] C. Rus. "Tras las pajitas de papel llega la botella de papel: coca-cola pondrá a prueba su botella biodegradable este mismo 2021". *Xataka* (2021). URL: https://www.xataka.com/ecologia-y-naturaleza/pajitas-papel-llega-botella-papel-coca-cola-pondra-a-prueba-su-botella-biodegradable-este-2021.

[18] S. R. S. Serope Kalpakjian. *Manufacturing engineering and technology*. Singapore : Pearson Education South Asia, 2016. ISBN: 9780133128741.

[19] N. Stevulova and V. Hospodarova. "Cellulose fibres used in building materials". In: 2015, p. 211. DOI: 10.7250/rehvaconf.2015.031.

[20] Uc3m. "Ciencia en ingeniería de materiales course. Polymers i and ii". 2016.

[21] ucbtae2. "The plastic island: what is it and what can we do?" *The Quagga* (2018). URL: https://mresbec.wordpress.com/2018/11/23/the-plastic-island-what-is-it-and-what-can-we-do/.

[22] L. University. "Modern experimental mechanics course. X-ray tomography in experimental mechanics". 2021.

[23] K. Wałęsa, I. Malujda, and K. Talaśka. "Krzysztof wałęsa * ireneusz malujda* krzysztof talaśka* hot plate butt welding of thermoplastic drive belts" (2018). DOI: 10.21008/j.2449-920X.2018.70.2.06.

[24] A. Wattanakornsiri, K. Pachana, S. Kaewpirom, P. Sawangwong, and C. Migliaresi. "Green composites of thermoplastic corn starch and recycled paper cellulose fibers". *Songklanakarin Journal of Science and Technology* **33** (2011), pp. 461–467.

A

Mechanical testing results from first shipment's samples

Biofiber Master Thesis

Tensile test developed at Biofiber Tech

In this report it will be shown the tensile test experiments developed by Biofiber Tech to their dog bone samples. This is just a summary report of the data that have been facilitated from the company to us, where the results will be explained and discussed

1 Introduction

Biofiber Tech is a start-up from Stockholm (Sweden) who has developed a new composite material composed of wood fibers and a polymeric matrix that reduce the dependence on fossil fuels to produce a thermoplastic polymer.

In order to understand the material behaviour it was done a series of different tensile test to the samples by following the ISO 527-1:2019. This results were sent in form of **.txt* files, with some information about the samples. This information have been tried to be summarized in this report with some discussion on it.

2 Samples

Different samples sets, composed of 5 different dog bones samples each, where tested. All of the samples are made from the RISE Mölndal compound, defined by Biofiber Tech. The material was processed at 180°C, And the injector had a: screw diameter of 25mm and a configuration of twin screws that co-rotates. All compounds are composed of 40%wt of fibers and 60%wt PP.

The name indicates the material the sample is made of and the parameters used for manufacturing. An example for the identification name of a sample would be:

120 D Fiber 8kg_h

The first name defines the type of wood that was used.

- **119:** It is the reference fibers, without any chemical treatment.
- **120, 121 and 123:** Different chemical treatments. Single compounding.
- **125:** Another chemical treatment was applied. Double compounded sample.

- **A14:** As 119, It is a reference fiber of another wood.
- **C18:** Fiber A14 with an applied chemical treatment.

Fibers 119, 120, 121, 123 and 125 are of the same batch, hence they are comparable between each other (This will be called Type 1). The same happens between A14 and C18 which will be called Type 2.

The third word indicates whether it comes from a Fiber or from Pellets. This tells how the material was formed in the compounder, either if the wood was introduced into the hopper in form of fibers or in pellets. The last number, indicates the mass flow rate used during the extrusion.

The double compounded sample refers to the fact that the material went through the compounder (machine where the fibers and matrix are combined) twice. This is brings the hypothesis that the fibers will be more mixed than the others. For this set of samples, the material was extruded first at 8 kg/h and then ant 10 kg/h.

More parameters about the injection molding can be found in Table 1, where the reference to name of the files of the samples can be found on Annex I

Sample Wood	**C18 F**	**C18 P**	**A14**	**119**	**120**	**121**	**123**	**125**
Melt T, °C	190	190	190	190	190	190	190	190
Mold T, °C	40	40	40	40	40	40	40	40
Injection p, bar	90	85	100	120	110	120	110	95
Holding p, bar	90	85	100	120	110	120	110	95
Holding time, s	25	25	25	25	25	25	25	25

Table 1: Injection parameters of the samples

3 Data analysis

As said, every material was composed of 5 different samples to analyze and compare every set of samples, the stress strain curve was plotted to see if any of the samples stood out from the rest. For those which did not stand out, the mean for a given stress was made.

As not the same stress was recorded for every sample, to obtain the mean curve, a linear interpolation for each curve was made extracting the values of the strain for different stresses. This was done from the initial point to the mean fracture point, only taking into account the values that were only interpolated (i.e. not extrapolated values were taking into consideration).

By doing this mean some discontinuities are found due to stop considering a curve when this fractures. However, this curve is wanted just to have an idea of how the sample behaves, and this discontinuities are not of big importance if it is known that those regions are not trustworthy. An example for this can be found in Figure 1, where the first sample tested was not taken into account.

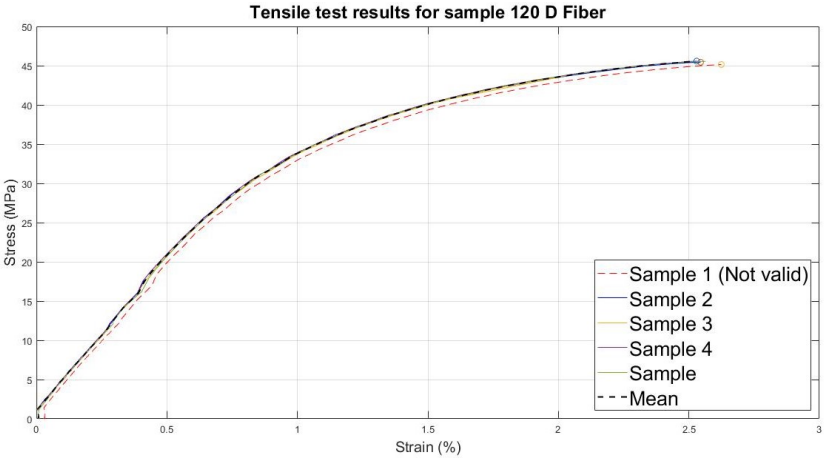

Figure 1: Calculation of the Stress-Strain mean curve of material 120D Fiber

As no difference necking can be found in the curve, it is hard to determine the Young's Modulus in the material. To do it it was used the method established in section 10.3.3. from the ISO 527-1:2012, where the Young's Modulus is calculated as the slope of the least-squares regression up to a strain of 0.25%.

Also to determine the Yield of Strength it was used the method where the Yield happens where the strain-stress curve crosses a line whose slope equals to the Young's Modulus, and it crosses the x-axis at 0.2% of strain. This value is used as an indicator of how quick the slope decreases, or how quick the creep begins.

Finally the toughness of the sample was calculated as the amount of energy that can be absorbed by a unit of volume before its fracture. To do it it was made the trapezoidal integral of the line.

4 Results

The processing explained in Section 3 was applied to all of the samples. By plotting all the results in just one plot (Figure 2) it can be seen how every sample has an

strain hardening behaviour along the whole deformation, and does not present the characteristic "necking" that many polymers have.

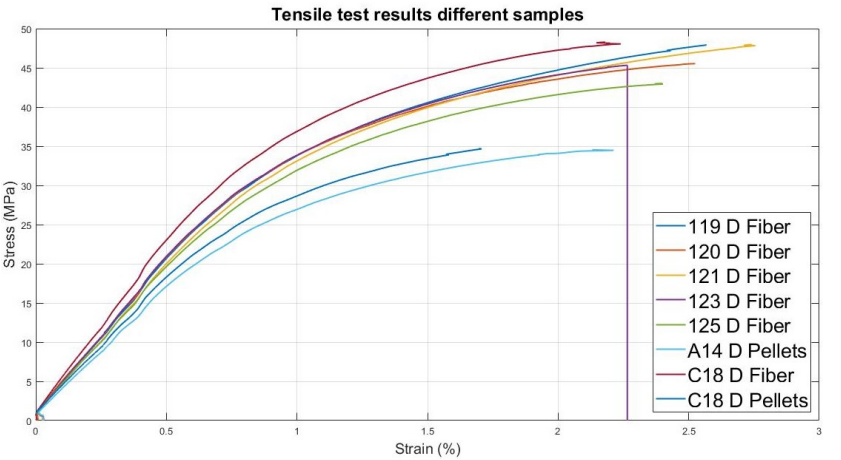

Figure 2: Tensile Test Results for all the different kind of samples

Due to the shape of the curves, the strain at the breaking point coincides with the Ultimate Tensile Strength (UTS).

To compare the samples a histogram of the main properties was made. As said before samples containing fibers 119, 120, 121, 123 and 125 are comparable between each other, and fibers A14 and C18 have to be compared apart.

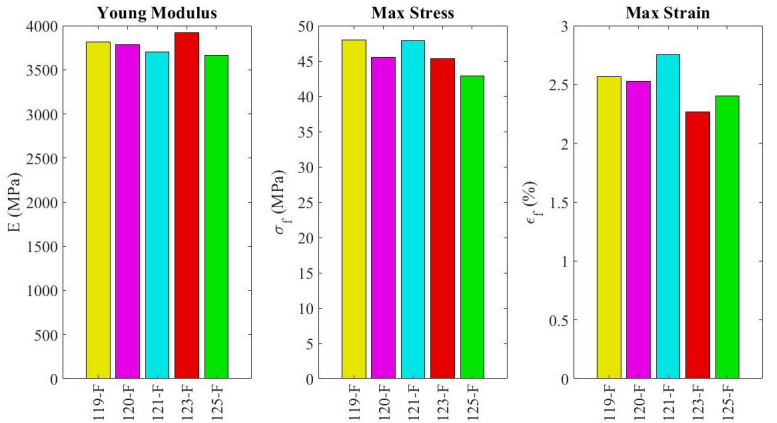

Figure 3: Young Modulus, UTS and Strain at fracture from the first set of fibers

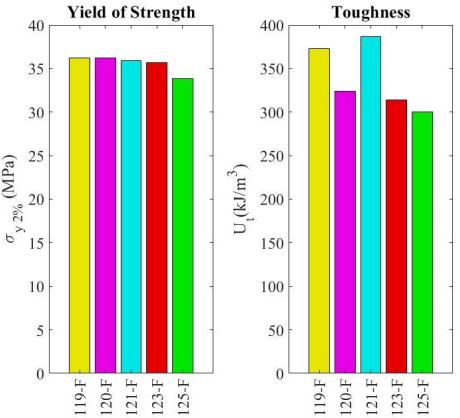

Figure 4: Yield of Strength and Toughness at fracture from the first set of fibers

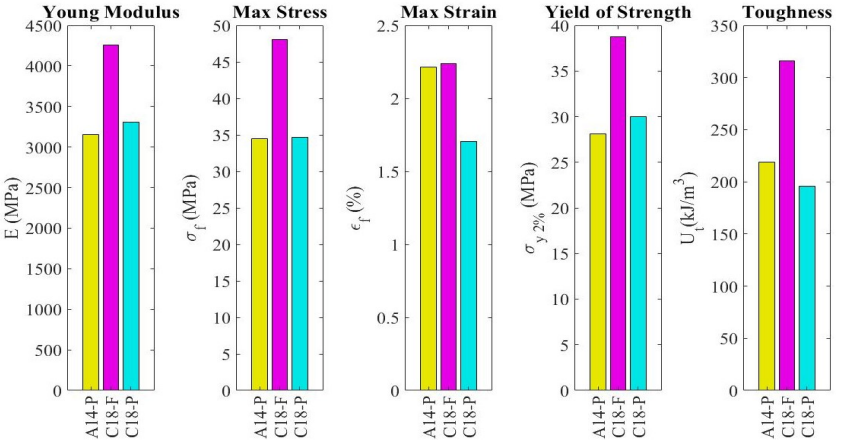

Figure 5: Young Modulus, UTS, Strain at fracture , Yield of Strength and Toughness at fracture from the second set of fibers

5 Discussion

To compare the results, it is important to take into account the properties found for the reference fibers *119-F and C14-P*. This samples presented very different results, which can be translated into the fact that samples coming from different

kind of fibers are difficult to be compared, although C18-F presented properties more similar to the Type 1, even though it is made out of the Type 2 fibers.

Taking a look at Figure 2, the properties from all the samples whose fibers where directly pressed into the compounder, seem to be higher than those where the wood was introduced in form of Pellets. This difference can be confirmed by analyzing the Type 2 fibers in Figure 5.

5.1 Fibers of Type 1

For the first set of samples, it was found that the Young's Modulus is very similar to one another, and these differences could be caused because the error of the data collected.

It seems that Sample 125-F has a tendency to be weaker than the rest of them, something that could be explained either because of the double compounding injection, or because of the chemical treatment that was implemented.

On the other hand, sample 121-F seems to have high tensile properties, being the one with the highest toughness of them all, explained by a high fracture strain and a similar UTS as the rest sample.

The sample whose fibers were not made any treatment, presents the highest properties after 121-F: highest Yield of Strength, Highest fracture stress and second highest fracture strain and toughness. A fact that could be kind of controversial, as initially a chemical treatment could seem likable for the fibers, but this treatment could be to aggressive and weak them.

In the end samples 119-F and 120-F had similar results until just before the fracture, and sample 121-F had similar properties than 119-F but lasted longer which lead to an increase of all the properties that take into account the plastic region of the curve (Toughness, Maximum Stress and Maximum Strain).

5.2 Fibers of Type 2

By looking at Figure 5, it is evident an outstanding difference by the sample C18-F, the only sample that whose compounding was made by directly introducing the fibers into the compounder (which can be the explanation for this to happen).

Again comparing the reference sample with the one which was subjected to a chemical treatment, the first one behaves similarly but with a higher strain at fracture. So chemical treatment applied to C18 seems to increase the hardness of the material, but with the result of reducing the fracture strain (It could be said

that it becomes more brittle). This result in an small decrease of the toughness but not critical.

6 Conclusions

Between all the samples that were analyzed there was found a main difference between those whose wood particles were implemented in the composite in form of fibers, and those who where introduced in pellets. The first ones achieved higher Young's Modulus, Yield of strength, Stress and Strain at fracture and Toughness, being this difference bigger than the one estimated in the beginning were it was said that the two different type of fibers should not be compared between each other.

Between the samples of fiber Type 1, the sample with the wood fiber that was subjected to no chemical treatment reached the highest parameters just after the sample 121-F which achieved the highest Stress and strain at fracture and toughness.

On the other hand, the sample that was manufactured with double injection (125-F) presented the smallest toughness, yield of strength, UTS and Young's Modulus with difference with the rest.

Analyzing the fracture mechanisms of the samples to understand the behaviour of the strain and force distribution would be useful to know the reasons the sample failed and find possible improvements to focus on.

7 Annex I

Here can be found the sames used for the different samples in the document, with the respective name of the file used:

- **119-F:** *119 D Fiber.txt*
- **120-F:** *120 D Fiber 8kg_h.txt*
- **121-F:** *121 D Fiber 8kg_h.txt*
- **123-F:** *123 D Fiber 8kg_h.txt*
- **125-F:** *125 D Fiber 2 komp.txt*
- **A14-P:** *A14 D Pellets 10kg_h.txt*
- **C18-F:** *C18 D Fiber 10kg_h.txt*
- **C18-P:** *C18 D Pellets 30kg_h.txt*

B

Phase Segmentation analysis of the first shipment samples

In the following document, it can be found the process followed to get to the final result of each phase segmentation step by step in the following order:

1. **Color histogram:** to prove the comparability between the different tomographies.
2. **Porosity segmentation**
3. **Aggregates segmentation**
4. **Fiber segmentation**

Color Histograms

There are two sets of tomographies that were made, ones with a lower resolution (11um) and others with a higher one (4um). To be able to analyze the samples properly, the same image analysis is going to be held to each one of them. With this analysis, the results will be comparable between each other.

To check that all the filtering analysis will be affect in a similar way to all the samples, there are different indicators that will do so, and one of them is to check that all the colors are distributed evenly. This would mean that (as we are looking to a set of samples that from the start are similar) every phase is represented in the same way for all tomographies.

Histogram of the tomographies with lower resolution

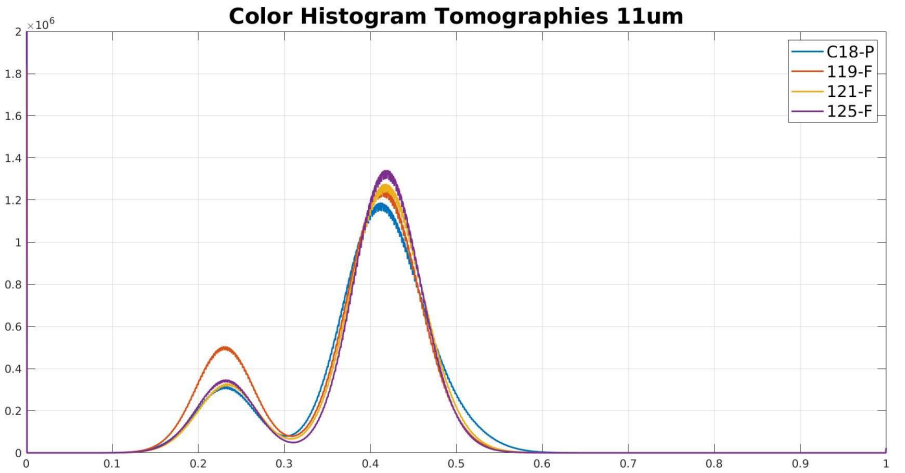

Histogram of the tomographies with lower resolution

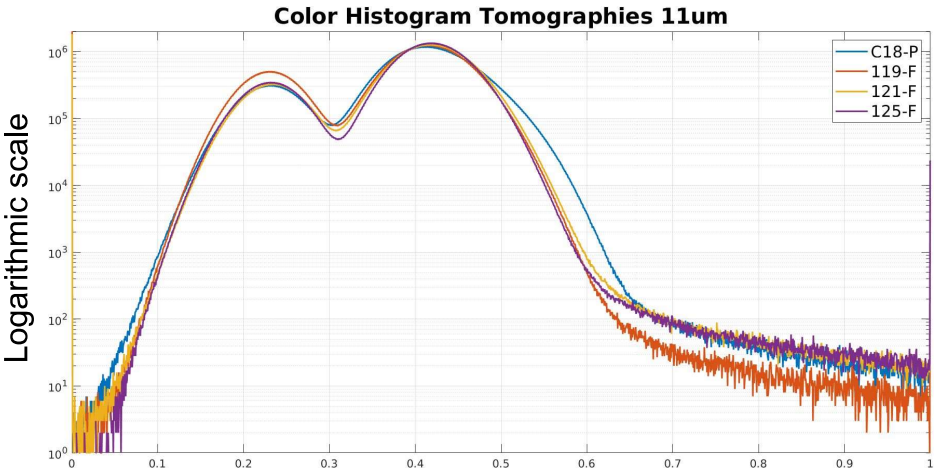

Histogram of the tomographies with higher resolution

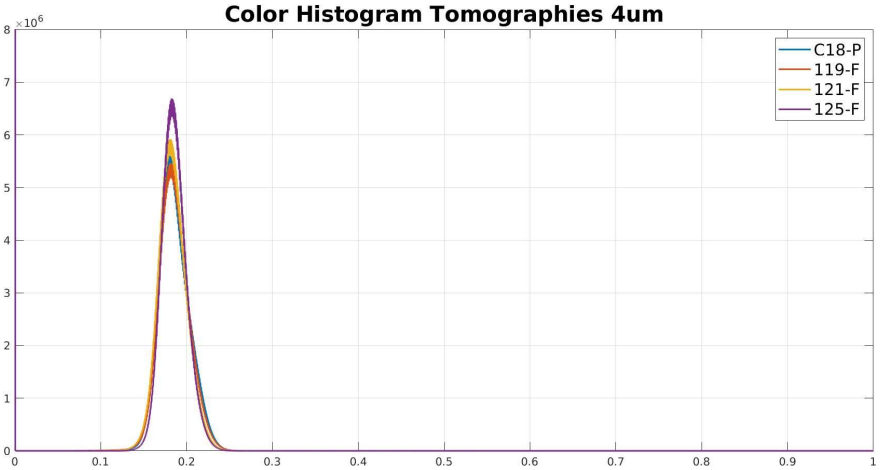

Histogram of the tomographies with higher resolution

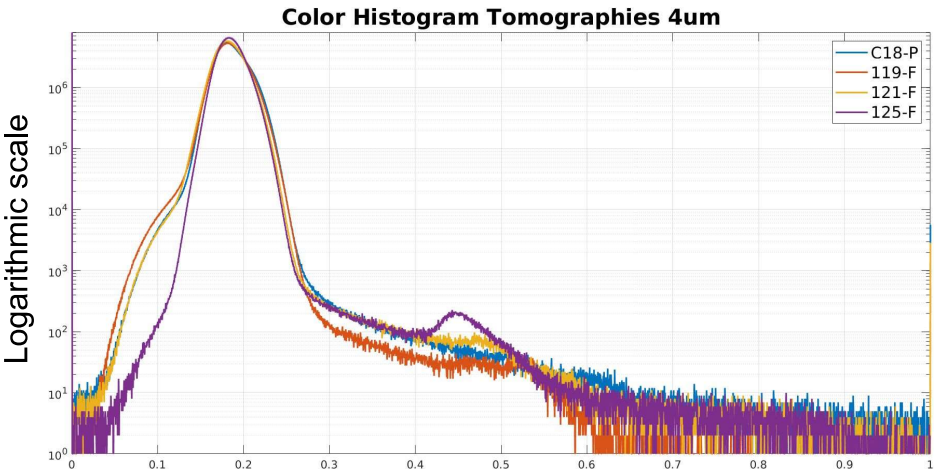

Adjusting contrast

High resolution tomography was made with a lower acquisition time. This meant that the contrast for the images found was much smaller than for the low resolution images. To solve this, a function where the contrast of the image is adjusted is used.

The following histograms show the color distribution of these contrast adjusted images (applied to the High and Medium Resolution tomographies). The function used to adjust the contrast was “imadjustn”

C18-P silice **without** contrast adjustment

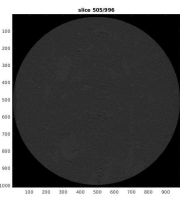

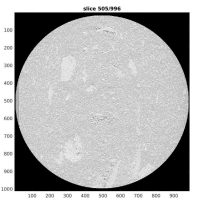

C18-P silice **with** contrast adjustment

Histogram of the tomographies with lower resolution

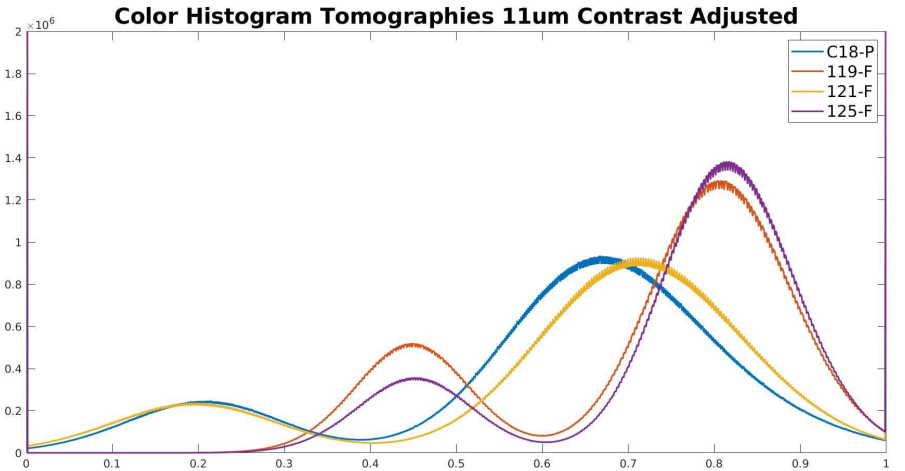

Histogram of the tomographies with lower resolution

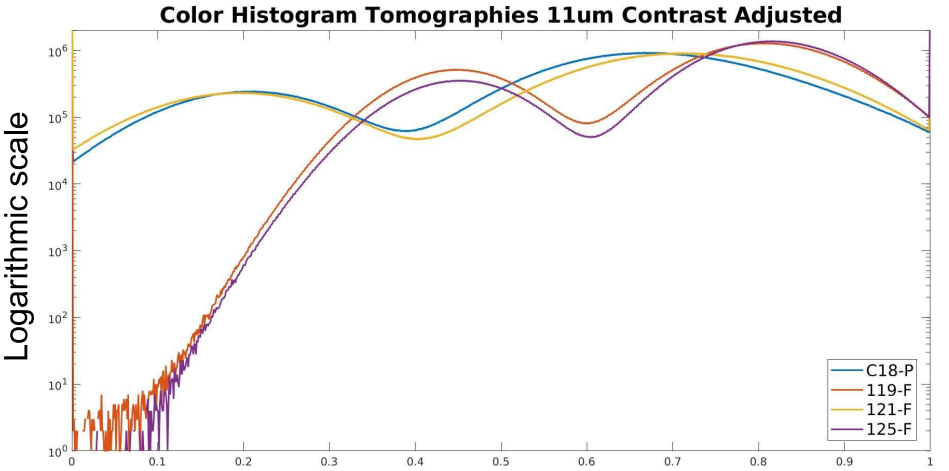

Histogram of the tomographies with lower resolution

The explanation of the redistribution of the peaks is thought to be the different values for the background outside the sample, so this was removed from the sample to see how it would influence it. This is the result of the cutted, contrast adjusted samples

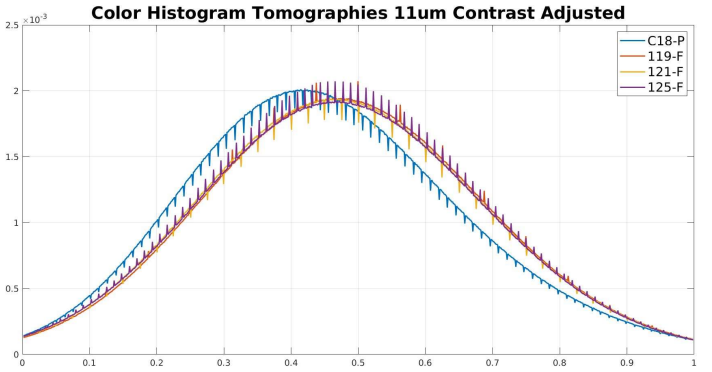

Histogram of the tomographies with lower resolution

The explanation of the redistribution of the peaks is thought to be the different values for the background outside the sample, so this was removed from the sample to see how it would influence it. This is the result of the cutted, contrast adjusted samples

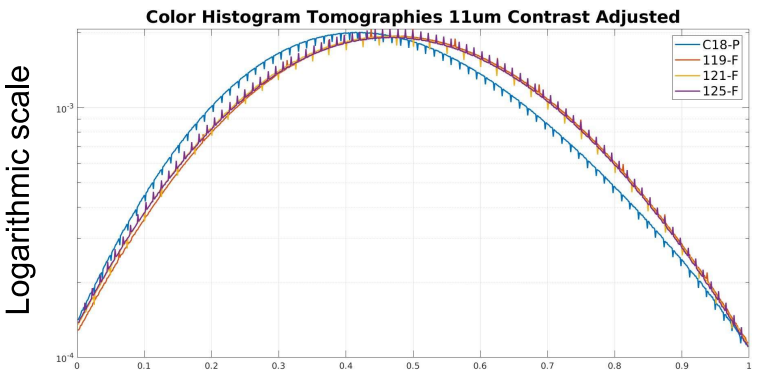

Histogram of the tomographies with higher resolution

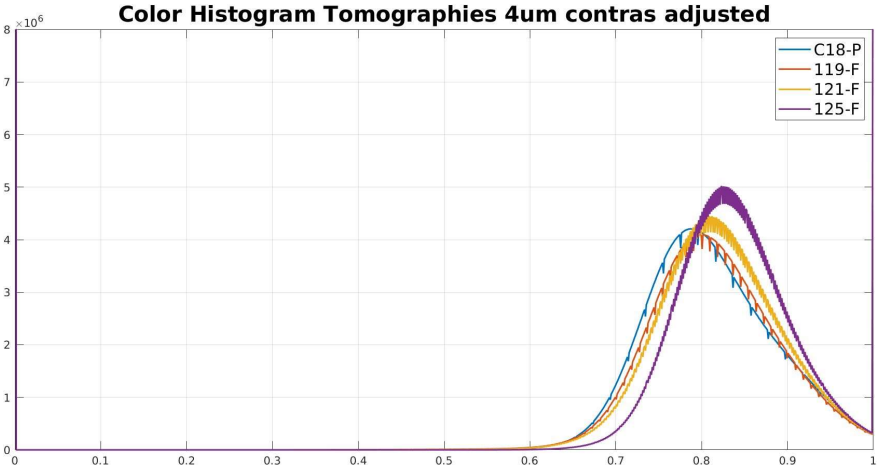

Histogram of the tomographies with higher resolution

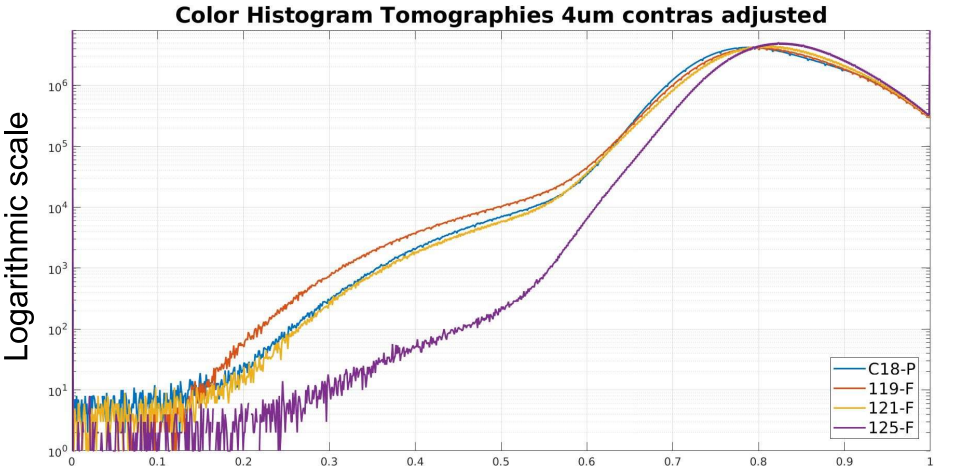

Void Filtering

To analyze the porosity found in each sample, it is going to be applied the same kind of filters to each one of them, so then they can be compared between each other.

The samples that are going to be analyzed are the medium resolution tomographies for the samples (11um). This tomographies will go first to through a contrast adjustment filter.

As it was mentioned in the document “Color Histograms” for the tomographies with this resolution, the distribution of colors is not the same. For this reason, when filtering and binarizing the images, it cannot be taken the same value for each one of them. In contrast, different methods will be tried.

Original slices

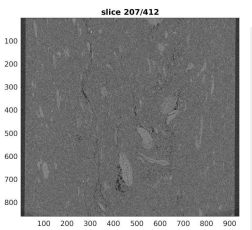

C18-P

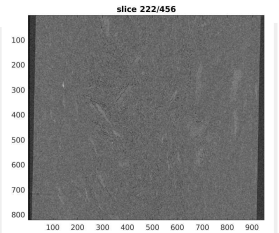

119-F

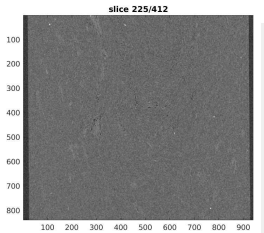

121-F

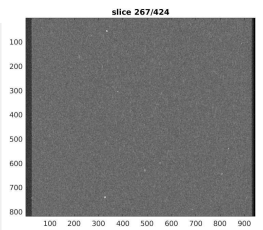

125-F

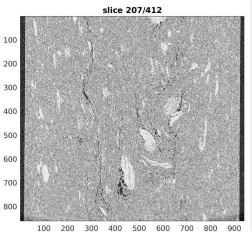

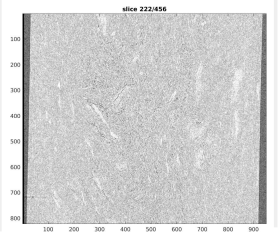

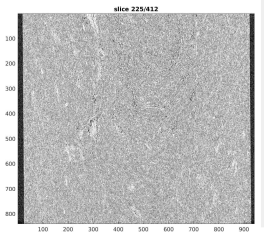

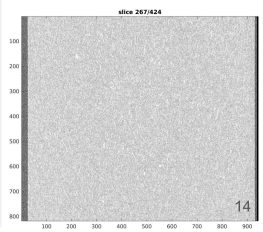

Binarize Image (segmentation)

As the voids in the image are very small, it has to be careful on which filters it is applied. If a smoothing filter is applied, there is a high risk where the voids may disappear, so the main operations that are going to be applied are binarizing eroding and dilating the image.

The problem is that as explained before, the color histogram of the tomographies when the contrast is adjusted do not coincide, so the same color may not mean same phase in the sample.

To avoid this two different approaches were made:

1. Applying the same threshold to every image without applying the contrast adjustment (Threshold = 0.32), or cutting the image before segregating.
2. ~~Obtaining the threshold value from an adimensional parameter from the color histogram.~~ (this was not used in the end, as removing the background worked good enough)

Segmentation 1.1:

- 1st row: Threshold value 0.32
- 2nd row: Grains bigger than 15 voxels

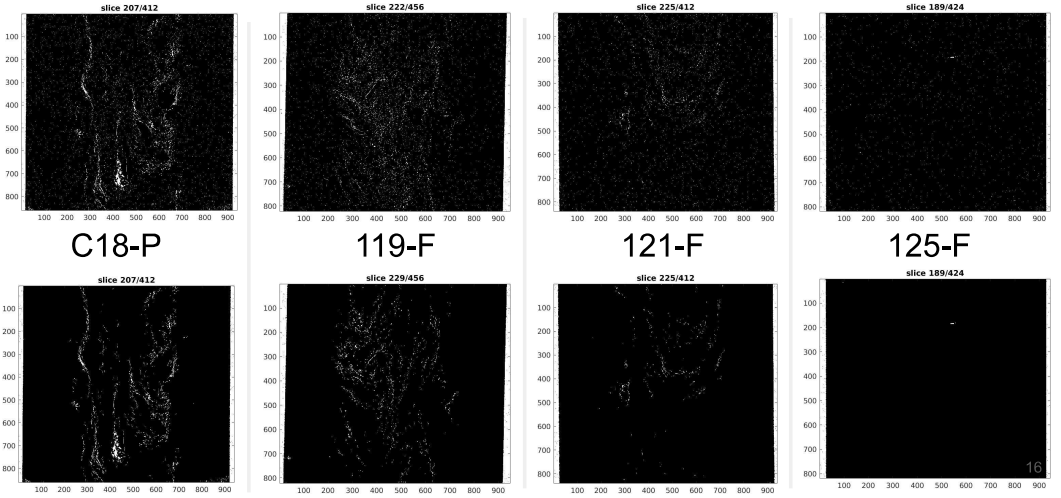

Segmentation 1.1: Background removed

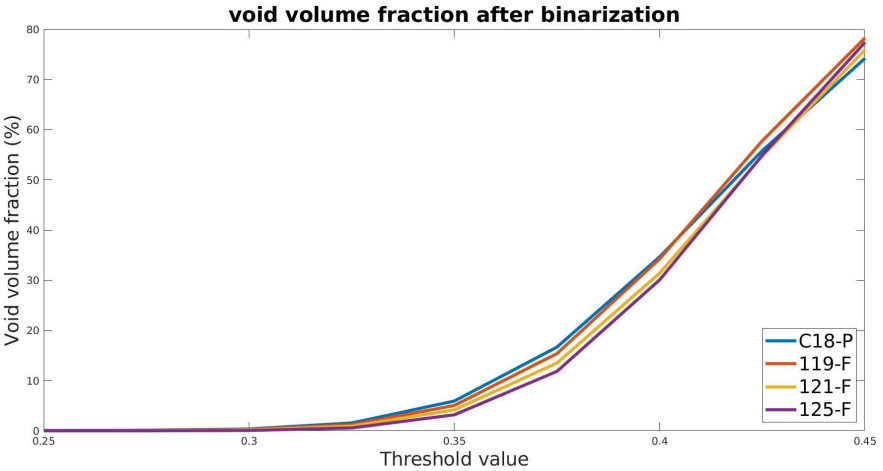

17

Segmentation 1.2: High resolution , background removed, contrast adjusted tomographies.

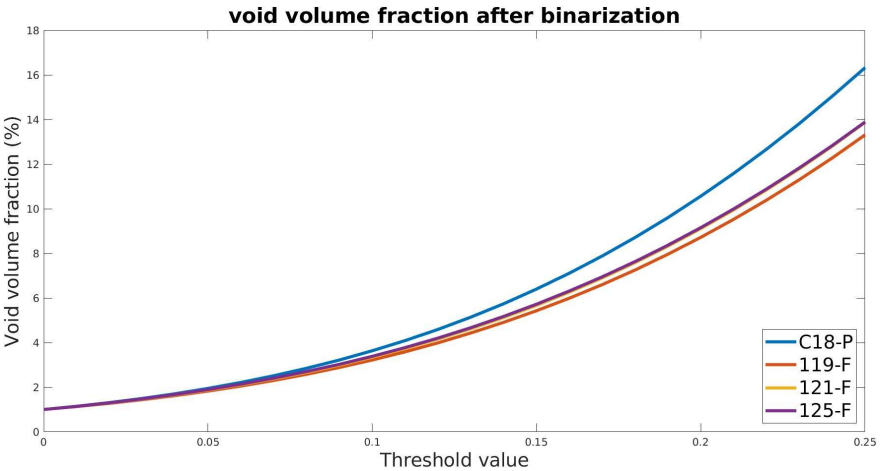

18

Segmentation 1:

- 1st row: 1.1: Threshold value 0.35 MH-Tom(Filtered out grains under 15 voxels)
- 2nd row: 1.2: Threshold value 0.05 HD-tom (Filtered out grains under 15 voxels)

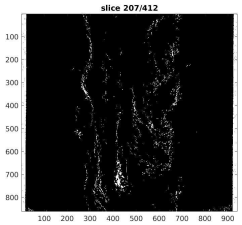

C18-P

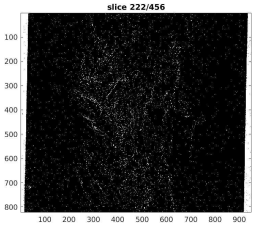

119-F

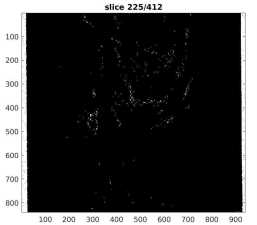

121-F

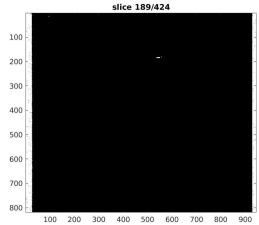

125-F

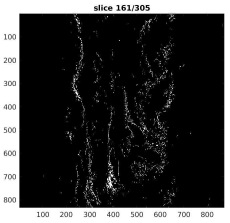

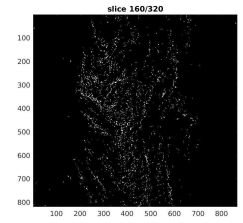

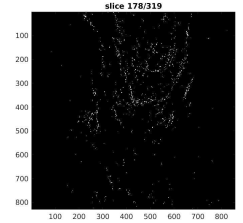

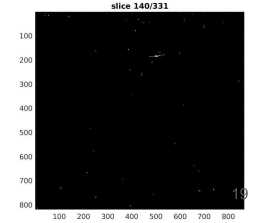

19

Binarized Image (segmentation 2)

To binarize the image it has been chosen, after analyzing the results previously shown, to use a mask segmentation for the tomographies without any contrast adjustment, whose borders have been cutted out of the image.

The filter will be made at the value of 0.33, value which seem to show a good fit for every sample, high enough so voids are seen in every sample (not only the ones that present big voids), and low enough so the matrix does not start to be included in the segmentation.

In order to get rid of the noise of the image, voids of a volume lower than x voxels^3 will be neglected out of the main analysis. This value will be 8 or 27 (to be consistent with cubic voids of side 2 or 3.

Segmentation 2: %V(void) in terms of the minimum size considered for the analysis.

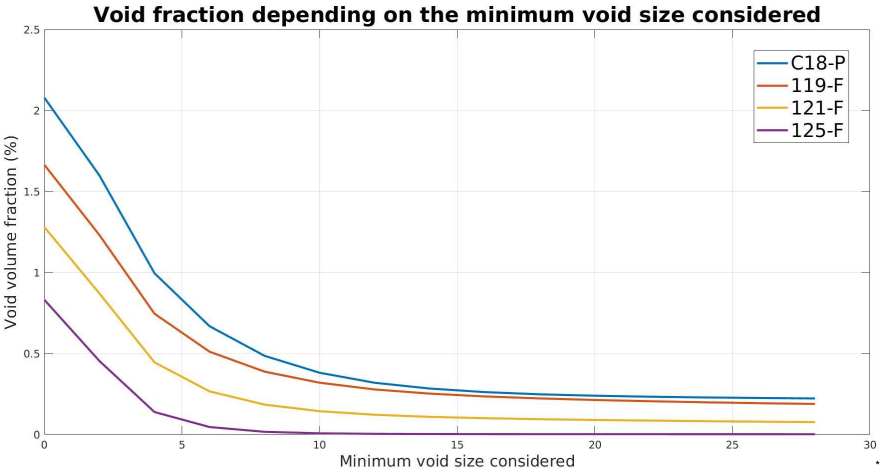

Min Void Size	Rel Void Frac*
0	100
4	36
8	15.8
14	9.4
20	7.9
27	7.14

* Mean of the relative Void volume fraction (%)

Segmentation 2: %V(void) reduction when small voids are neglected

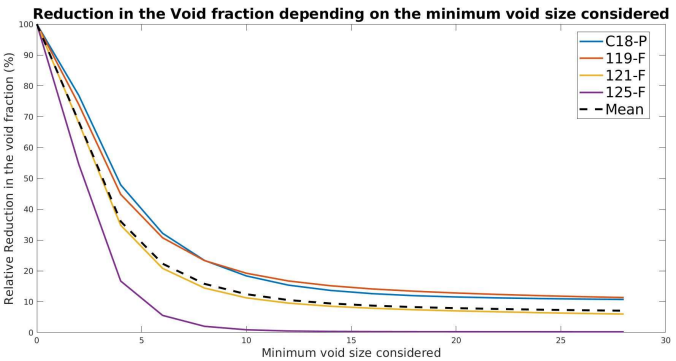

It can be seen that the reduction in voids is much faster in the sample 125-F than the rest of the samples. This is an indicator that when filtering we are actually removing some porus that we are considering as noise, as if it was noise, it would reduce in a similar way for all the samples as it happens with 119-F and C18-P. This does not mean that for this two samples we are just removing some noise, but it means that for 125-F we are actually removing something that definitely is not noise, and although this is not going to be solved, is something that should be taken into account.

Segmentation 2:

- 1st row: Filtered out grains under 4 voxels
- 2nd row: Filtered out grains under 8 voxels

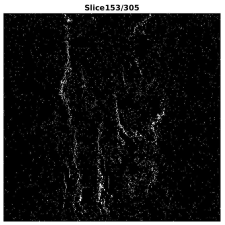

C18-P

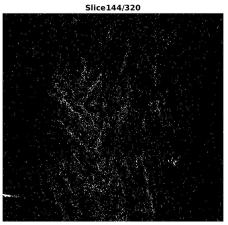

119-F

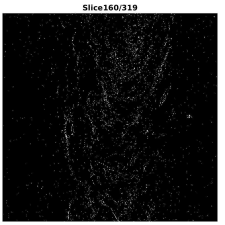

121-F

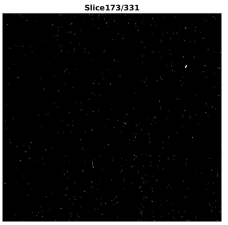

125-F

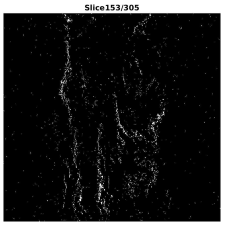

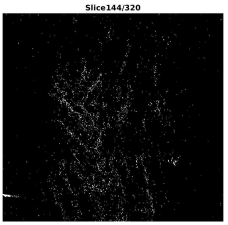

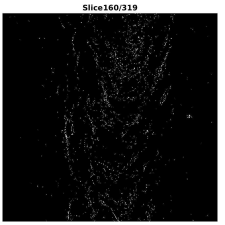

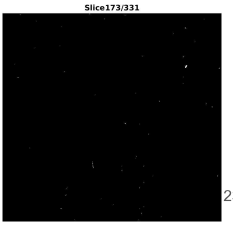

Dilate - Eroding filtering (D - E 1)

From the previous analysis done it has been decided to focus the analysis on the voids that are bigger than 8 voxels. 4 voxels could also be chosen, but as in this filtering the void fraction will increase, this can suppose a balance.

The following analysis will be to unite voids that from a first view are separated, but we would like to consider as one, because of its size and proximity with each other. This filter leaves intact the voxels that are isolated (i.e. if there is a void of 5 voxels that has nothing in its surroundings, at the end of the filter it will be of the same size), but unites groups that might be close to each other.

This analysis basically will consist on a continuous set of filters of dilating the image and then eroding it with different sphere radius. By doing this those grains that are of a considerable size and are next to each other will be united, and although the number of voxels considered as voids will increase, this will suppose a “redemption” to the pores that were eliminated in the previous filtering.

D-E 1:

In this plot it is represented both the void fraction and the number of voids development when it is applied a D-E filter on the sample for the C18-P sample

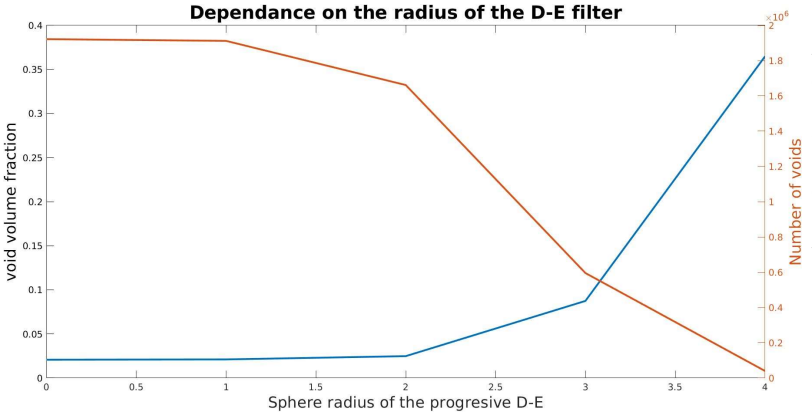

It can be seen how when the radius of the dilating sphere is increased to 3 the void volume fraction increases a lot, just the opposite as the number of voids, which decreases drastically as a consequence of the connection between big porus.

D-E 1:

This is the same plot as in the previous slide but for all the samples. The dotted line is referenced to the number of voids (left axes), while the other represents %V

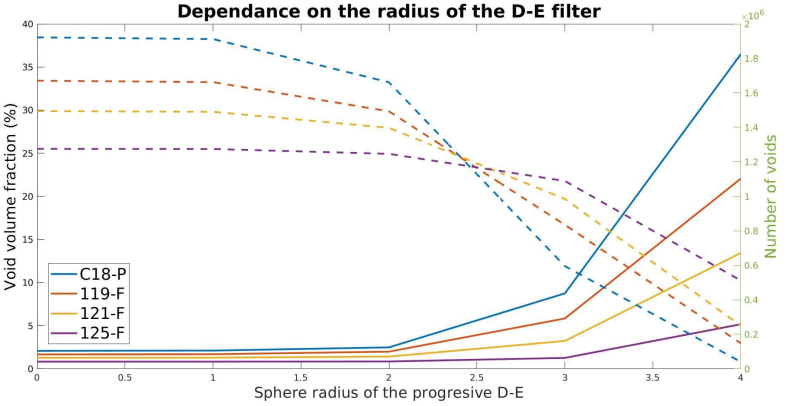

When the radius used is of 2 voxels, the fraction does not increase as much, but the number of voids decreases a noticeable amount. Because of this the analysis will be focused on a D-E filter of radius between 2 and 3 voxels

Segmentation 2:

- 1st row: Original picture with a segmentation at 0.33
- 2nd row: D-E picture with a sphere radius of 2 voxels

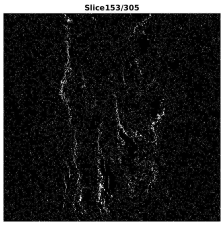

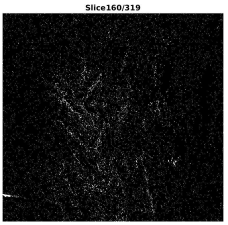

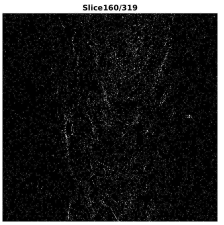

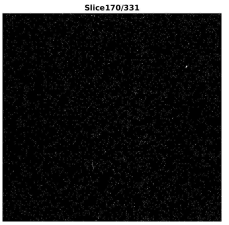

C18-P | 119-F | 121-F | 125-F

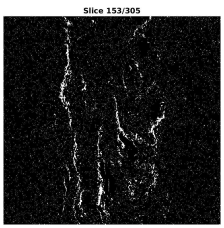

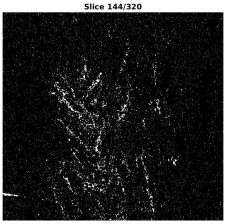

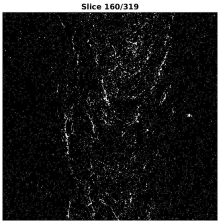

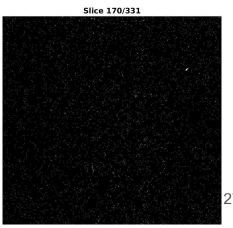

Minimum void size after D-E filter:

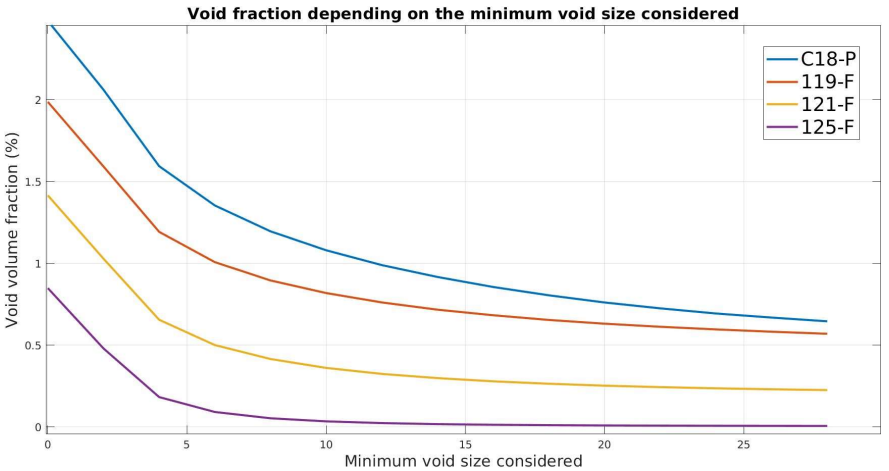

Final results:

After some analysis to the image it has been decided that the image will be first cutted to get rid of the surroundings, then the segmentation will be done with a threshold value of 0.33.

Also to get rid of the noise, it will be considered voids only those that represent a set bigger than a number (either 4 or 8 voxels^3). Apart from that, a progresive dilating eroding analisis will be held with an sphere shape of radius 2 at its maximum.

The question to analyze know, is whether the size filter is applied before or after the D-E filter. If it is done before we avoid noise dots to grow bigger and risk ourselves to afterwards consider them as real voids. However, if we do it after, then we are able to unite better the bigger voids between each other by taking advantage of these small voids between them (which make sense for them to happen).

Final results:

Here it is plotted the different volume fractions found depending on the order the filters are applied on the samples

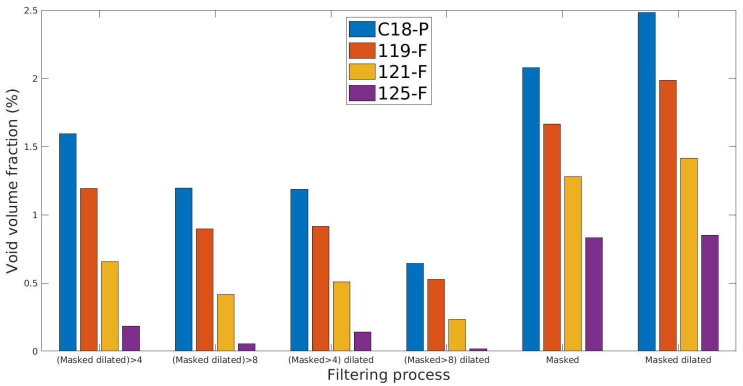

It has been decided for the final analysis to first grow and connect the porous by subjecting them to a dilating-eroding filter of radius 2, and then eliminate the “not anymore considered voids” smaller than 8 voxels. By using this value instead of 4, those false grains that were together and have grown to a bigger one are discarded here.

Final results:

- 1st row: Original picture
- 2nd row: Resultant picture for analysis

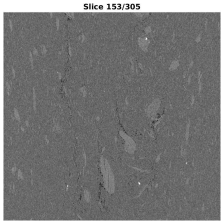

C18-P

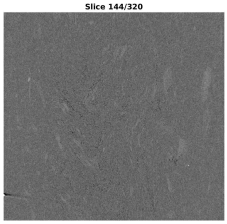

119-F

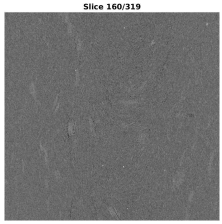

121-F

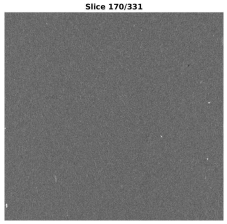

125-F

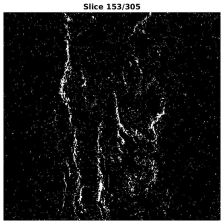

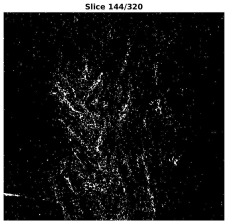

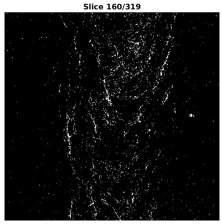

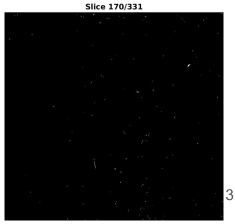

Aggregations Filtering

It is easier to segmentate the just aggregations out of the picture instead of all the fibers, as these could be easily differenced taken out of the noise, and the analysis could be more personalized.

To analyze the aggregations found in the picture, unlike porosity, it could be applied different filters to smooth and sharpen regions, because we are just analyzing the big clumps and small ones can be neglected.

In this analysis it is going to be used medium resolution tomographies (11um) for the samples C18-P, 119-F, 121-F, 125-F. All the samples in the end will be subjected to the same set of filters so the comparison can be significative.

Im_adjusted after cutted

Tomographies are cutted to analyze just the sample, ignoring the background of it. Once this pictures are cutted, the images contrast can be adjusted without influencing in its later analysis, as seen in the “Color Histogram” document.

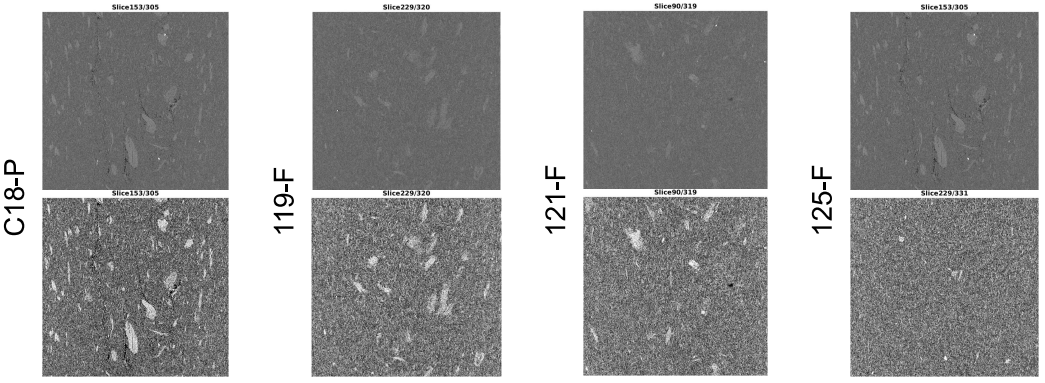

Erode-Dilating filter

In order to get rid of the fibers and segregate correctly purely the aggregations, it is tried a filter of E-D, this could reduce the size of the small fibers. On top the E-D filter is applied to the original (cutted) images, and then a contrast adjustment is done, on the bottom is the other way around. (E-D sphere radius = 3)

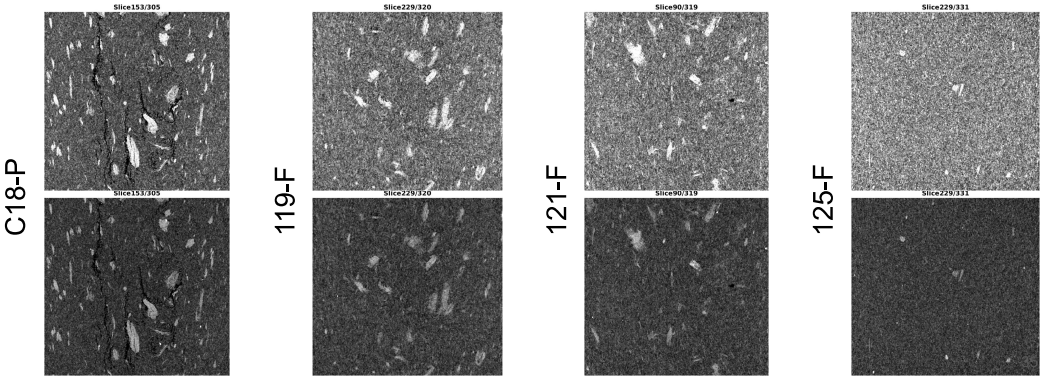

Dilate-Eroding filter

In E-D filtering, it was thought that when eroding first the image, the matrix/voids would absorb the fibers avoiding them to grow again when dilating. But as shown, when there are not many aggregations, the result is that as the last filter is a dilating filter, the white colors are enhanced. To try to have the opposite effect, it is tried a D-E filtering.

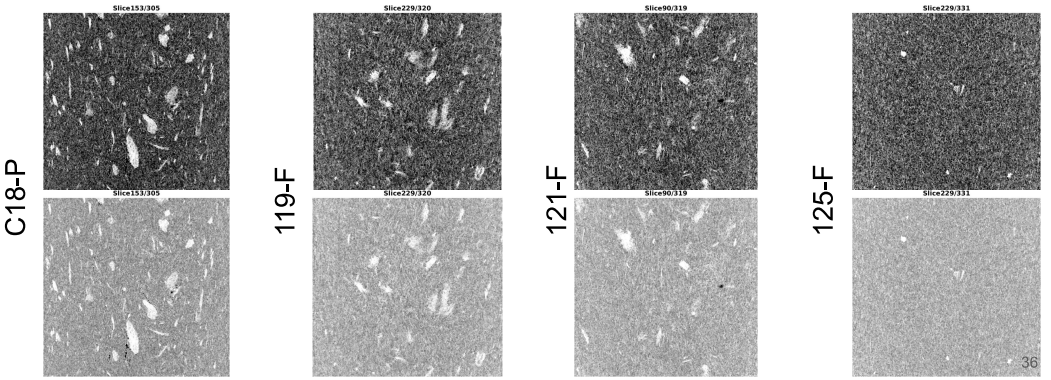

Dilate-Erode filters considerations

- When the aggregations are less noticeable in the sample, the fibers are more difficult to eliminate from the picture, and it looks like there is more “noise” (which is not real noise) in the picture.

- In the previous slides it could be seen how after applying this E-D filtering the picture darkens, and for that reason if we apply the contrast adjustment later, the aggregations are more noticeable.

- The preadjusted contrast image seem to enhance the colors of the first filter applied, while the filter on the post-contrast-adjusted seems to grow the extremes (the aggregations and voids in our case), with a bigger grow on the color that modifies the second function on the small structures and on the first function for the bigger structures.

Smoothing filters 119-F

Unlike voids an porus, smoothing filters could be used in our pictures to treat as noise the small fibers, and make them disappear while keeping the aggregations. In this case it is tried different filters to see how these affect the samples. Again, the top row shows the results for the tomographies where first the filter is applied, and then the contrast adjustment, and on the bottom, the other way. (note that the no local filter is a 2D filter applied to each slice)

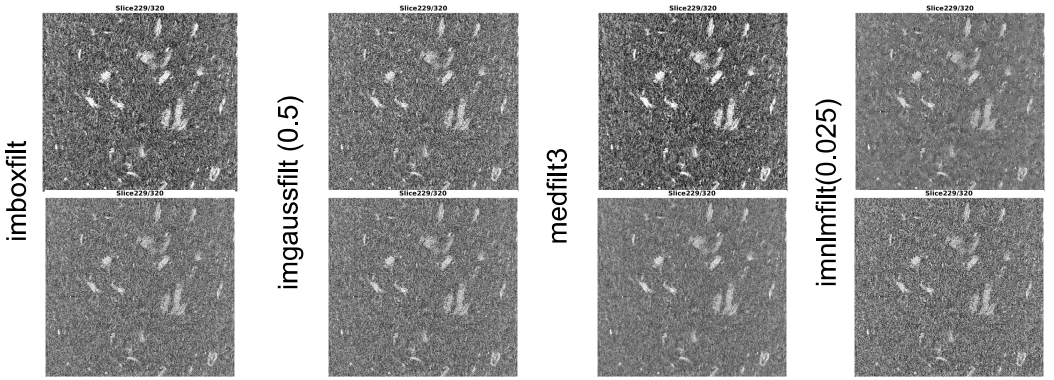

Smoothing filters

119-F

Unlike voids an porus, smoothing filters could be used in our pictures to treat as noise the small fibers, and make them disappear while keeping the aggregations. In this case it is tried different filters to see how these affect the samples. Again, the top row shows the results for the tomographies where first the filter is applied, and then the contrast adjustment, and on the bottom, the other way. (note that the no local filter is a 2D filter applied to each slice)

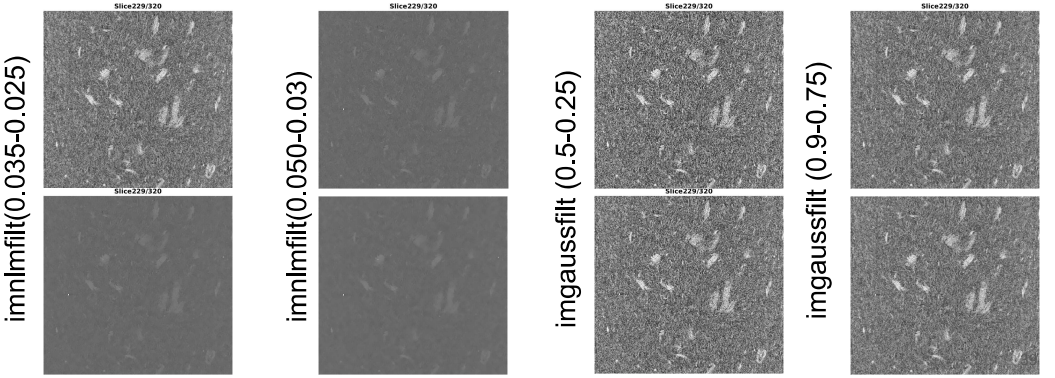

Smoothing to DE images

From the smoothing filter analysis it can be seen that non local filters smoothes drastically the picture, but the value used cannot be very high, and it darkens the picture a lot. If this filter is enhanced by the DE filter seen previously, aggregations of high intensity will be highlighted. On the top row it can be seen images have been subjected to (in order): DE filter of radius 3, imnlfilt(0.03), contrast adjust. And on the bottom: DE filter of radius 3, contrast adjust, imnlfilt(0.03), contrast adjust.

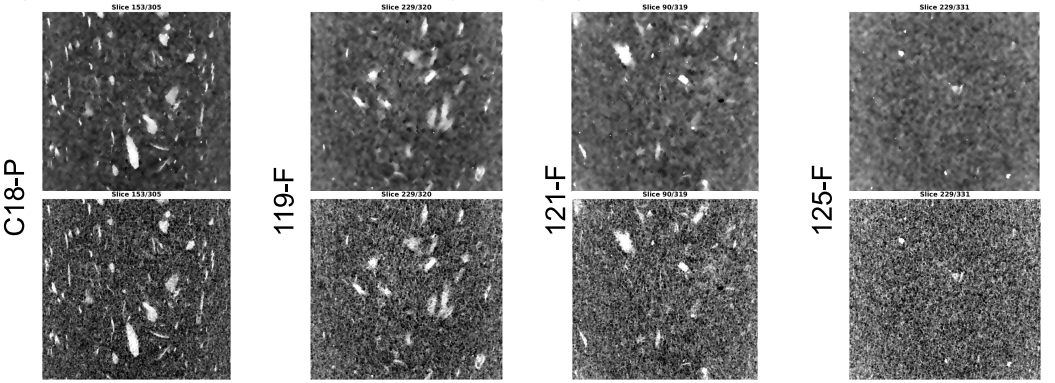

Smoothing to DE images

New tries:
Top row: Non local mean (0.05) > E-D (2) > Non local mean (0.05) > Contrast adj
Bottom row: D-E(3) > Non local mean (0.05) > Contrast adj

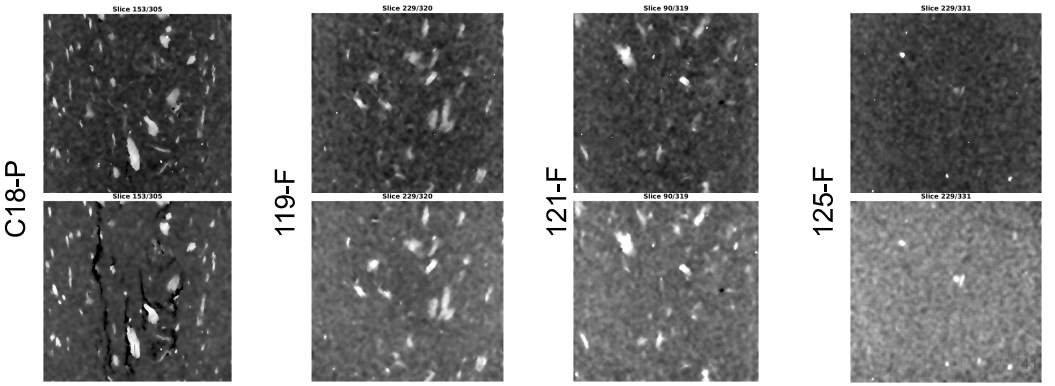

Color histogram check

After color adjusting the images and applying the filters used in the analysis it has to be checked before binarizing that the filter applied to the pictures has the same effect on all of them and then comparison between pictures is reliable. The first histogram shows the results for the pictures with: DE filter of radius 3 > imnlfilt(0.03). The second histogram the same but with a contrast adjustment.

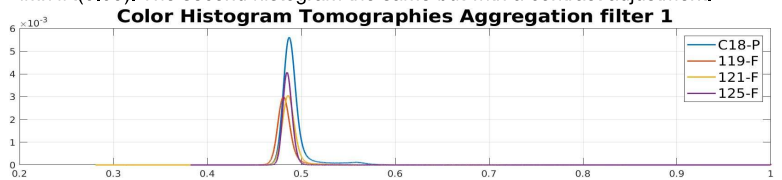

The color histogram shows that the comparison between samples cannot be done by just applying the same threshold in the binarization of the sample. At least on the contrast adjusted picture

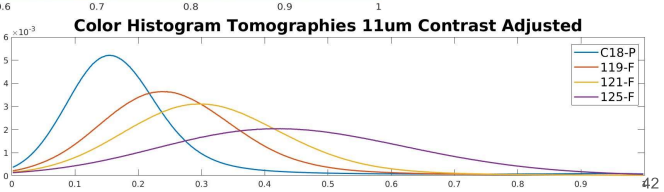

Color histogram check

After color adjusting the images and applying the filters used in the analysis it has to be checked before binarizing that the filter applied to the pictures has the same effect on all of them and then comparison between pictures is reliable. The first histogram shows the results for the pictures with: ED filter of radius 3 > imnlfilt(0.03). The second histogram the same but with a contrast adjustment.

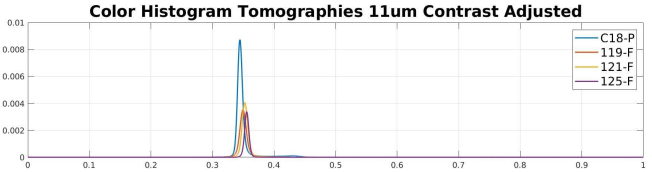

As before, when applying a contrast adjustment, the color distribution between samples differs. This may be because the different presence of voids and aggregations on them.

It has been found visually that for those pictures where the contrast was not adjusted the difference in contrast is not noticed, but the change in shape of the color histogram lays in the fact that some samples have more voids and aggregations.

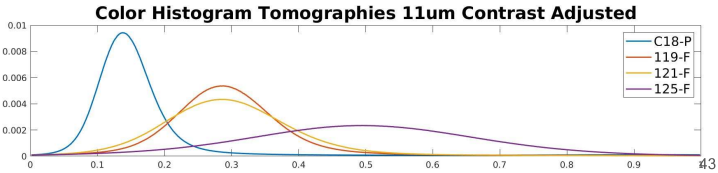

Aggregation binarization

As it is shown here, when applying a filter without adjusting the contrast of the samples, the color values of the aggregates look the same. Here it can be seen an slice for each one of them.
In the following analysis it will be performed a binarization on the tomographies that went through the process: **ED filter of radius 3 > imnlfilt(0.03)**, by changing the threshold value of binarizing and checking how the slopes of the %aggregates change.

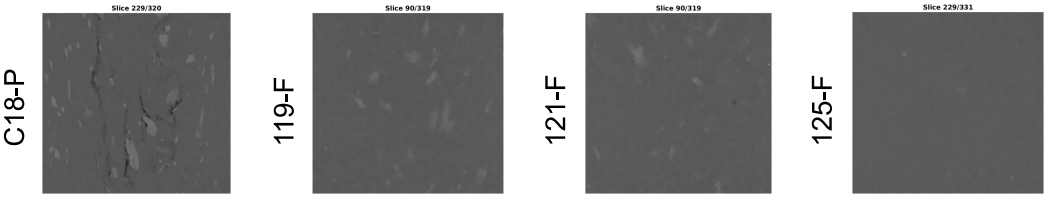

The aggregates seem to have a value between 0.39-0.45, and the rest of the matter between 0.33 and 0.35.

Aggregation binarization

In the following analysis it will be performed a binarization on the tomographies that went through the process: **ED filter of radius 3 > imnlfilt(0.03)**, by changing the threshold value of binarizing and checking how the slopes of the %aggregates change.

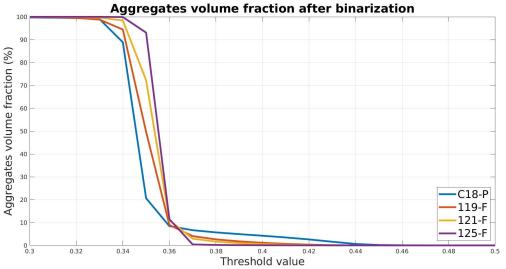

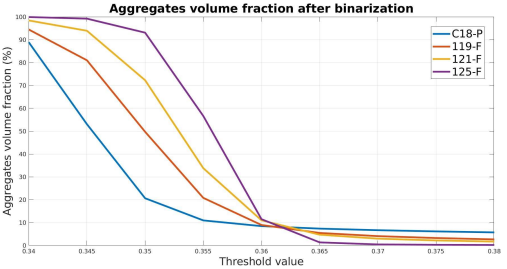

A reasonable value to use in this binarization would be between 0.36 and 0.365. In the curve there could be identified 3 different change in slopes: from horizontal to a very steep curve, then to a not so steep one, and finally to almost horizontal. As in 0.36 this “not so steep slope” has already occurred at a lower threshold (0.35-0.355), the threshold value for all the samples chosen will be of 0.365

Aggregation binarization

Comparison between the original picture and the binarized one with a threshold value of 0.365

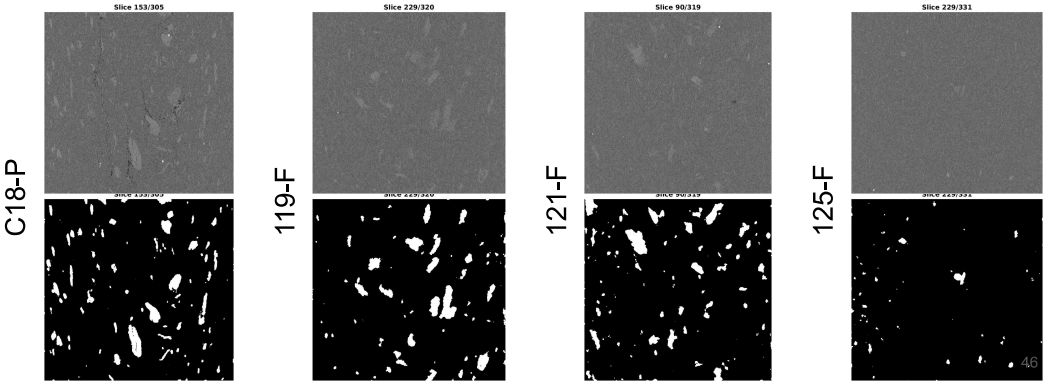

Aggregation binarization

Comparison between the original picture and the binarized one with a threshold value of 0.37

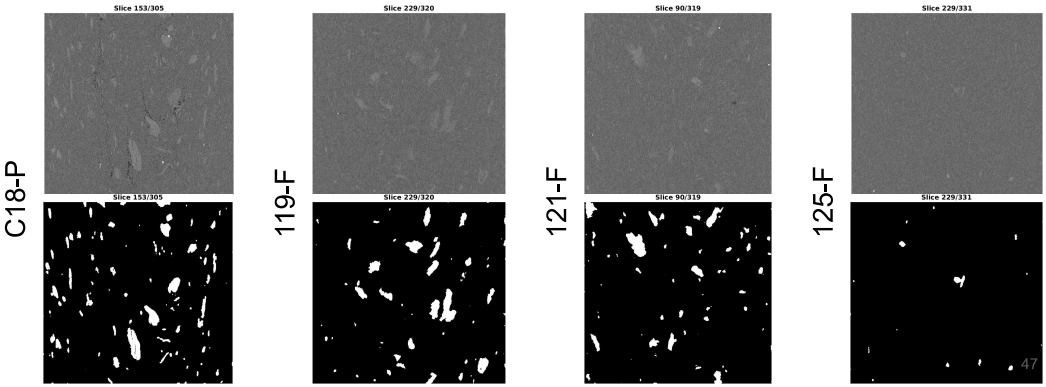

Aggregation binarization

Comparison between the original picture and the binarized one with a threshold value of 0.38. This seems like a threshold value that would fit with the original picture.

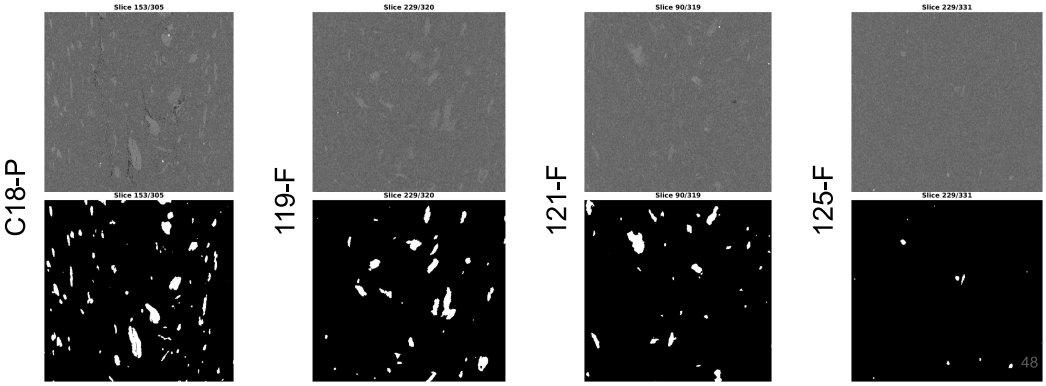

Fibber Filtering

After the void and aggregation analysis it is going to be worked with the Fibers, this is the most difficult segmentation to make, as the fibers are very thin, and every filtering that is made to them can represent on a change in the image that doesn't reflect the reality. Because of this, the analysis that is going to be made in the mask it is very important

In this analysis it is going to be used high resolution tomographies (4um) for the samples C18-P, 119-F, 121-F, 125-F. All the samples in the end will be subjected to the same set of filters so the comparison can be significative.

The area analyzed in this high resolution tomographies is the one shown in the picture, smaller than the sample cross section so this should be taken into account when the analysis is made.

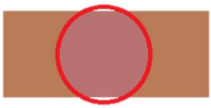

Original Picture

On the top row it can be seen the original image from each sample, and on the bottom it is seen the same image with contrast adjustment applied. As it can be seen in the "Color Histogram" document, when this adjustment is made, the color histogram curve decentres from one another, so this filter should be avoided, but it can be useful for visualization.

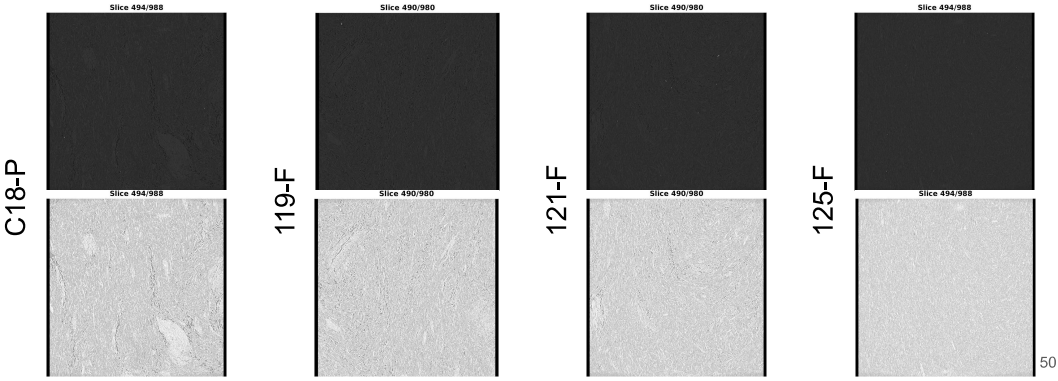

Fiber volume fraction*

From the previous void analysis and data such as the PP density and the sample density, we are able to get the expected volume fraction from each the matrix and the fibers. This information, although should be taken carefully can give us a guide of the values we should expect to get. It has to be said also that this value might not be relevant for our tomography, as the high resolution tomography that we are going to use does not involve 2 of the 4 sides of the samples (so the void fraction of this part of the tomography should be higher)

$$\begin{cases} \%V = \dfrac{\rho_{composite}}{\rho_{fiber}} * \%w \\ (1 - \%V - \%void) = \dfrac{\rho_{composite}}{\rho_{matrix}} * (1 - \%w) \end{cases}$$

- ρ_composite: 600 kg/m3
- ρ_PP: 900 kg/m3
- %w: 40%

C18-P

- %void: 1.196%
- %V: 58.8%
- fiber: 408 kg/m3

119-F

- %void: 0.896%
- %V: 59.1%
- fiber: 406 kg/m3

121-F

- %void: 0.415%
- %V: 59.6%
- fiber: 403 kg/m3

125-F

- %void: 0.053%
- %V: 59.95%
- fiber: 400 kg/m3

Mask analysis

Again the image is binarized to isolate the fibers. To do so it has to be taken into account the background from the image. This background is a result of the high definition tomography, because for this resolution not the whole cross section is analyzed, so a cylindrical shape appears in the analysis, and the rest of it (to make an square picture) is filled with pure black.

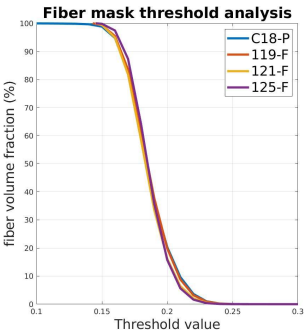

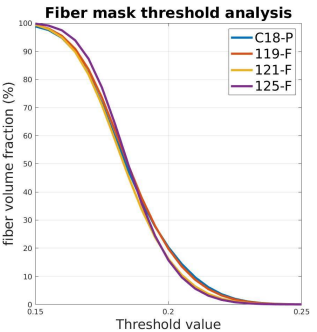

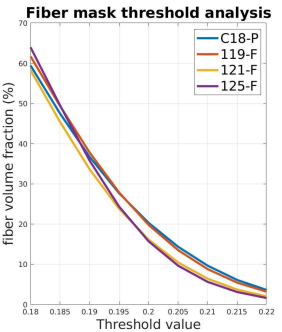

Mask analysis

In our analysis it is expected a fiber volume fraction of around 60% (a value that should be a bit smaller, considering that we are analyzing just the middle part of the sample, where voids tend to accumulate). However, there does not seem to be an inflexion value that could be defined as the value where “we start to introduce some matrix in our binarization”. Furthermore, in a visual analysis, this threshold value should be between 0.19 and 0.22, but for this values the fiber volume fraction is much smaller than the one expected which could be because the resolution of the tomographies.

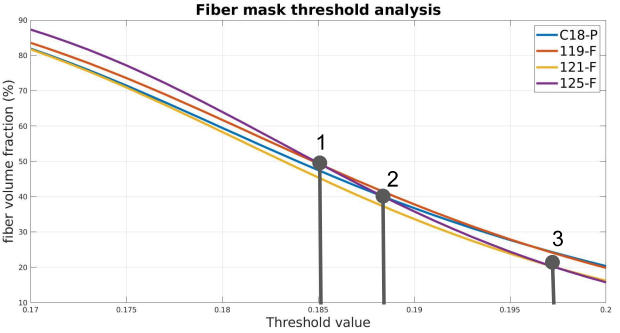

Mask Visual analysis

As it has been seen, there is no outstanding point that could mean like a good starting point to look for the segmentation threshold value. Because of that it is tried a segmentation with a visual approach starting with threshold values that may look interesting form the previous analysis.

Original - Adjusted | Thrsld - 0.185 (1) | Thrsld - 0.189 (2) | Thrsld - 0.1955 (3)

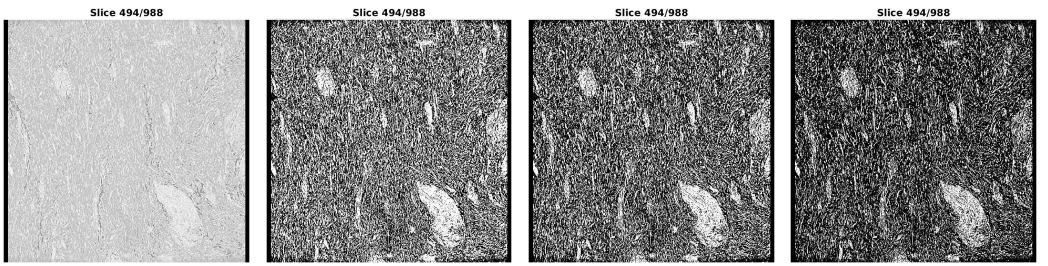

Mask Visual analysis On a zoomed region of the C18-P sample, slice 494 in the zx plane

Thrsld - 0.189 (2)

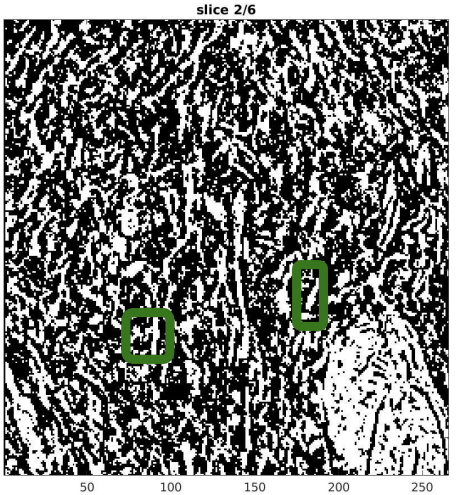

Thrsld - 0.2

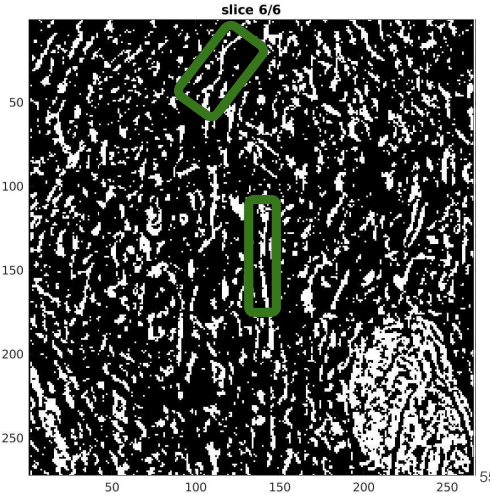

Mask Visual analysis On a zoomed region of the C18-P sample, slice 494 in the zx plane

Thrsld - 0.1955 (3)

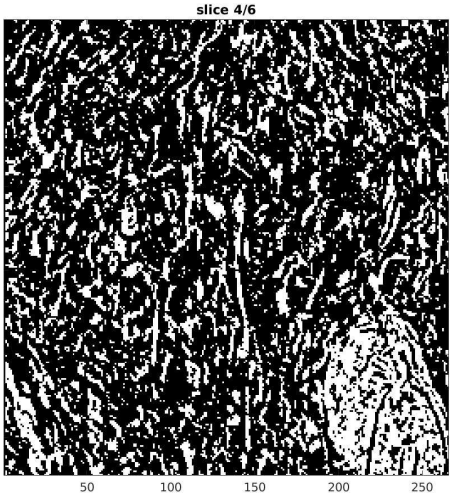

Thrsld - 0.198

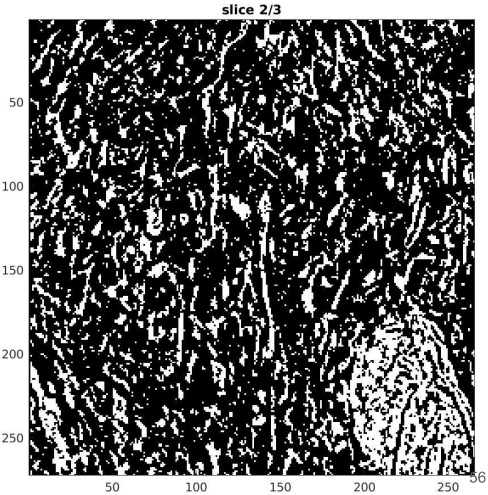

Problems

By using a binarization value of 0.1955 some problems appear, because although the visual analysis seemed to work properly, the are some flaws, like the fact that the void fraction with this value is 20%, or that when it is said to mark brighter just one fiber (the biggest one which would correspond to an aggregate we suppose) it is found out that all of the sample brightens up.

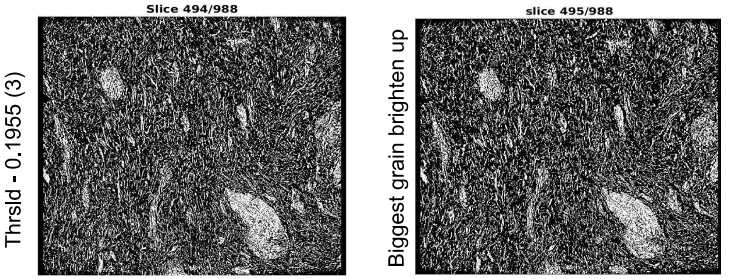

This problems indicate that the threshold value could be too high for some things (as the %v is to low), and too small for others (as all the fibers are connected to each other). These problems can be a cause of the resolution of the tomography and making such an strong cut when doing the binarization, instead of a progresive one, but it is something that has to be done for our analysis

Mask Visual analysis On all the samples with a threshold value of 0.1955

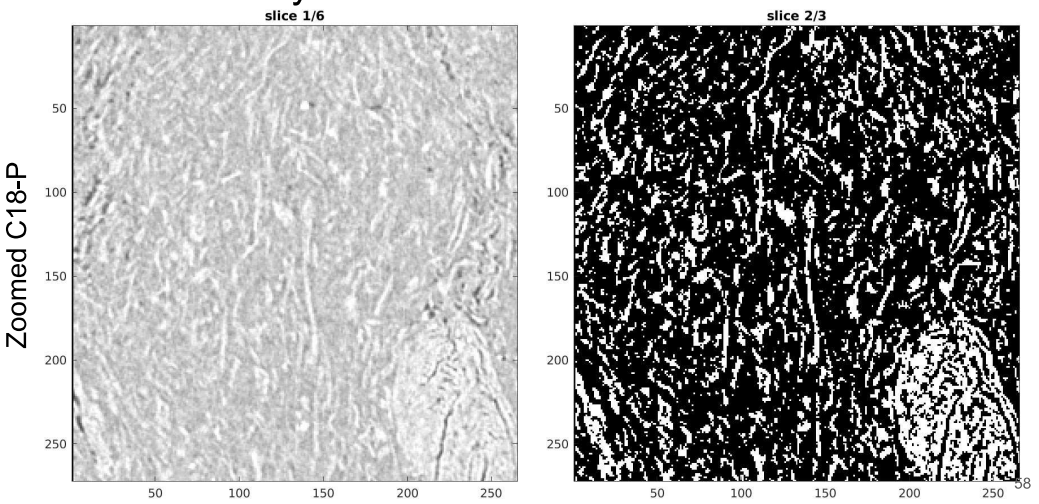

Mask Visual analysis On all the samples with a threshold value of 0.1955

Zoomed 119-F

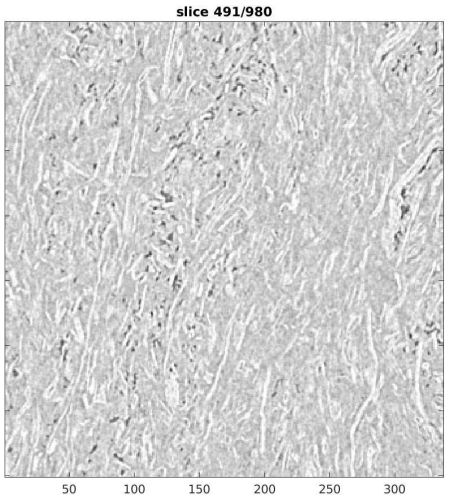

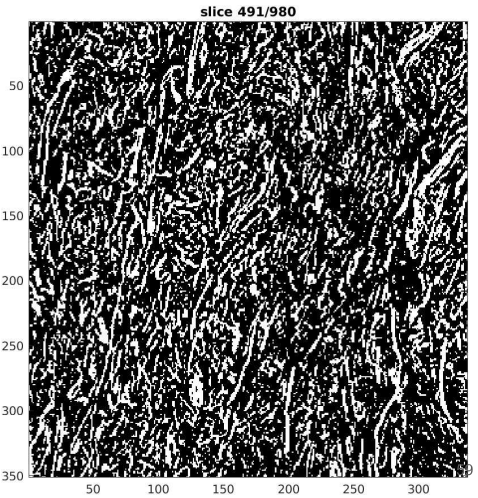

Mask Visual analysis On all the samples with a threshold value of 0.1955

Zoomed 121-F

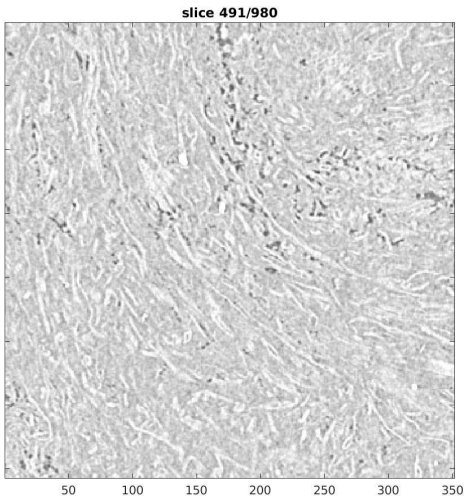

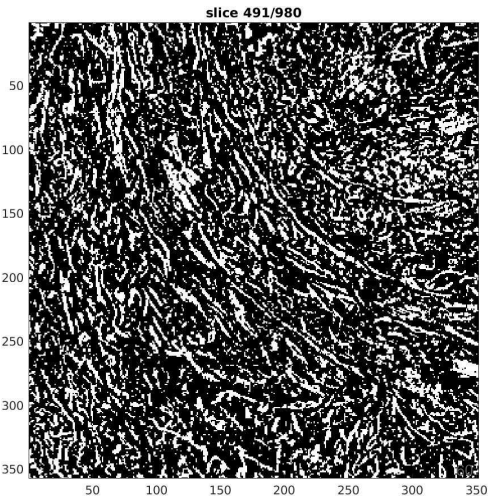

Mask Visual analysis On all the samples with a threshold value of 0.1955

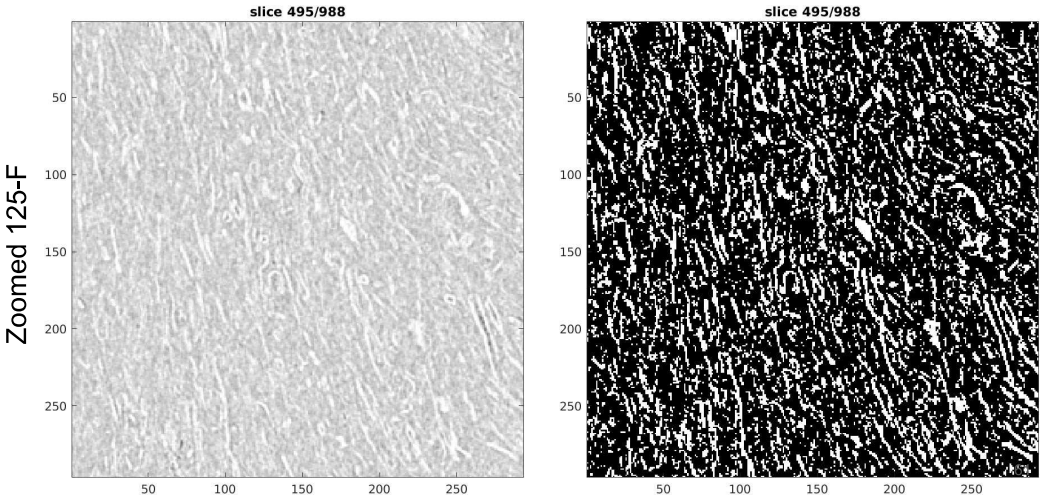

Aggregations suppression

The orientation analysis with the structure tensor code is designed to be used in fibers, and the analysis in the aggregations could lead to some random orientations. To avoid this, we delete the aggregations that were found in the previous analysis where we segmented the aggregations.

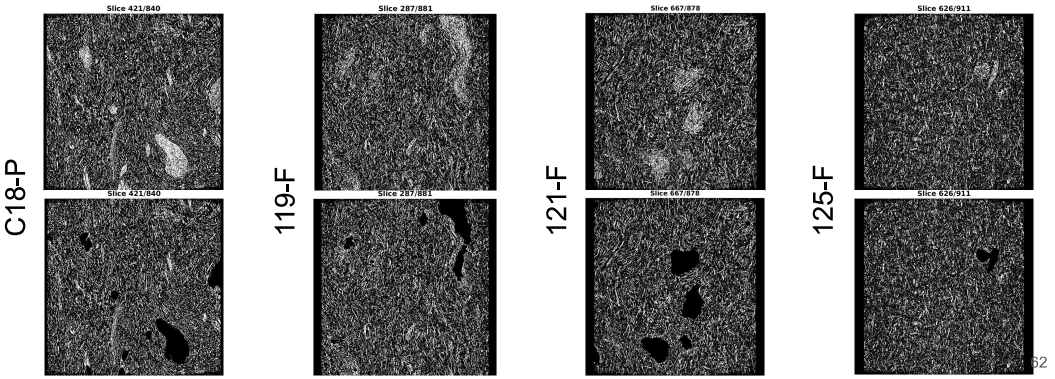

C

First shipment tomography results

This document contains the resultant information and pictures obtained after the segmentation of the first shipment sample tomographies, containing volume pictures, heat maps of the different phases, bar plots of the main data and orientation distribution calculations.

The document is divided into three different parts containing:

1. **Porosity analysis**
2. **Aggregates analysis**
3. **Fiber analysis**

Void analysis

This is a porosity analysis for the set of samples that was first send by Biofiber Tech to Lund University. The analysis is carried out by doing four tomographies, each belonging to a different kind of the samples received. Notice that here only lies an analysis for four out of the eight different kinds received.

The tomography done for the sample has a resolution of 11um, and it is focused at the middle of it. To segmentate the voids the following process was made to all of the tomographies: Cutting the tomographie to get rid of the borders of the image that only shows the surroundings of the sample, binarization with a threshold value of 0.33, dilate-eroding filter with an sphere shape first with a radius 1 and then with radius of 2 voxels, finally filtering out all the voids smaller than 8 voxels in the image.

Segmentation result:

- 1st row: Original picture
- 2nd row: Resultant picture for analysis

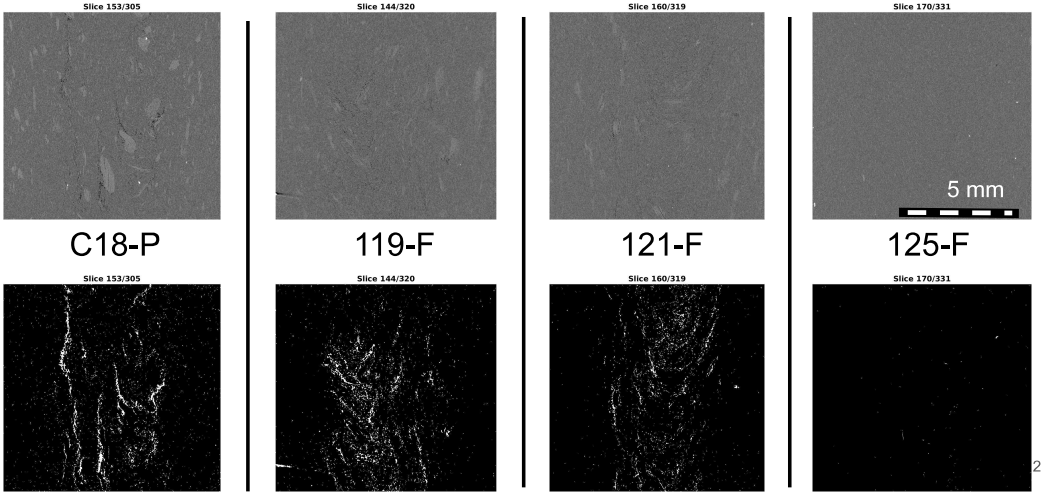

Volume Viewer Pictures

C18-P

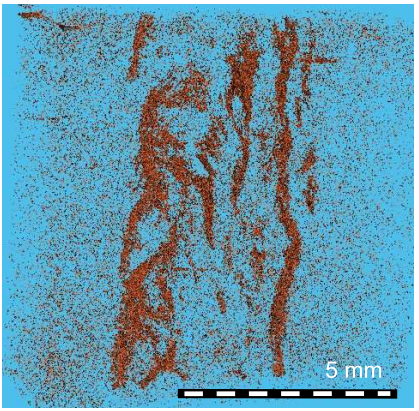

119-F

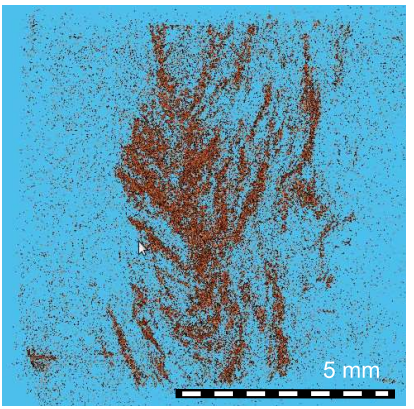

Volume Viewer Pictures

121-F

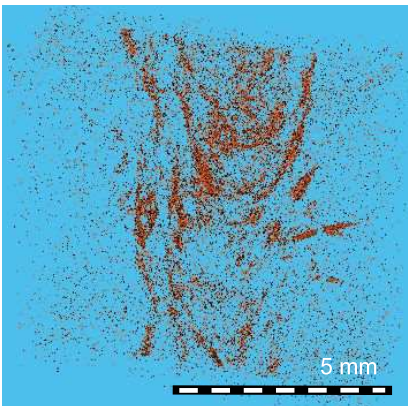

125-F

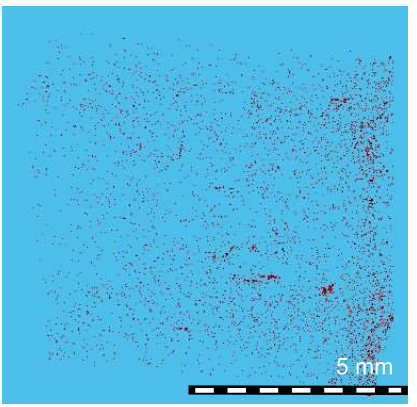

C18-P

Heat map with histogram of pores along the sample:

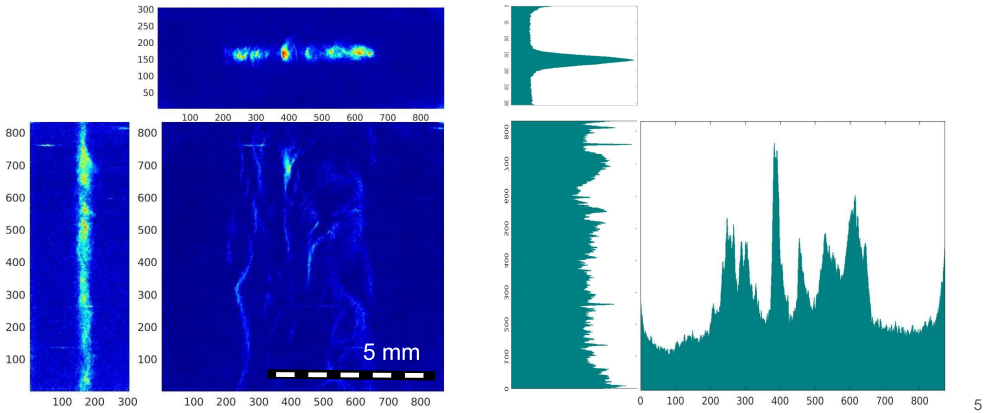

119-F

Heat map with histogram of pores along the sample:

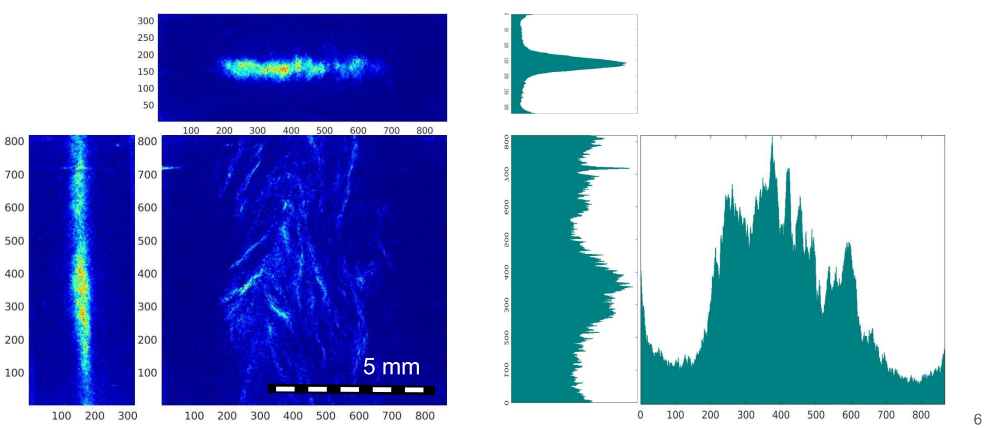

121-F

Heat map with histogram of pores along the sample:

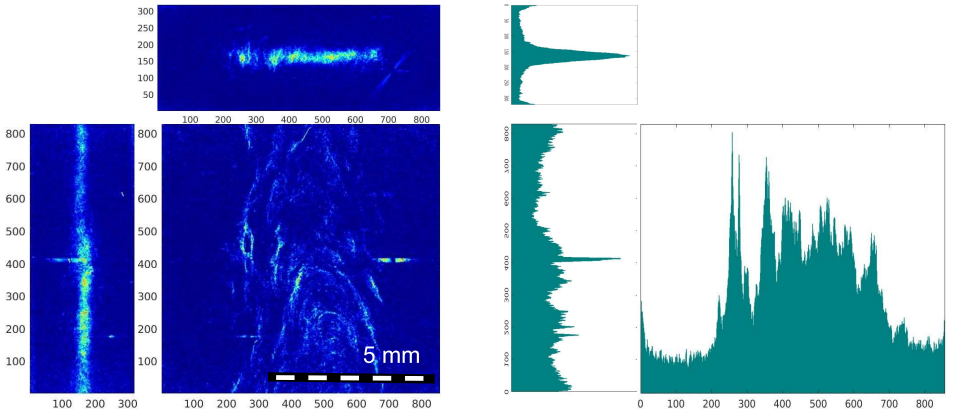

125-F

Heat map with histogram of pores along the sample:

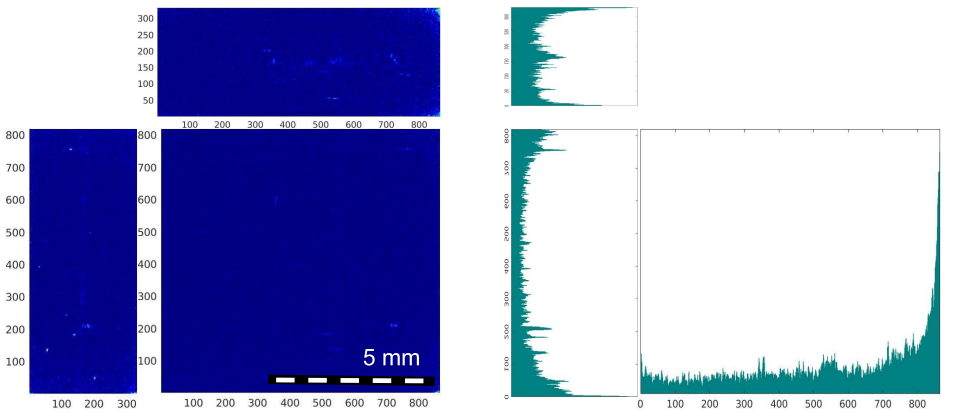

Porous Properties

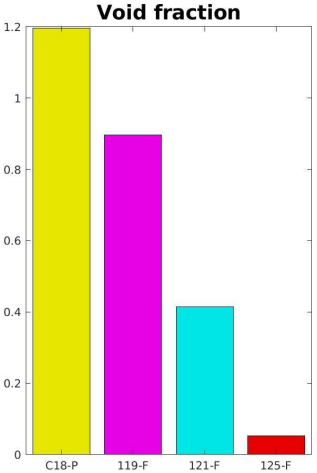

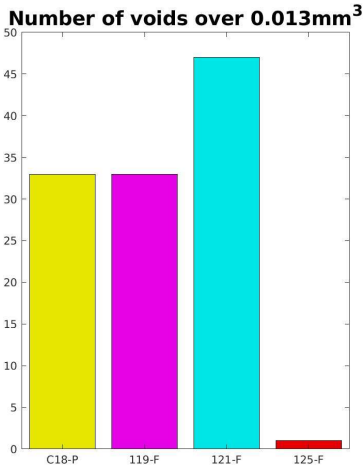

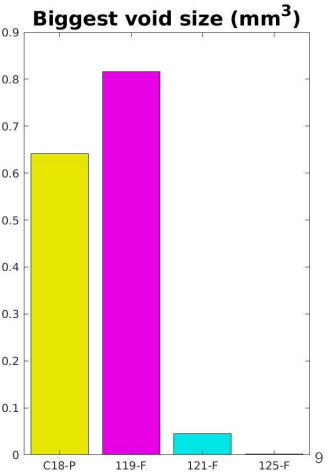

Porous Properties

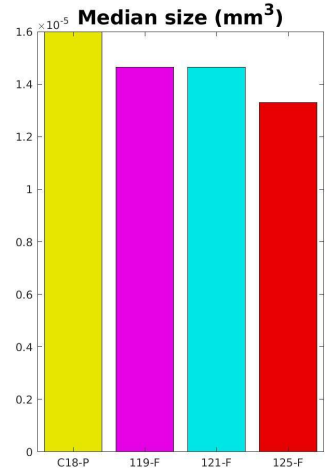

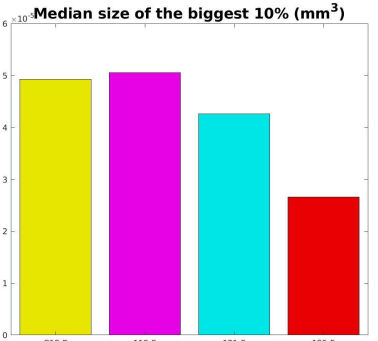

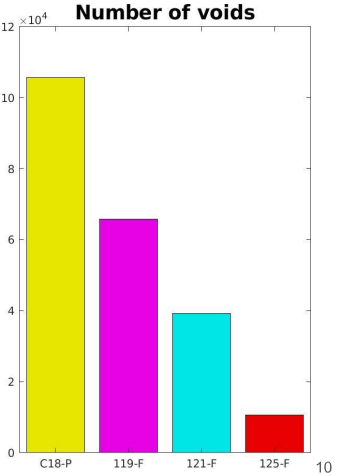

Orientation of the voids

Interactive tomography

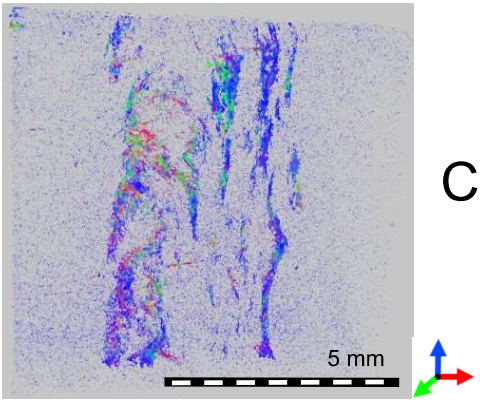

C18-P

Angle with the vertical

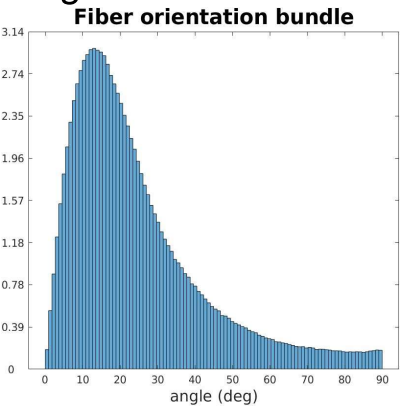

Orientation of the voids

Interactive tomography

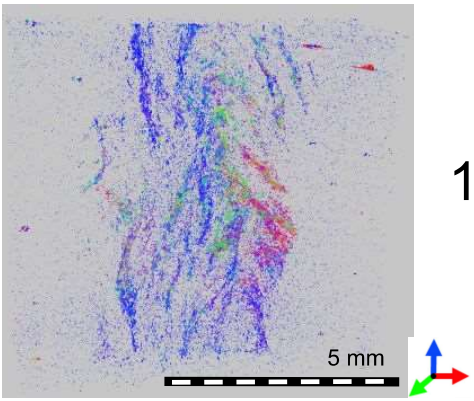

119-F

Angle with the vertical

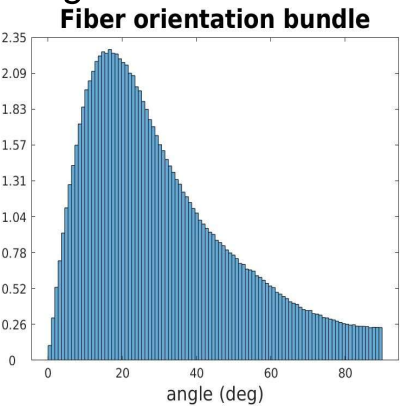

Orientation of the voids

Interactive tomography

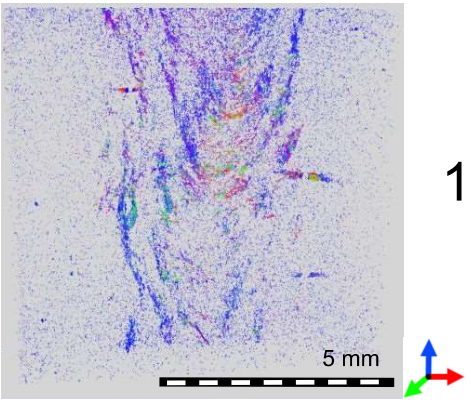

121-F

Angle with the vertical

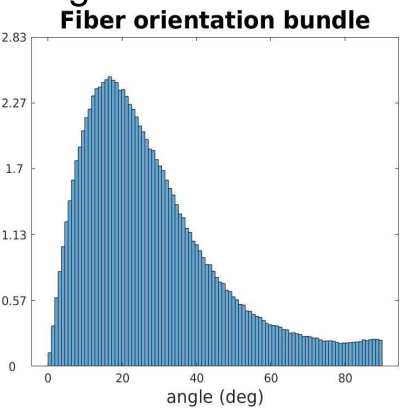

Orientation of the voids

Interactive tomography

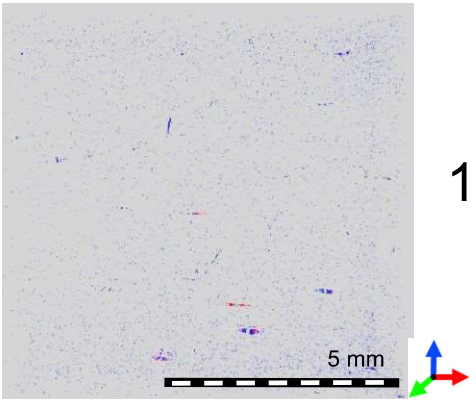

125-F

Angle with the vertical

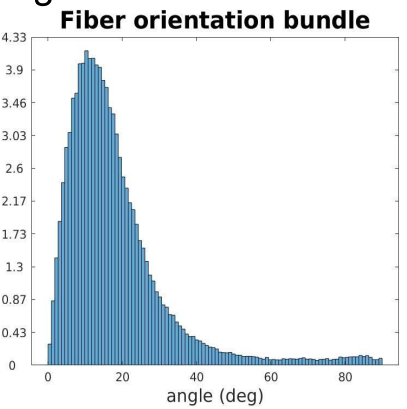

Aggregations Analysis

This is the aggregations analysis for the set of samples that was first send by Biofiber Tech to Lund University. The analysis is carried out by doing four tomographies, each belonging to a different kind of the samples received. Notice that here only lies an analysis for four out of the eight different kinds received,

The tomography done for the sample has a resolution of 11um, and it is focused at the middle of it. To segmentate the aggregations the following process was made to all of the tomographies: Cutting the tomographie to get rid of the borders of the image that only shows the surroundings of the sample, E-D filter of radius 3, non local mean filter to each slice in the xz plane with a “Degree of Smoothing” equal to 0.03, a binarization with threshold value 0.38 and a filter of grains smaller than 10x10x10 voxels.

If more information wants to be known about this analysis refer to **“Aggregations Filtering”** document.

Aggregation binarization

Comparison between the original picture and the segmented picture.

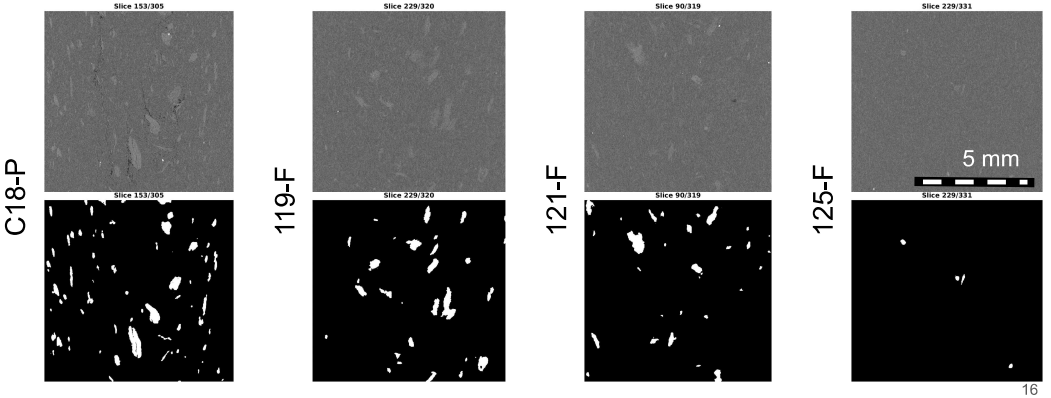

Volume Viewer Pictures

C18-P

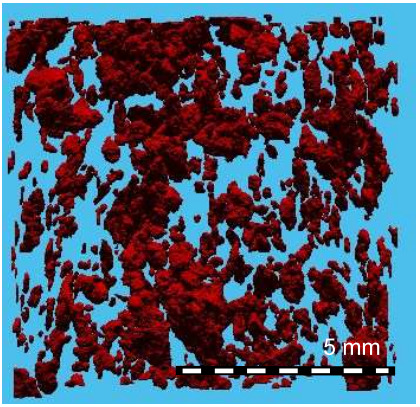

119-F

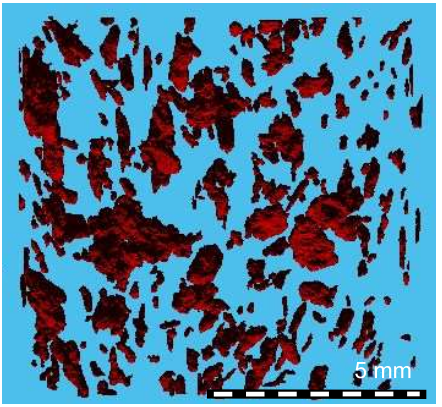

Volume Viewer Pictures

121-F

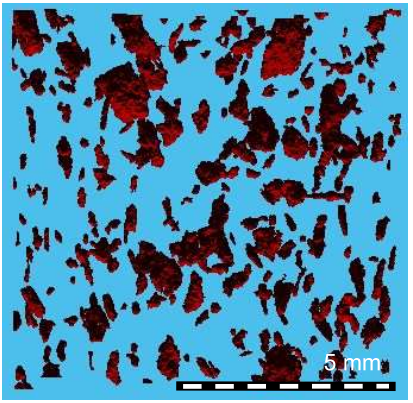

125-F

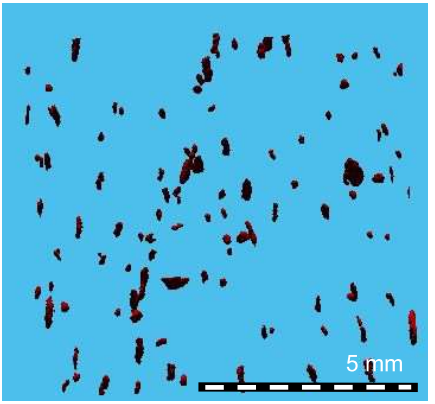

C18-P

Heat map with histogram of Aggregates along the sample:

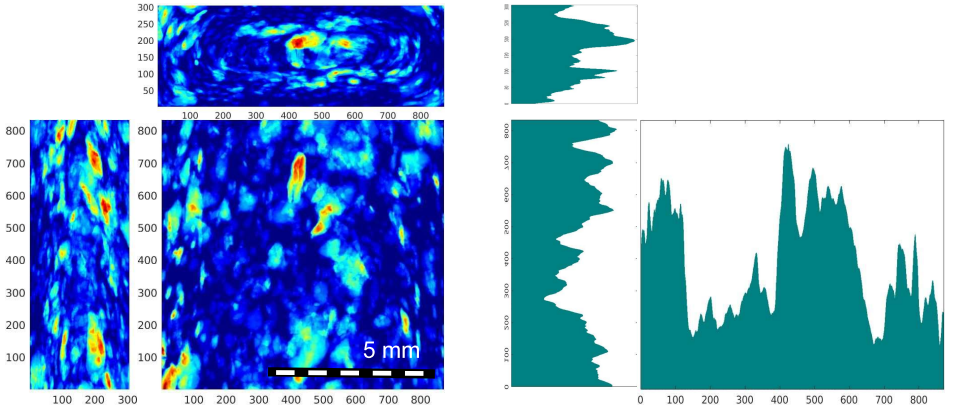

119-F

Heat map with histogram of Aggregates along the sample:

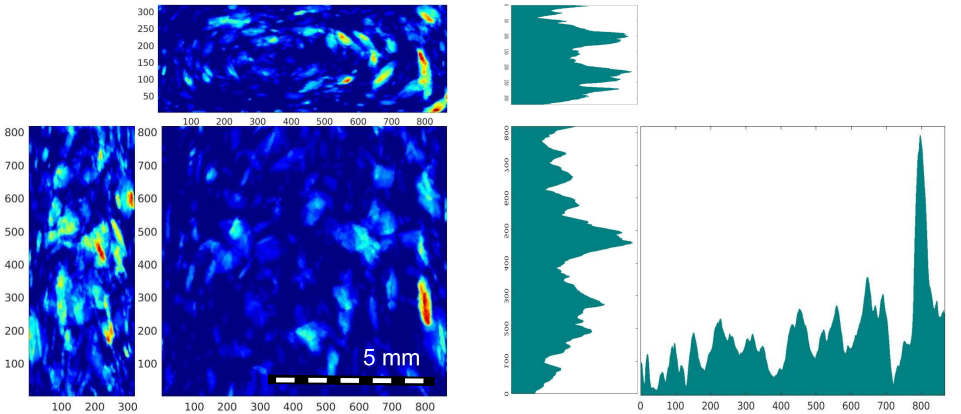

121-F

Heat map with histogram of Aggregates along the sample:

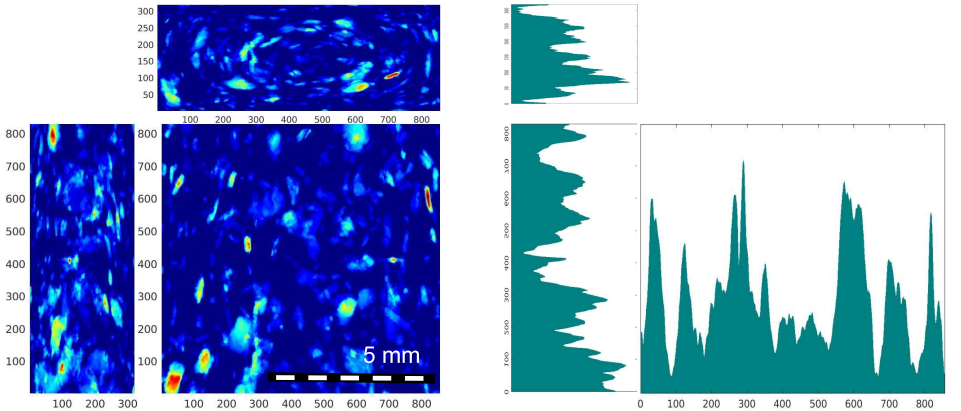

125-F

Heat map with histogram of Aggregates along the sample:

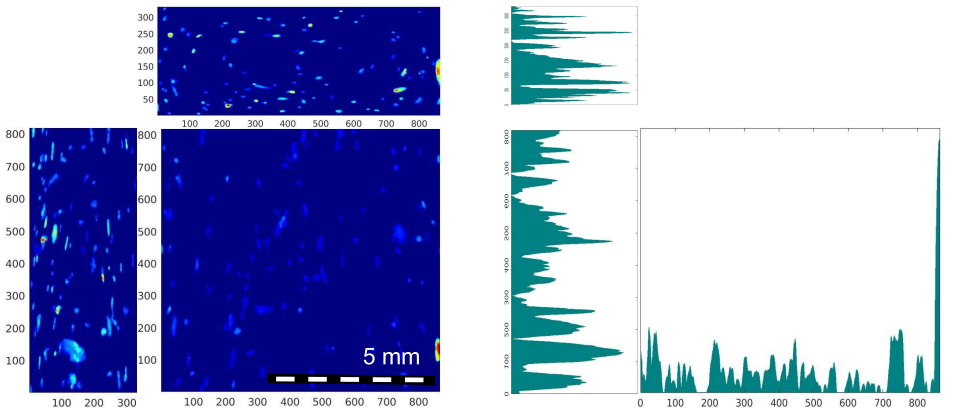

Porous Properties

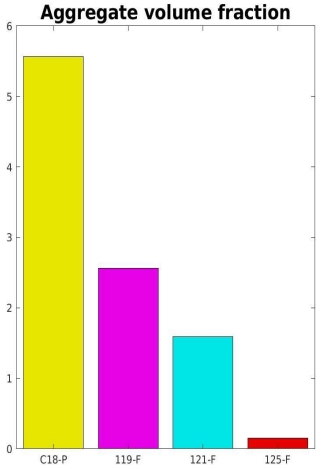

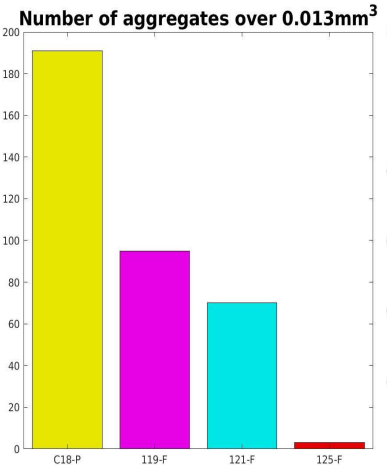

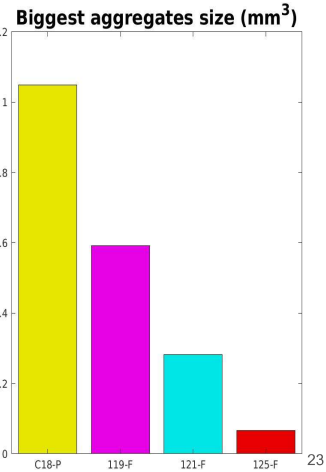

Porous Properties

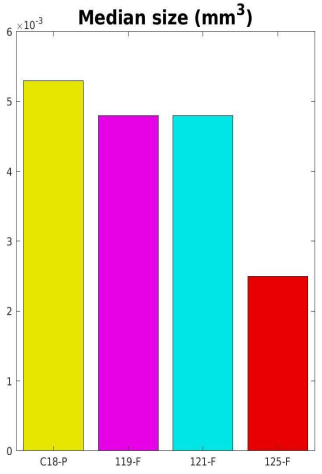

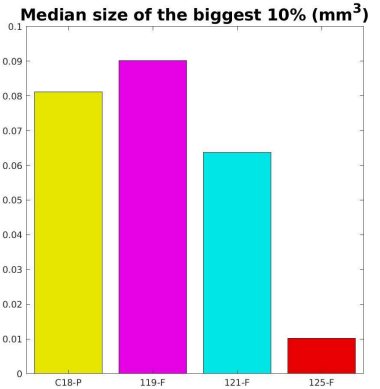

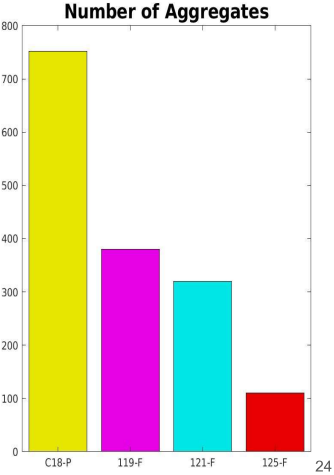

Shape of the aggregations

These were calculated by using the regionprops3 function in matlab, with the property “eigenvalues” and then relate them to each other as the Structure Tensor Code does

C18-P

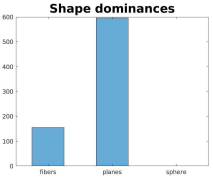

119-F

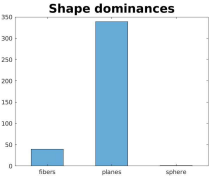

121-F

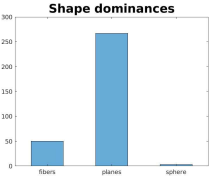

125-F

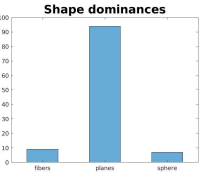

It is seen that mostly none of the samples present non-spherical aggregates, and the shape that predominates is the plane, which means that the aggregates usually are longer in two of the three dimensions, but does not mean that the third one is an small size

Orientation of the aggregations C18-P

These were calculated by using the regionprops3 function in matlab, with the property “orientations”

YZ plane histogram - roll

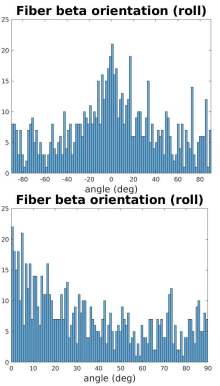

XZ plane histogram - pitch

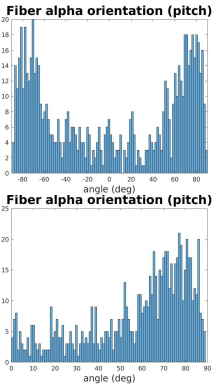

XY plane histogram - yaw

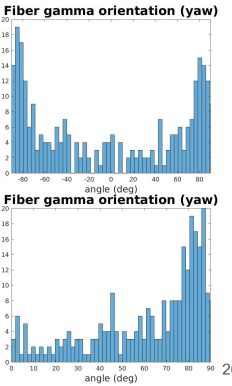

Orientation of the aggregations 119-F

These were calculated by using the regionprops3 function in matlab, with the property “orientations”

YZ plane histogram - roll

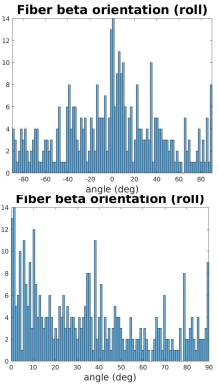

XZ plane histogram - pitch

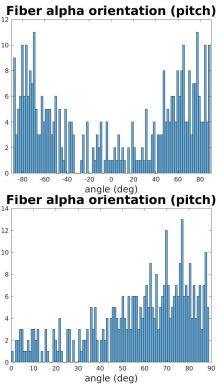

XY plane histogram - yaw

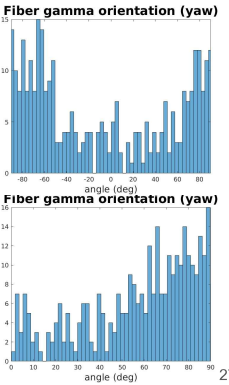

Orientation of the aggregations 121-F

These were calculated by using the regionprops3 function in matlab, with the property “orientations”

YZ plane histogram - roll

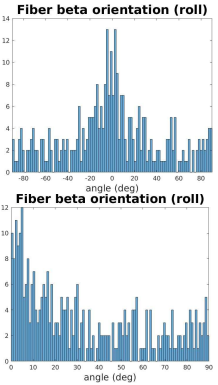

XZ plane histogram - pitch

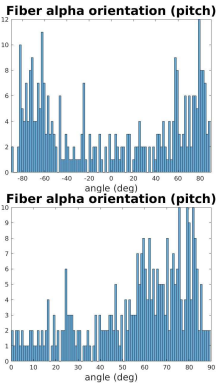

XY plane histogram - yaw

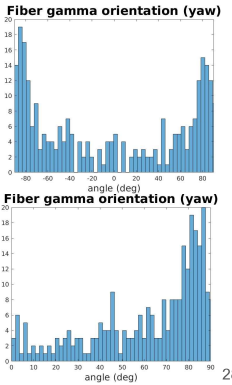

Orientation of the aggregations 125-F

These were calculated by using the regionprops3 function in matlab, with the property “orientations”

YZ plane histogram - roll

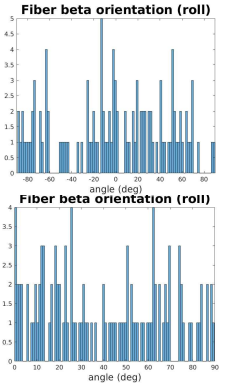

XZ plane histogram - pitch

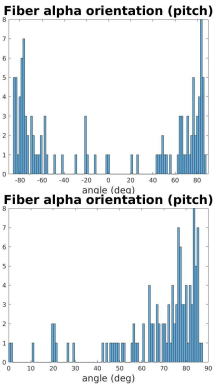

XY plane histogram - yaw

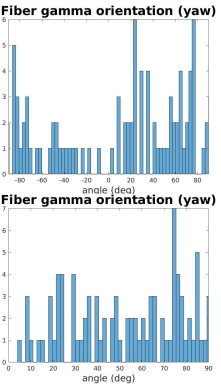

Fibber analysis

This is the analysis that has been conducted to estimate the wood fibber influence in the samples provided by Biofiber Tech. to Lund University. The analysis is carried out by doing four tomographies, each belonging to a different kind of the samples received. Notice that here only lies an analysis for four out of the eight different kinds received.

The tomography done for the sample has a resolution of 4um, and it is focused at the middle of it. To segmentate the fibbers the following process was made to all of the tomographies: binarization of the image with a threshold value of 0.1955, reshape and resizing of both the aggregates mask obtained in the previous analysis and the binarized image to fit it with each other and eliminate the aggregates from the image so just the fibers are left.

If more information wants to be known about this analysis refer to **“Aggregations Filtering”** document.

Fiber binarization

Comparison between the original picture and the segmented picture.

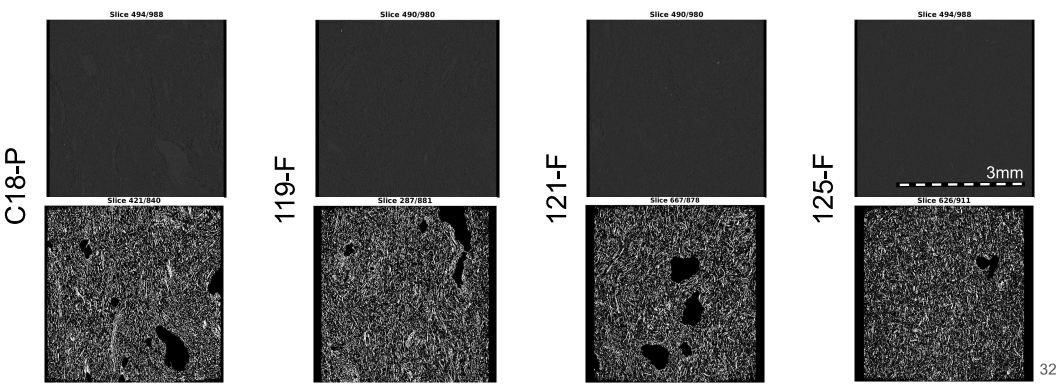

Heat mapping

The only heat maps that are of interest in our case are the ones of the xy-plane because the rest of the heat planes do not take into account the black borders of the picture that are not part of the sample but a fill for the image to be square

Example:
C18-P

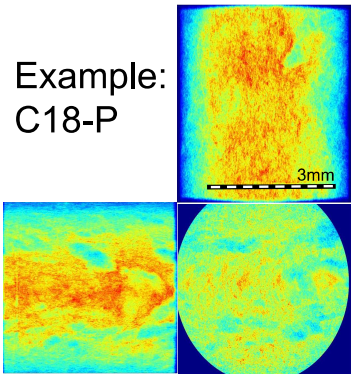

Heat mapping

The only heat maps that are of interest in our case are the ones of the xy-plane because the rest of the heat planes do not take into account the black borders of the picture that are not part of the sample but a fill for the image to be square.

C18-P

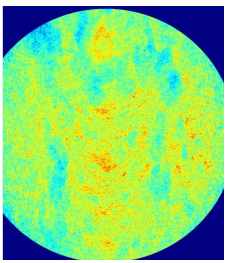

119-F

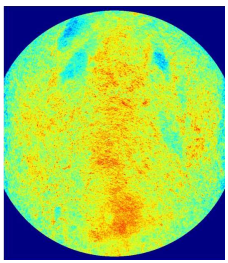

121-F

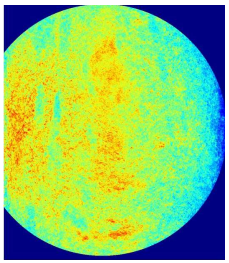

125-F

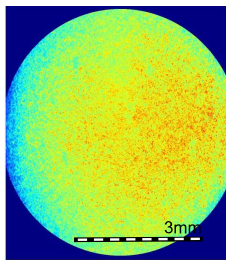

Orientation of the fibbers

These were calculated by using the structure tensor code, and getting four angles considered of relevance.

C18-P

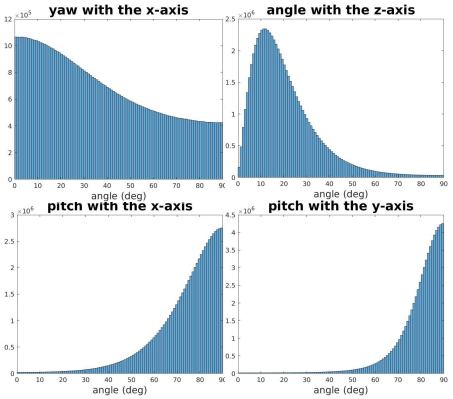

119-F

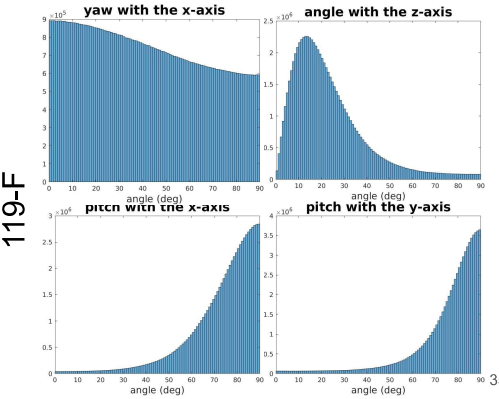

Orientation of the fibbers

These were calculated by using the structure tensor code, and getting four angles considered of relevance.

121-F

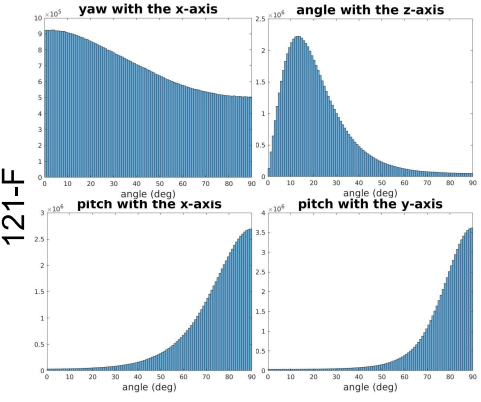

125-F

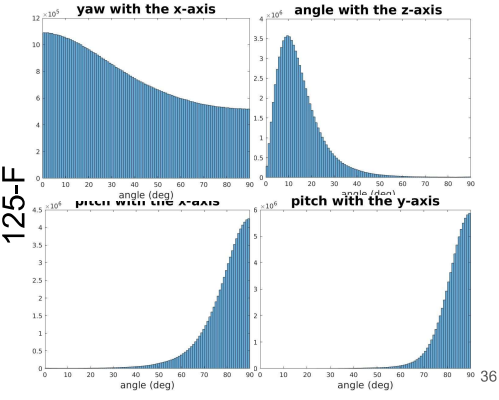

Complete segmentation

Complete segmentation where it can be identified the different phases analyzed: fibers, aggregates and porous. The porous and aggregates where taken from the

C18-P

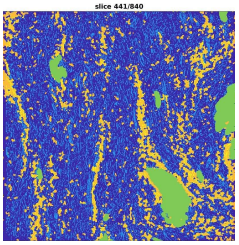

119-F

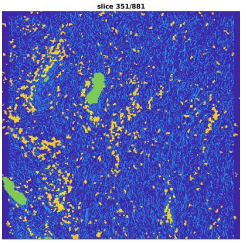

121-F

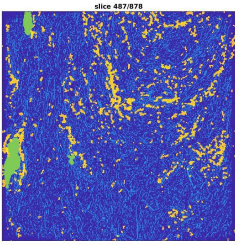

125-F

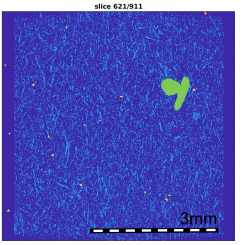

D

Phase Segmentation analysis of the second shipment samples

In the following document, it can be found the process followed to get to the final result of each phase segmentation for the second shipment sample. The order followed for the segmentation was de next one:

1. **Porosity segmentation**
2. **Aggregates segmentation**
3. **Fiber segmentation**

Porosity segmentation (2)

To analyze the porosity found in each sample, it is going to be applied the same kind of filters to each one of them, so then they can be compared between each other.

The samples that are going to be analyzed are the medium resolution tomographies for the samples (7um). This tomographies will go first to through a contrast adjustment filter.

The filtering this samples will go through will be similar to the one done to the samples from the first shipment, so if a deeper explanation is wanted, that analysis is more detailed.

Color Histogram

To assure that a reliable comparison between samples can be performed, the sampe steps have to be followed for every segmentation, and similar color histograms must be presented for every sample, so the segmentation filters work similarly in every tomography

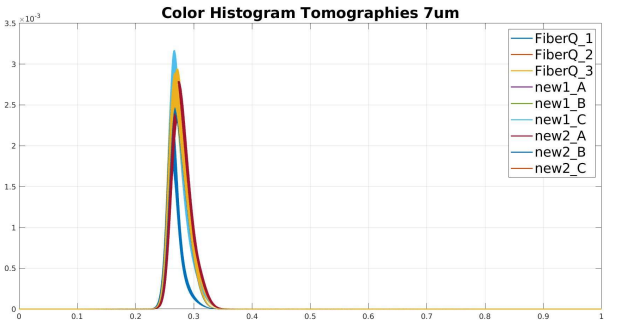

Void volume fraction

Starting with a binarization threshold analysis, it can be seen how the curve behaves with some differences to the previous tomographies. The shape of the curve in the big picture is similar, but when zooming in to the area where the void fraction starts to increase there is a bigger change in the first derivative, the steps are bigger. This more abrupt change may be caused by the increase of resolution of the tomography, which leads to sharper differentiation of phases. It may also be caused by the different surface treatment that these samples were subjected to.

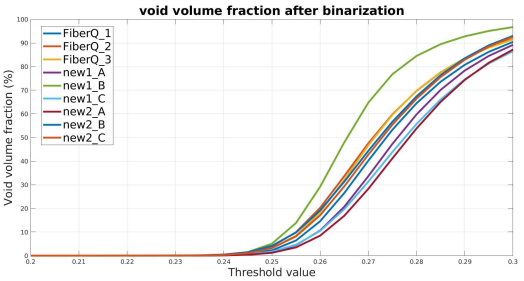

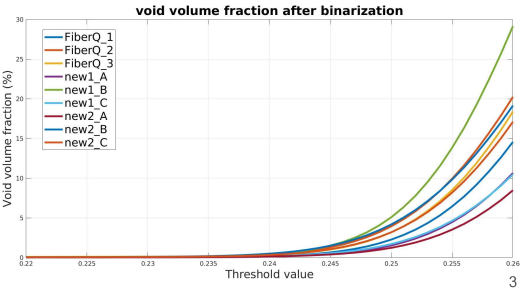

Void volume fraction

Plotting the same curves for the three different samples analyzed it is seen how the curves resemble to each other, meaning that the comparison between the images will be reliable. The difference between sample 2 and the rest might be caused by the fracture that is presented in the two other samples.

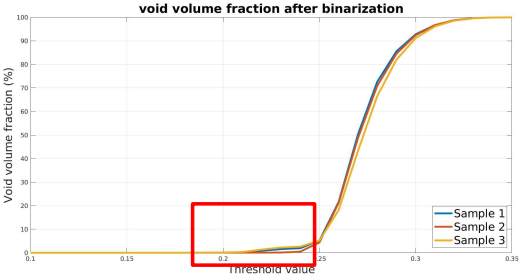

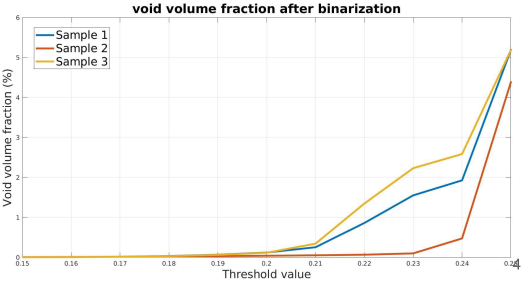

Binarize value 0.247 (1)

A value between 0.245-0.255 seems an optimum for the segmentation. Although there is a considerable difference for new1-B, which may indicate that either this sample

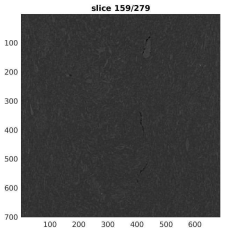

FiberQ-1

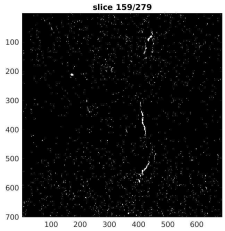

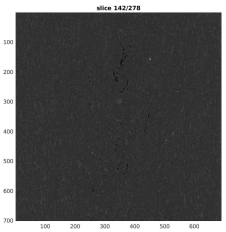

FiberQ-2

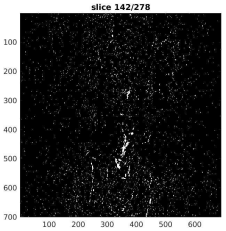

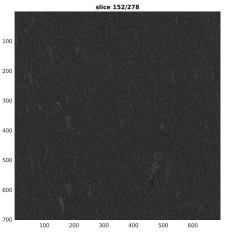

New1-A

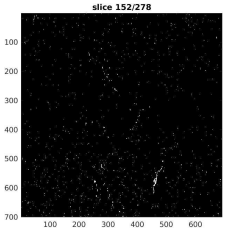

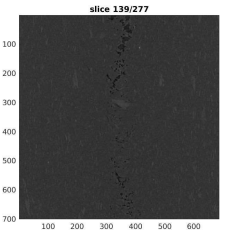

New1-B

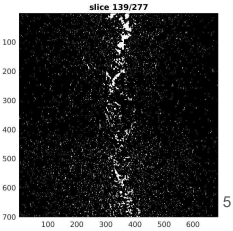

Binarize value 0.247 (1)

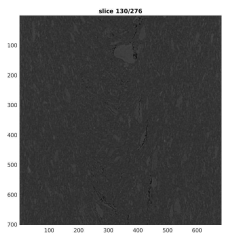

New1-C

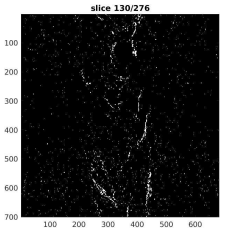

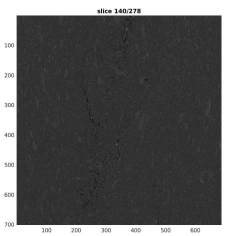

New2-A

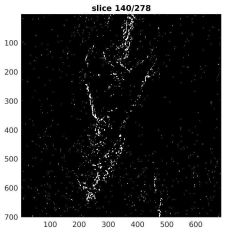

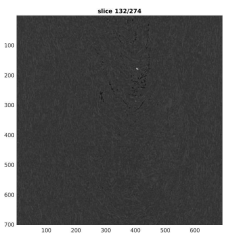

New2-B

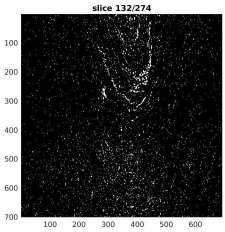

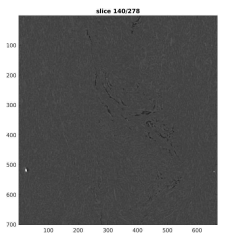

New2-C

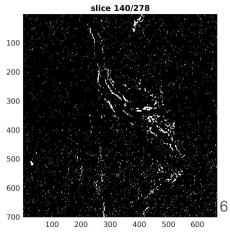

Binarize value 0.25 (2)

A value between 0.245-0.25 seems an optimum for the segmentation. Although there is a considerable difference for new1-B, which may indicate that either this sample

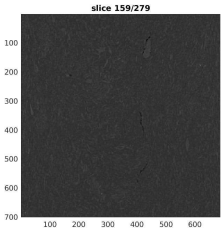

FiberQ-1

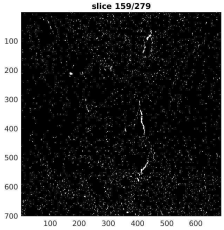

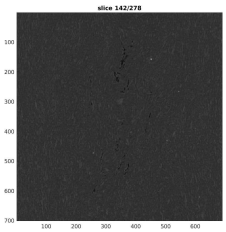

FiberQ-2

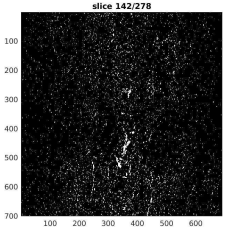

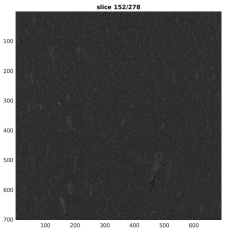

New1-A

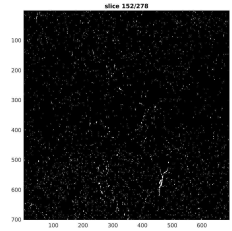

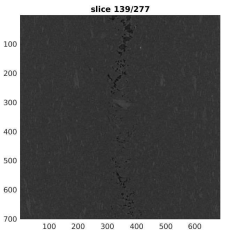

New1-B

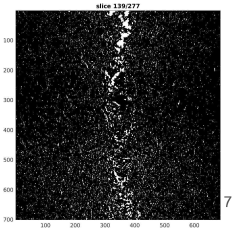

Binarize value 0.25 (2)

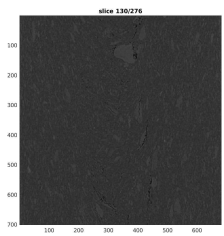

New1-C

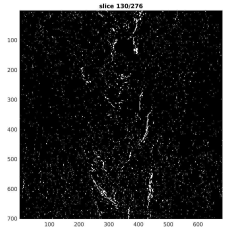

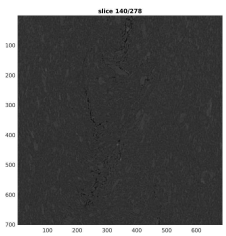

New2-A

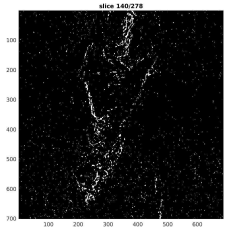

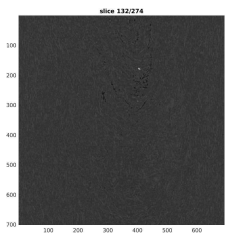

New2-B

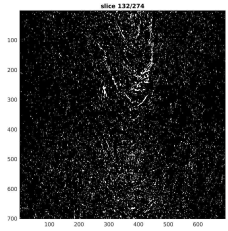

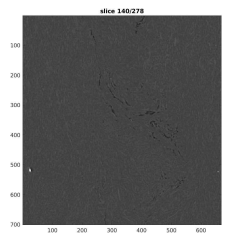

New2-C

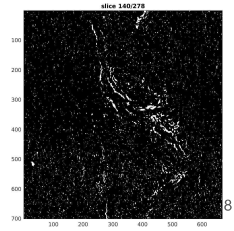

Binarize value 0.253 (3)

A value between 0.245-0.25 seems an optimum for the segmentation. Although there is a considerable difference for new1-B, which may indicate that either this sample

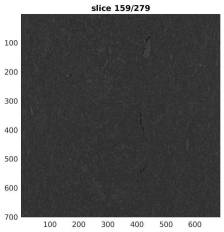

FiberQ-1

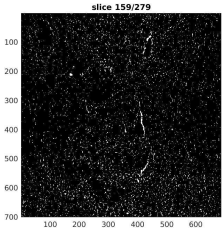

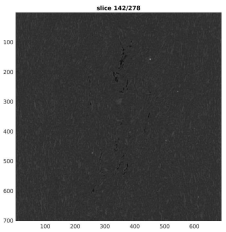

FiberQ-2

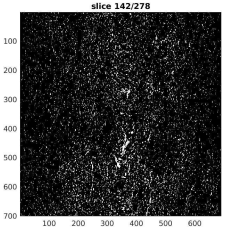

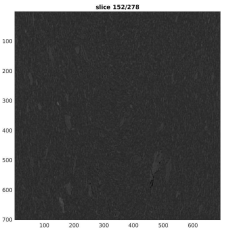

New1-A

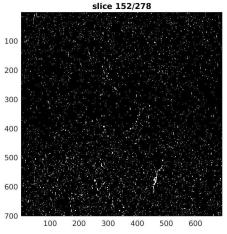

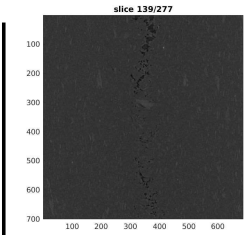

New1-B

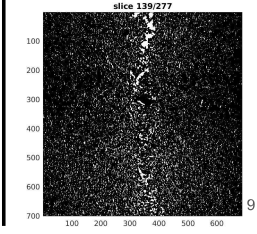

Binarize value 0.253 (3)

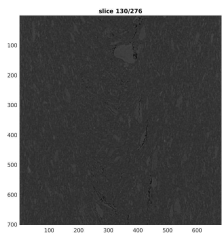

New1-C

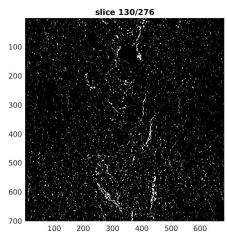

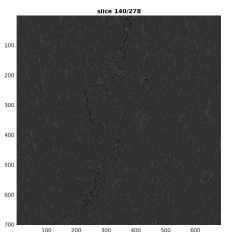

New2-A

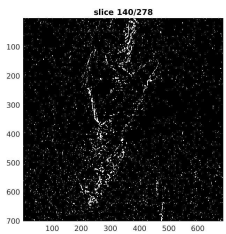

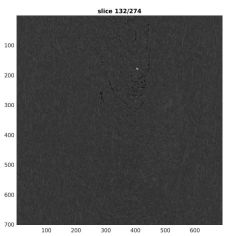

New2-B

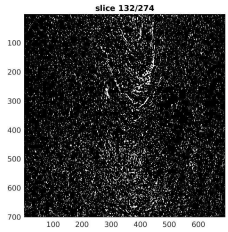

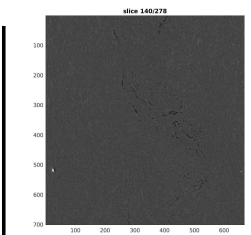

New2-C

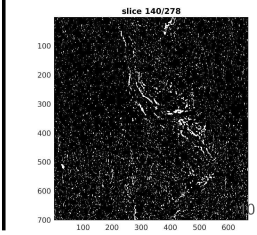

Dilate - Eroding filtering (D - E)

From the previous analysis done it has been decided to binarize the image for a threshold value of 0.25, as it suited the best for every sample in general.

The following analysis will be to unite voids that from a first view are separated, but we would like to consider as one, because of its size and proximity with each other. This filter leaves intact the voxels that are isolated (i.e. if there is a void of 5 voxels that has nothing in its surroundings, at the end of the filter it will be of the same size), but unites groups that might be close to each other.

This analysis basically will consist on a continuous set of filters of dilating the image and then eroding it with different sphere radius. By doing this those grains that are of a considerable size and are next to each other will be united, and although the number of voxels considered as voids will increase, this will suppose a “redemption” to the pores that were eliminated in the previous filtering.

D-E: This is the same plot as in the previous slide but for all the samples. The dotted line is referenced to the number of voids (left axes), while the other represents %V

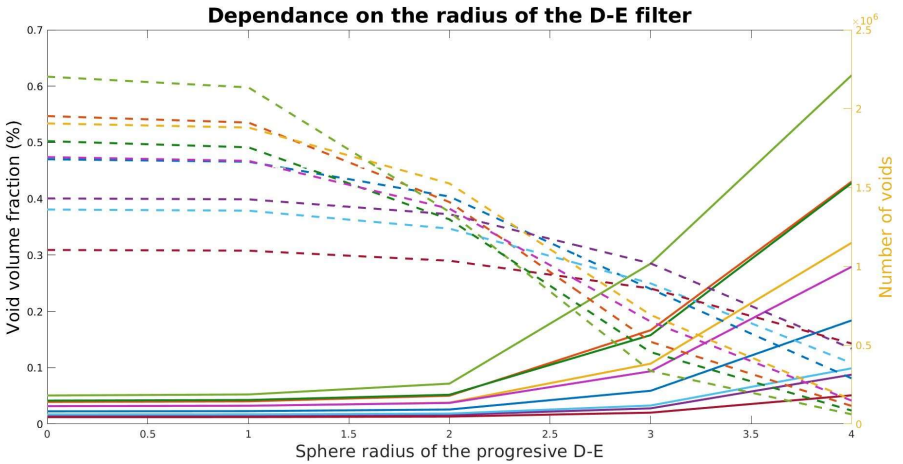

D-E 2

As it was seen in the previous plot, a radius for the D-E filtering equal to 2, reduced considerably the number of voids from the sample without compromising the volume fraction of the sample. For that reason this radius was chosen for the segmentation

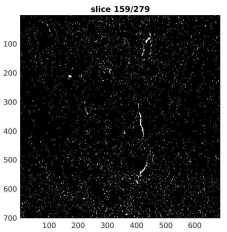

FiberQ-1

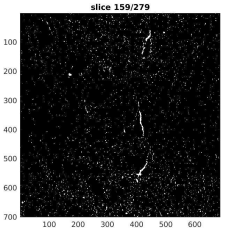

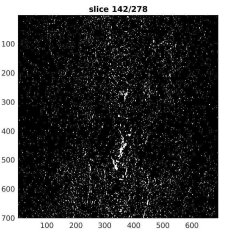

FiberQ-2

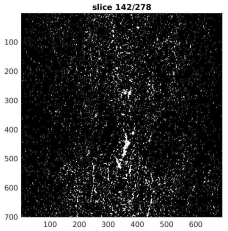

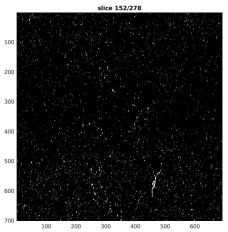

New1-A

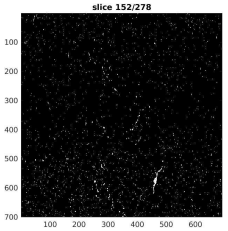

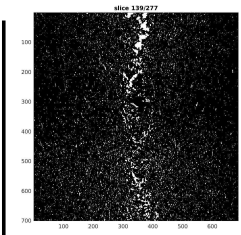

New1-B

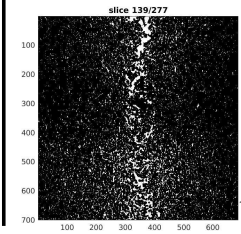

D-E 2

As it was seen in the previous plot, a radius for the D-E filtering equal to 2, reduced considerably the number of voids from the sample without compromising the volume fraction of the sample. For that reason this radius was chosen for the segmentation

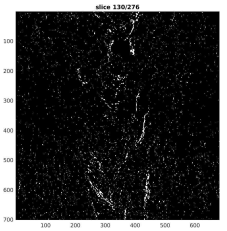

New1-C

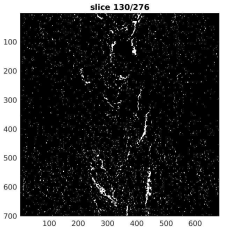

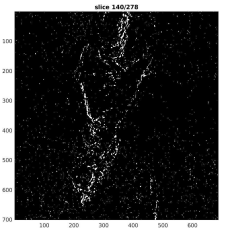

New2-A

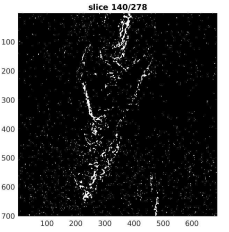

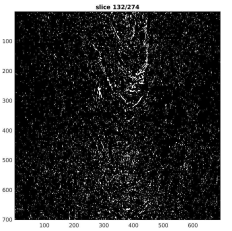

New2-B

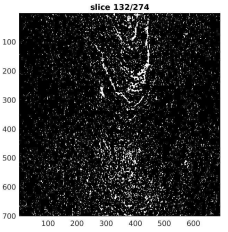

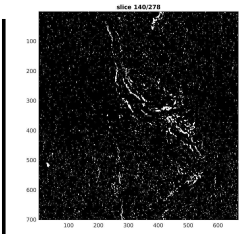

New2-C

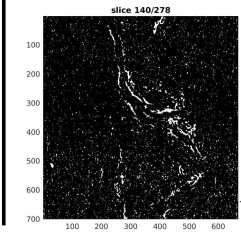

Minimum void size analysis

After the D-E filter, it has to be taken out some of the noise from the sample as “invalid” voids that were segmented in the image but might not be considered porosity. To get rid of this, it is plot the volume fraction of the sample, depending on the minimum void size to be considered valid (the size below the chosen value will be treated as noise).

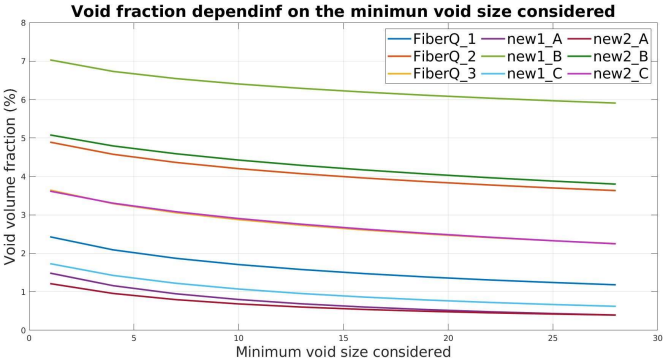

Minimum void size 8

As it is seen in the previous figures, similar distribution of the porosity is found, as the porosity of the samples seem to decrease almost parallel to each other. Consequently this filter won’t have a very big influence on the comparison, however it was chosen a threshold size of a cube of side 2 voxels (8 in total) = 2.74*10^-6 mm^3

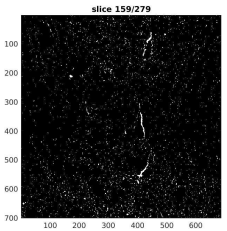

FiberQ-1

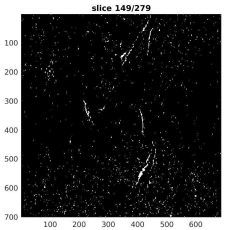

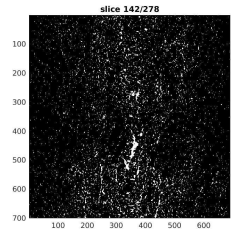

FiberQ-2

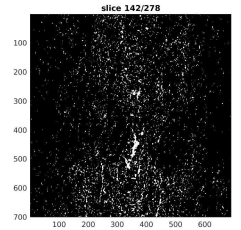

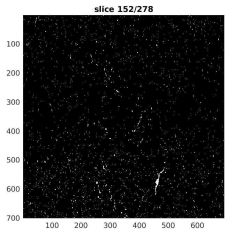

New1-A

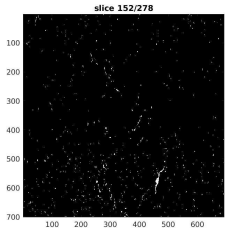

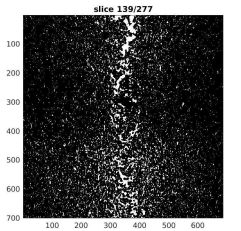

New1-B

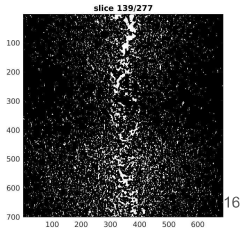

Minimum void size 8

As it is seen in the previous figures, similar distribution of the porosity is found, as the porosity of the samples seem to decrease almost parallel to each other. Consequently this filter won't have a very big influence on the comparison, however it was chosen a threshold size of a cube of side 2 voxels (8 in total) = 2.74*10^-6 mm^3

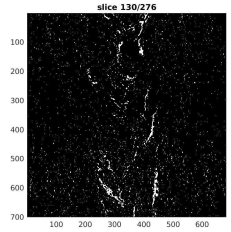

New1-C

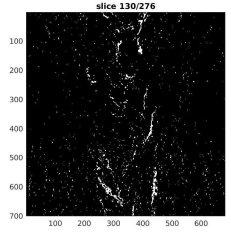

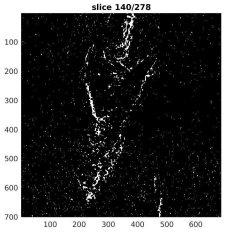

New2-A

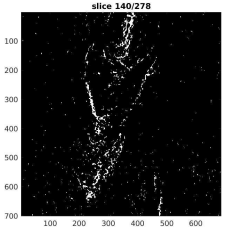

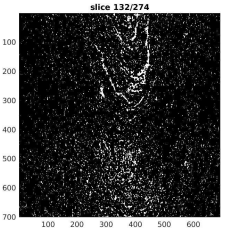

New2-B

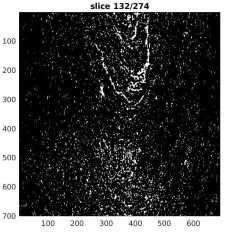

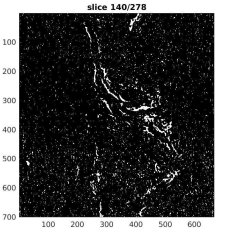

New2-C

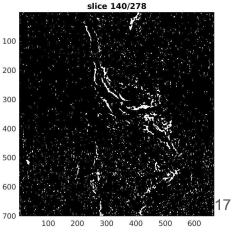

Final porosity segmentation

For the segmentation it has been performed the following procedure: Binarization with a threshold value of 0.25, Progresive Dilate-Erode filtering with spheres of radius 1 and 2, and a final filter out of the voids smaller than 8 voxels.

FiberQ-1

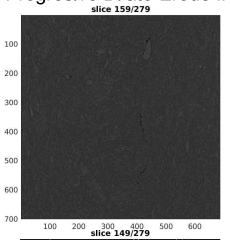

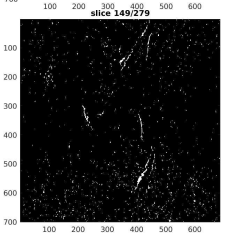

FiberQ-2

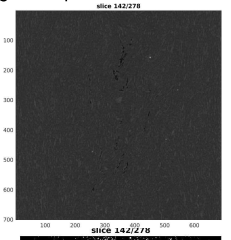

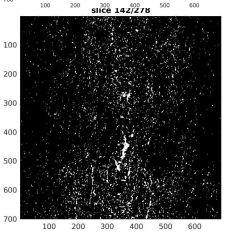

New1-A

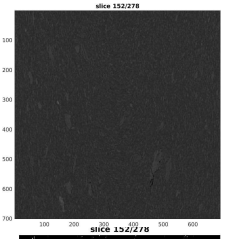

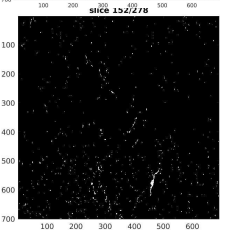

New1-B

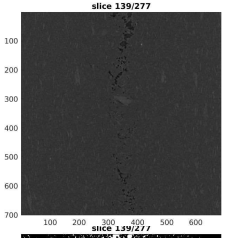

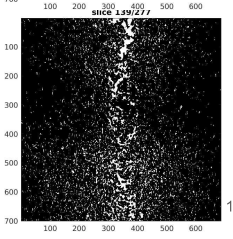

Final porosity segmentation

For the segmentation it has been performed the following procedure: Binarization with a threshold value of 0.25, Progresive Dilate-Erode filtering with spheres of radius 1 and 2, and a final filter out of the voids smaller than 8 voxels.

New1-C

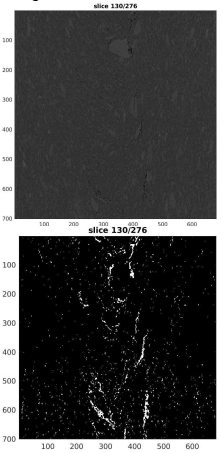

New2-A

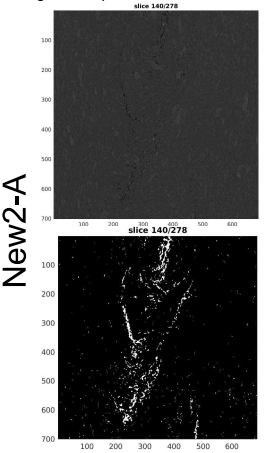

New2-B

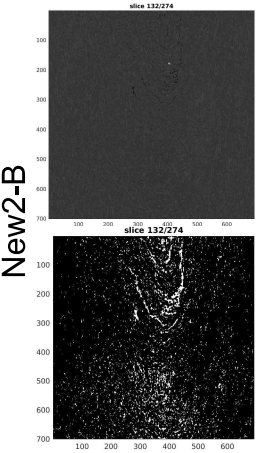

New2-C

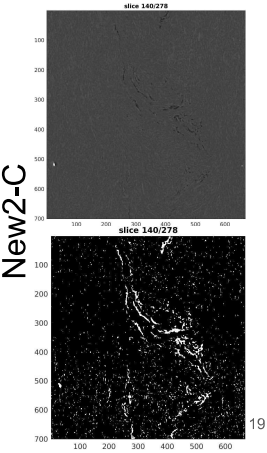

Aggregations filtering (2)

It is easier to segmentate the just aggregations out of the picture instead of all the fibers, as these could be easily differenced taken out of the noise, and the analysis could be more personalized.

To analyze the aggregations found in the picture, unlike porosity, it could be applied different filters to smooth and sharpen regions, because we are just analyzing the big clumps and small ones can be neglected.

In this analysis it is going to be segmented the aggregations for the samples sent by Biofiber Tech. to LU in the known as “second shipment”. All the samples in the end will be subjected to the same set of filters so the comparison can be significative.

Contrast adjust filter

Although it was learnt from previous analysis that if wanting to compare the samples a sample adjustment should not be used, it is useful to see how this affects the images, because aggregations tend to be highlighted

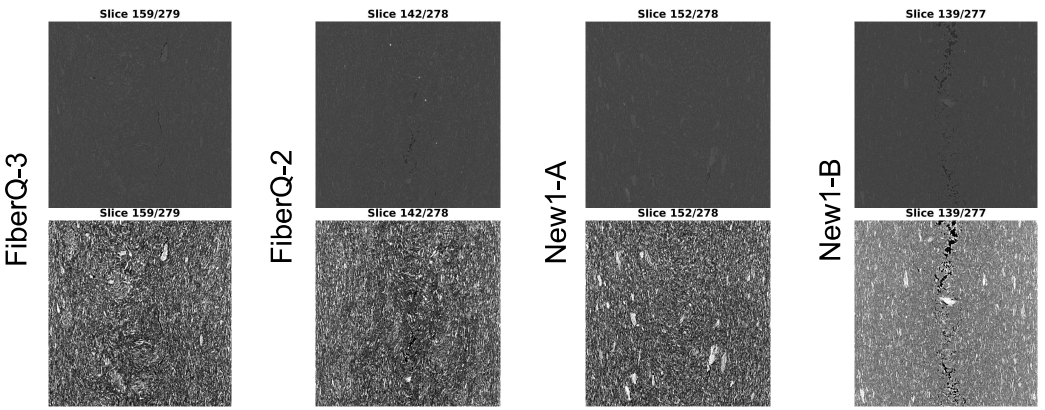

Contrast adjust filter

Although it was learnt from previous analysis that if wanting to compare the samples a sample adjustment should not be used, it is useful to see how this affects the images, because aggregations tend to be highlighted

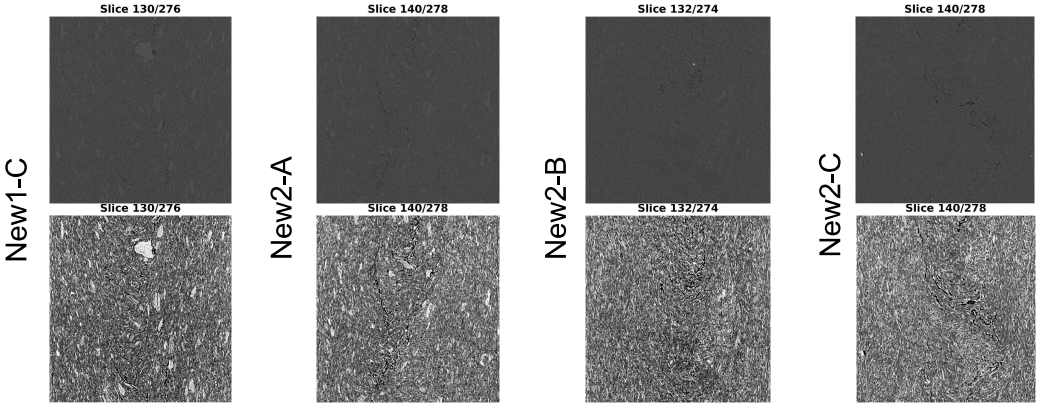

E-D (3) filter + Non-local mean

For a first approach to the method it was tried to apply the same one as the used for the first shipment samples, just changing the binarization threshold, to adjust with the contrast of the image. Here is shown the processing steps

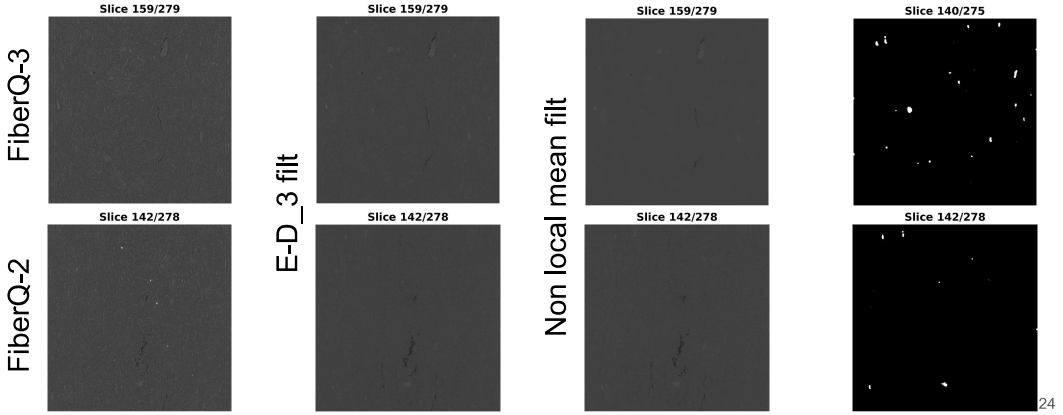

E-D (3) filter + Non-local mean

For a first approach to the method it was tried to apply the same one as the used for the first shipment samples, just changing the binarization threshold, to adjust with the contrast of the image. Here is shown the processing steps

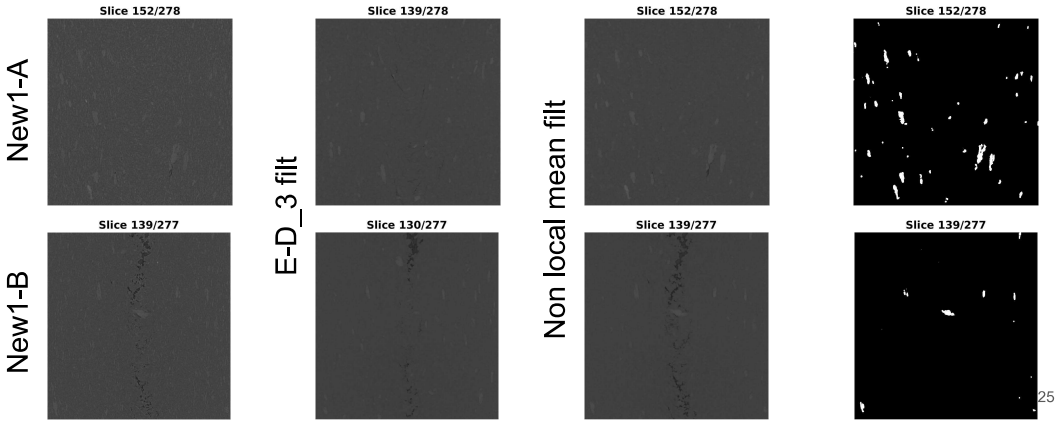

E-D (3) filter + Non-local mean

For a first approach to the method it was tried to apply the same one as the used for the first shipment samples, just changing the binarization threshold, to adjust with the contrast of the image. Here is shown the processing steps

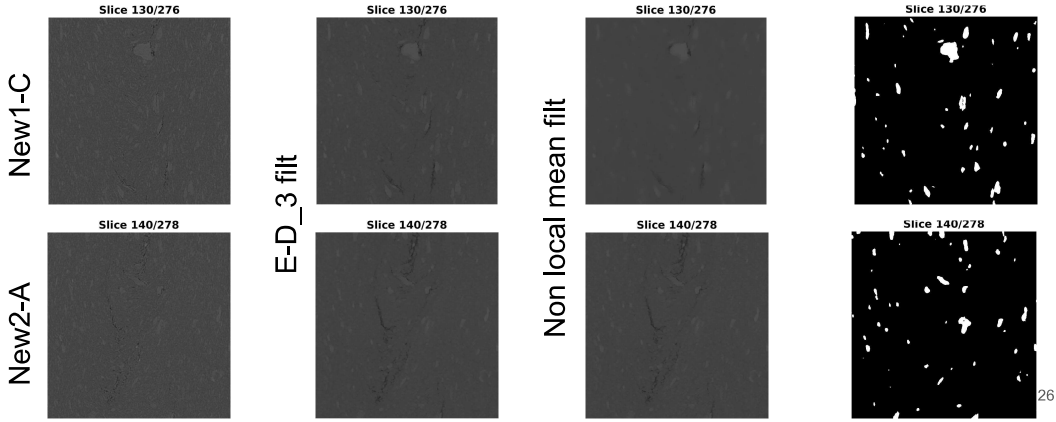

E-D (3) filter + Non-local mean

For a first approach to the method it was tried to apply the same one as the used for the first shipment samples, just changing the binarization threshold, to adjust with the contrast of the image**.** Here is shown the processing steps

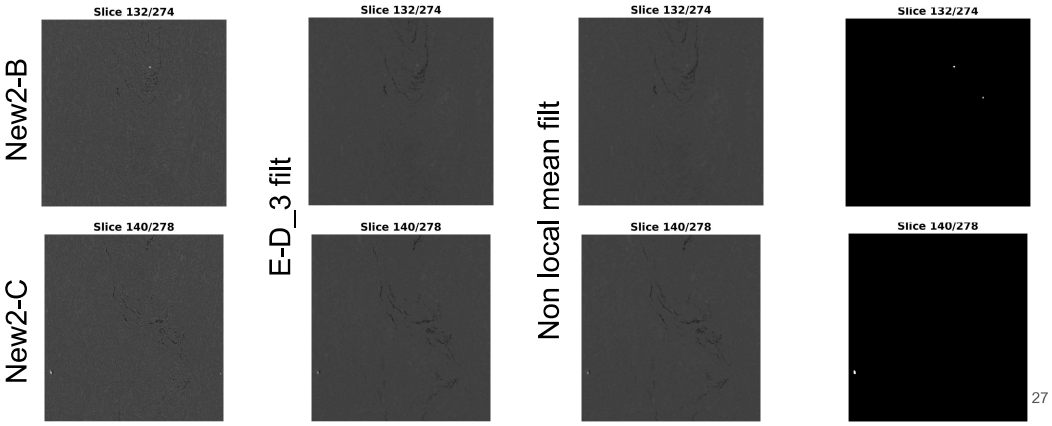

Aggregates fraction analysis (E-D + Non-linear)

To choose a threshold value for the binarization it is plot the aggregates fraction in terms of the said variable.

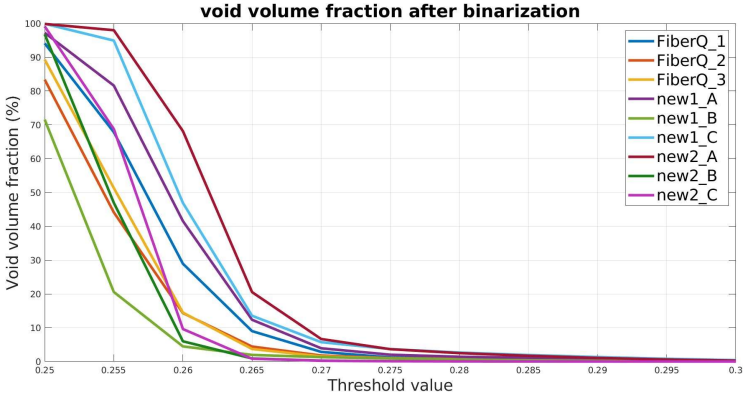

Aggregates fraction analysis (E-D)

After a qualitative check if the aggregates mask obtained with the same procedure as the one applied to the previous samples (first shipment) it was noticed that in this case independently of the mask threshold, the aggregates segmented did not fit to the ones seen in the original picture. The reason for this, it was found to be an excessive filter of the picture, so it is tried the segmentation without the non-local mean.

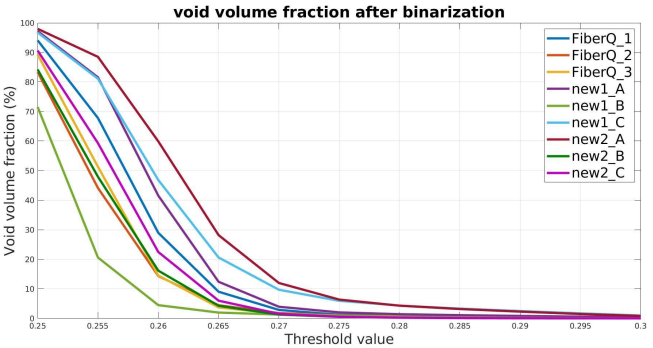

Aggregates segmentation

By just using a progresive E-D filter of radius 3, the results obtained were much more accurate that with the previous filter used. However, this came with the consequence that there were a lot of fibers that did not disappear with the binarization of the pictures.

This problem would not be able to be fixed by just masking out the small aggregates, as there were found a lot of gaps that were so close to each other that they always ended up to connect to one another in a similar way to what happened to the fiber segmentation in the first shipment samples.

To solve this problem it was found out that by combining both the non-local mean filtered image with the new one, the results obtained were improved for both images.

Aggregates segmentation

Example: new2-C

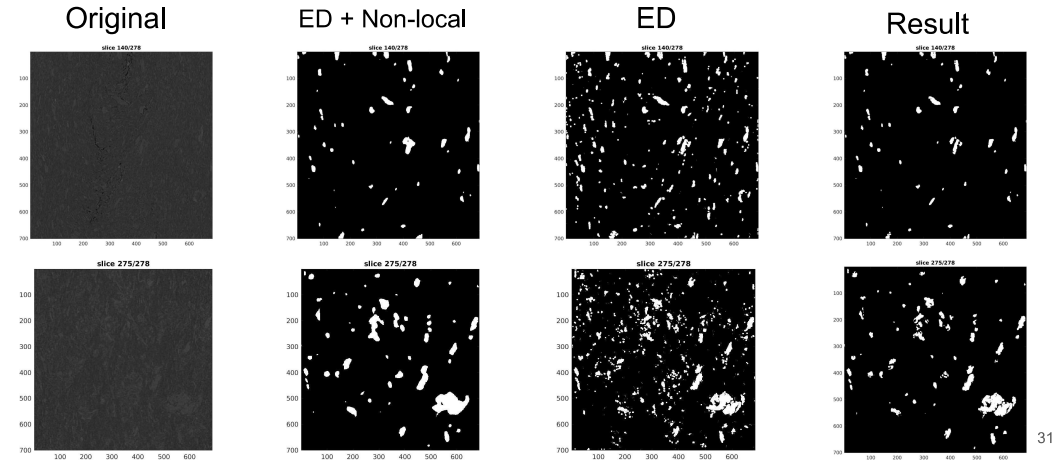

Aggregates segmentation result

After the segmentation is made, grains smaller than 0.0013mm³ are filtered out. This number is the correspondence of a cube of side 10 voxels in a tomography resolution of 0.011mm.

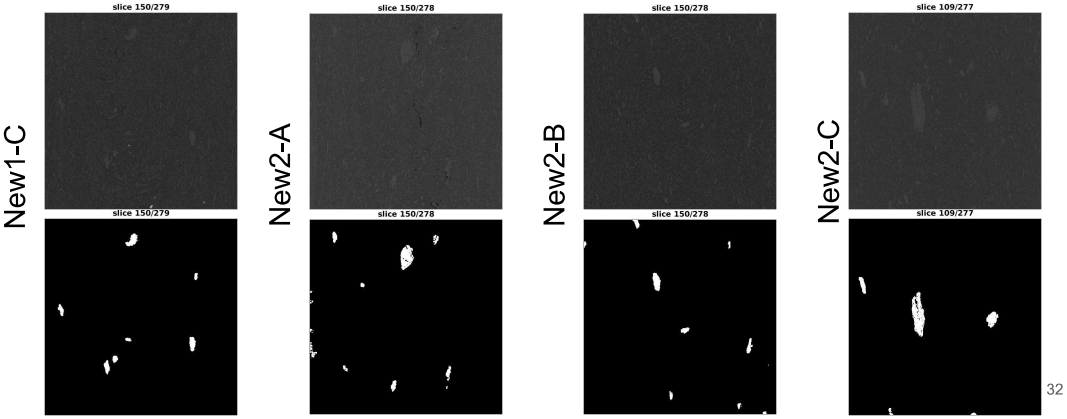

Aggregates segmentation result

After the segmentation is made, grains smaller than 0.0013mm³ are filtered out. This number is the correspondence of a cube of side 10 voxels in a tomography resolution of 0.011mm.

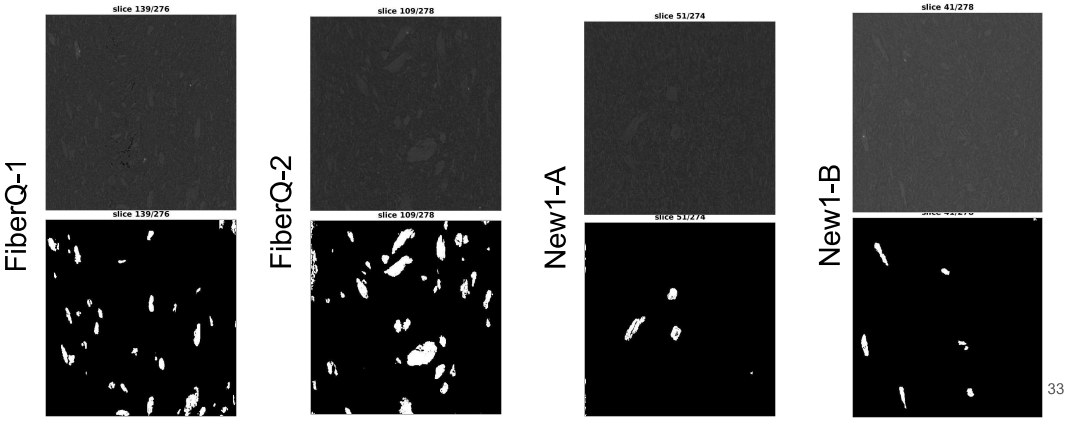

Fiber filtering (2)

After the porosity and aggregate segmentation the fiber segmentation works in a similar way than the one made to the first shipment samples, where the image can just be binarized without applying any filters. If filters were applied to the sample images, fibers could be compromised because their thin cross-section.

Functions that enhance fibers with a known thickness could be investigated (fibermetric3), however this enhances fibers with a known and constant section.

For this reason, being able to choose the right threshold parameter for the sample is of great importance, as this will define the whole analysis.

Samples

Top row: original picture | Bottom row: Contrast adjusted picture

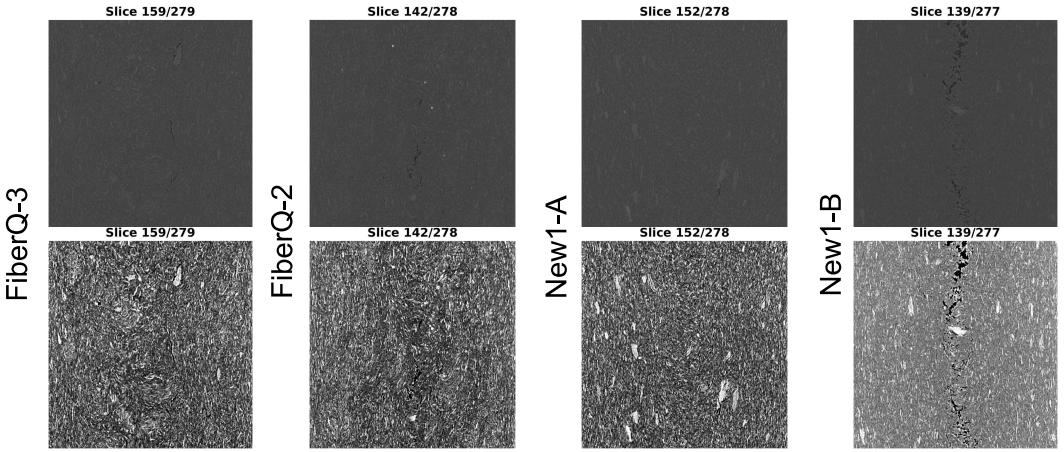

Samples Top row: original picture | Bottom row: Contrast adjusted picture

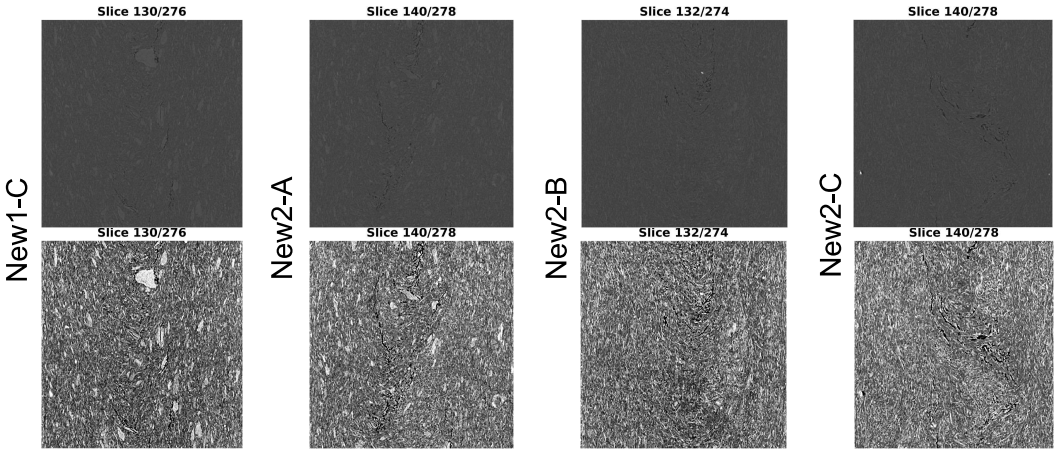

Binarization analysis

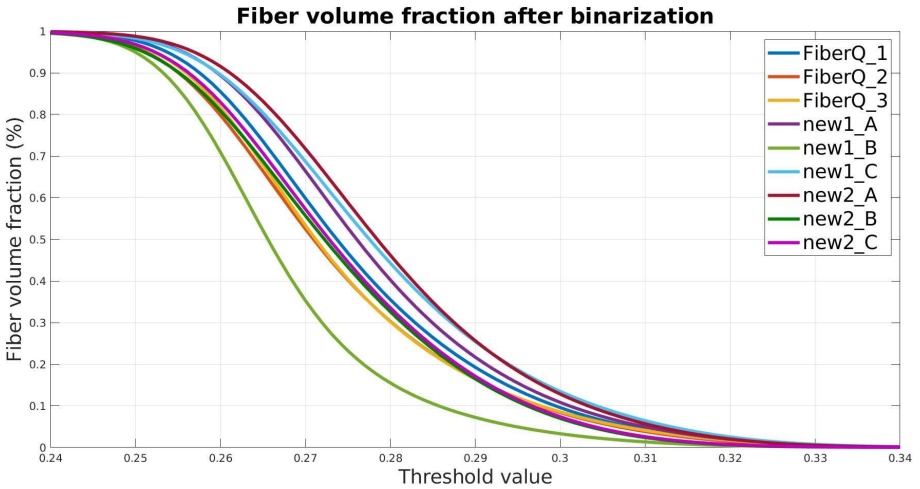

Binarization analysis

Points of reference are shown below, where two volume lines cross each other.

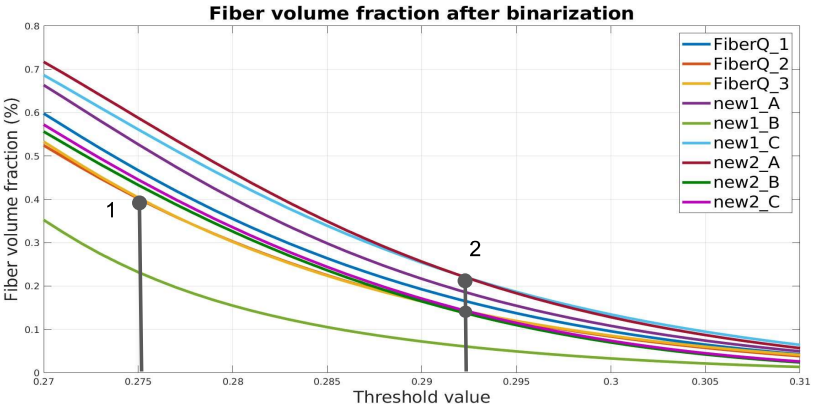

Binarization threshold (0.275)

Top row: original picture | Bottom row: Binarized

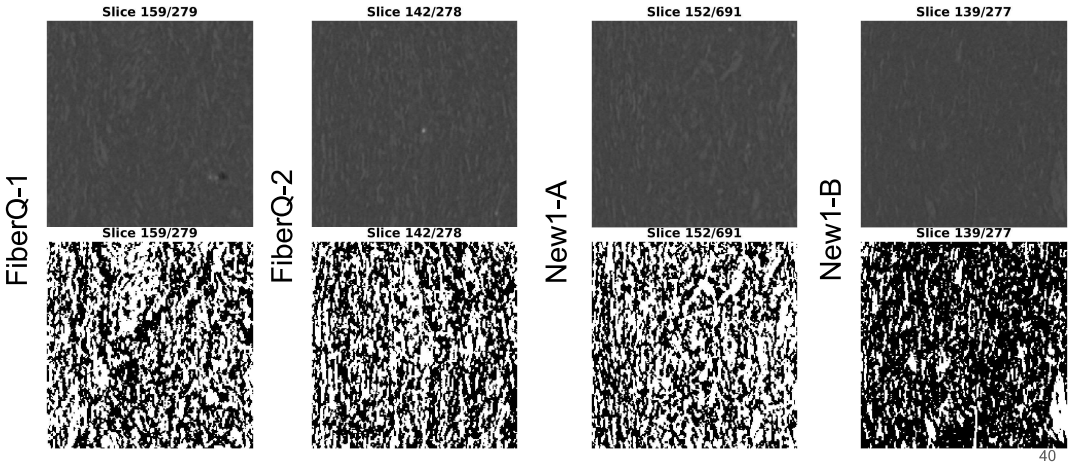

Binarization threshold (0.275)

Top row: original picture | Bottom row: Binarized

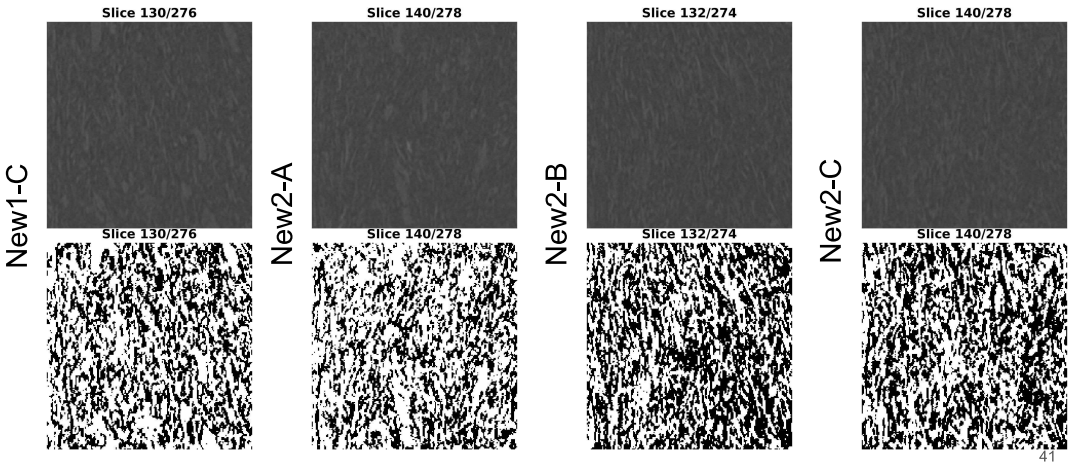

41

Binarization threshold (0.2925)

Top row: original picture | Bottom row: Binarized

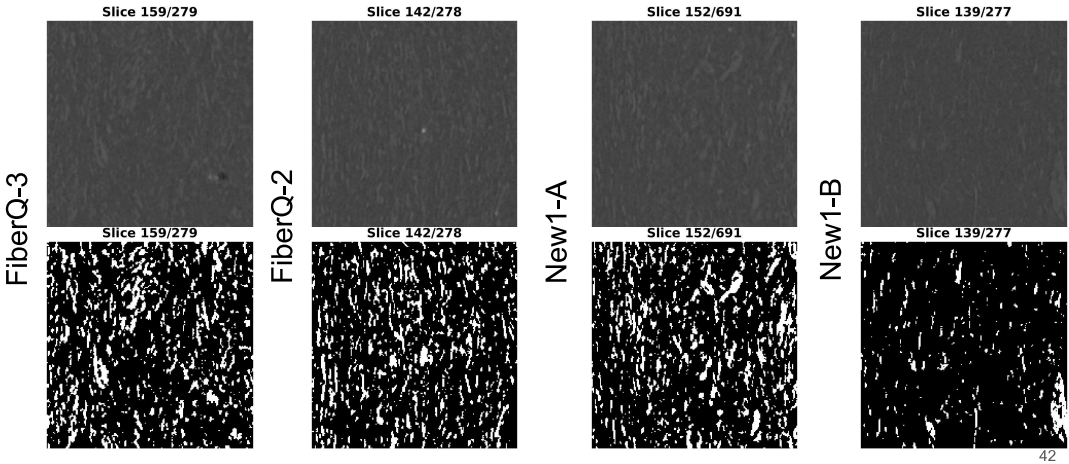

42

Binarization threshold (0.2925) Top row: original picture | Bottom row: Binarized

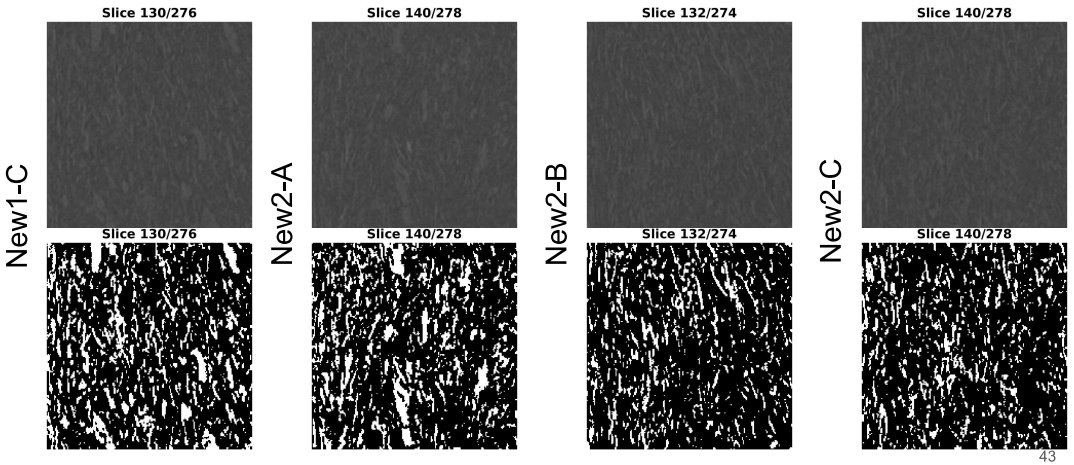

Fiber Segmentation

Again as in the previous fiber segmentation the problem lays that the same threshold value for the binarization adapts the fibers differently depending on the sample and region.

For the threshold value 0.2925, the segmentation works correctly for some samples such as FiberQ-1/2/3, New2-B, New2-C… curves more in the inner region of the volume fraction plot. However it seems that this value is oversized for other samples in the upper part of the plot (New2-A, New2-C) and undersized for the one in the bottom (New1-B).

The value 0.2925, was the one found that fitted the best for most of the samples and most of the regions, so it was the chosen one to segmentate the samples. After the segmentation, the aggregates were removed from the sample to omit them in the analysis.

E

Fracture volume analysis

Fracture analysis

Although due to the artifact found in the tomographies these are not ideal to calculate parameters quantitatively, they can still be used for many things such as to understand the breaking mechanisms of the samples.

To analyse the fractures it is used the segmented tomographies which present a color depending on the phase identified of the material: dark blue for matrix, light blue for fibers, green for fiber aggregations and orange for voids/air. This is useful for analysing how the fracture happened referring to the phases, and as it is an small distance along the z-axis, the change in brightness won't be of much relevance.

It is important to to keep in mind that different slices from the tomography do not indicate how the fracture developed in time, but it is just a snapshot of the whole fracture at the end of it, so when referring to it starts from a group of voids that grow and fusion with each other it can perfectly be the other way around, that a big grain collided with the small ones that was in top/bottom of them

Fib-30_1

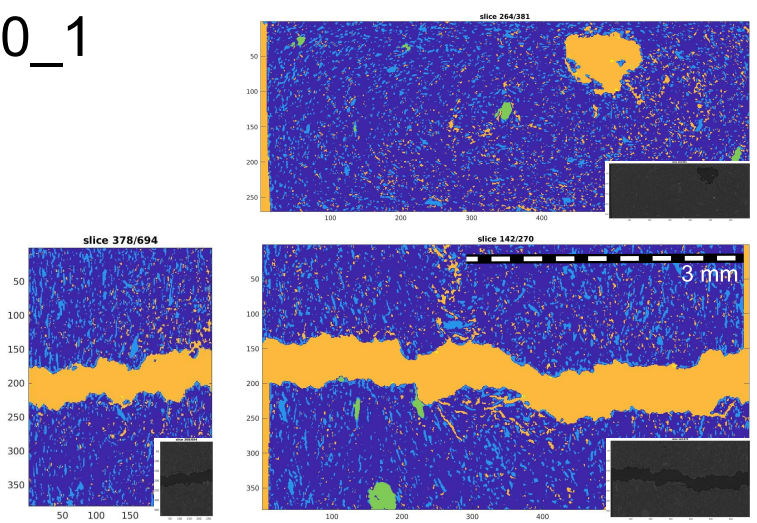

Fib-30_1 bottom to top

In figures (a), (b) and (c) it is seen how a group of pores that act as stress concentrators and expand, then while expanding they meet and fusion with other pores acting as a bigger stress concentration.

Some parts of the failure can be identified as an adhesion fiber/matix failure where the fracture starts in the matrix and voids move along the sample avoiding the fibers. Isolated fibers can be found inside voids in most of the pictures, and in figure (e) it can be noticed that the border between the main void and the rest of the sample is mainly composed of fibers.

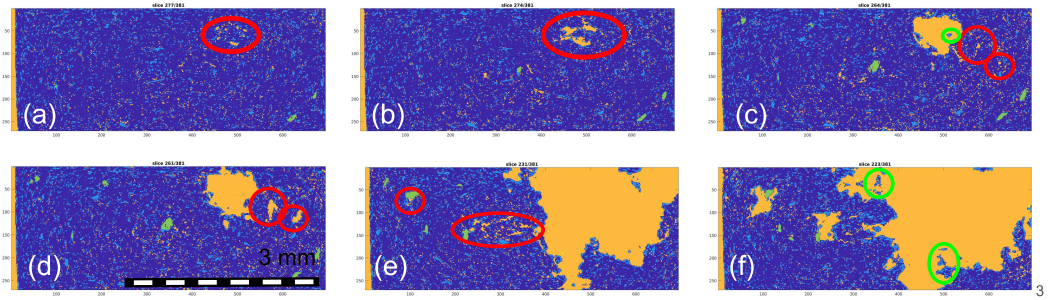

Fib-30_1 top to bottom

Similar to previous pictures, the voids first can be seen along matrix spaces, and it is when they surround a fiber when this one is absorbed by the void, meaning that the fiber did not fail but the matrix did as it was not able to adhere properly to the matrix.

It also can be seen in figure (f) that the same happens with the aggregations. This is surrounded by voids before detaching from the sample. The fracture develops from back to front in an inclined plane.

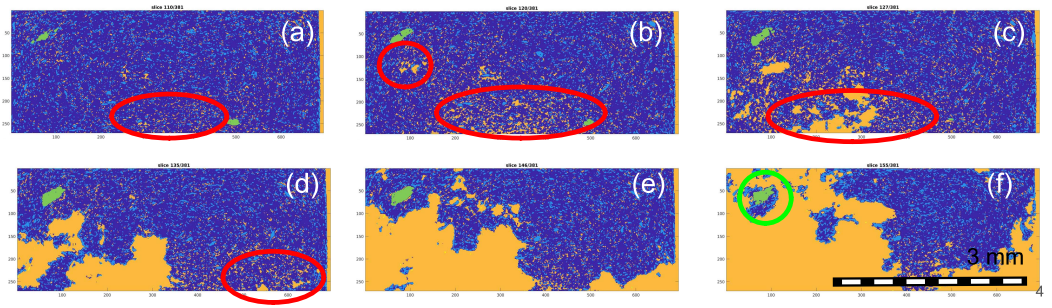

Fib-30_1 font to back

From the side view pictures different fractures reasons can be found. On (f) an aggregate is divided in two different pieces, meaning that the failure was due to cohesion of the fibers (and not adhesion in the fiber/matrix phase). In Figure (b) it can be seen how porosity has a significant presence along near the fracture area.

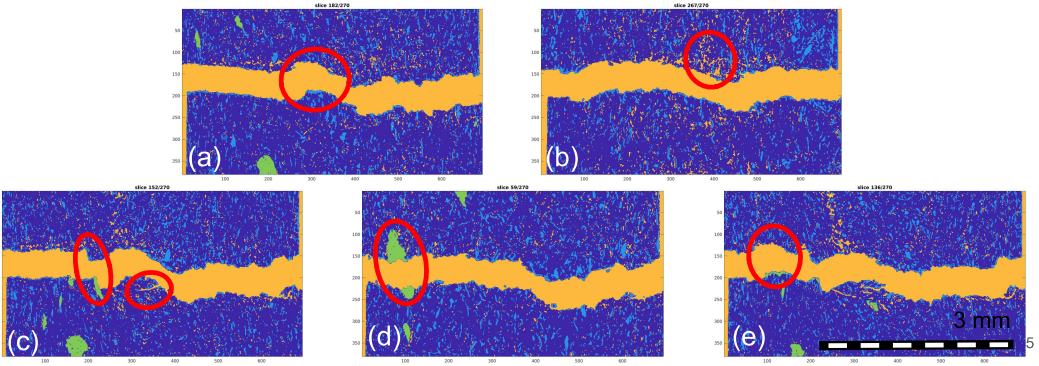

5

F92-40

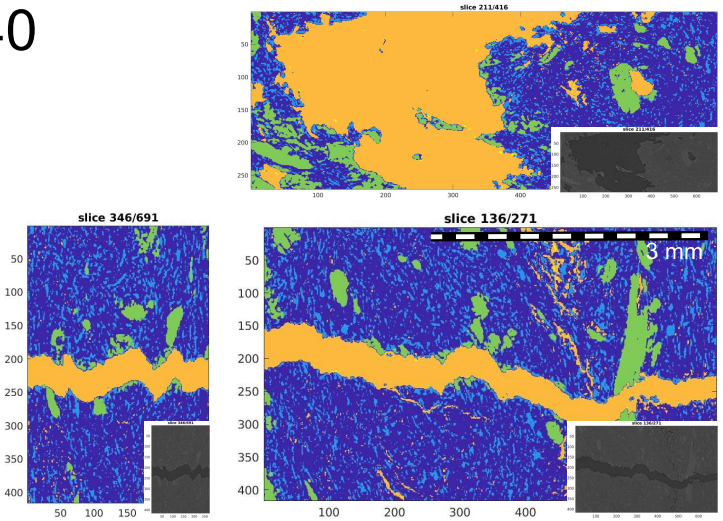

6

F92-40 bottom to top

From the top of the sample (a) there is a large void that is constant along the longitudinal axes. This void is where the fracture propagates around in the lowest part of the sample. The void grows (b) and brakes an aggregation appart.
It has to be taken into account that the sample parts were so close in the tomography that the fibers seen in the green circle in (c) correspond already to the top part of the sample. However, this area's border is composed of mainly fibers, indicating another failure for matrix, fiber adhesion, where fibers are found separated from the matrix.
In (d) it can be found both top and bottom parts of the sample next to each other, an indicator of how steep the fracture was made.

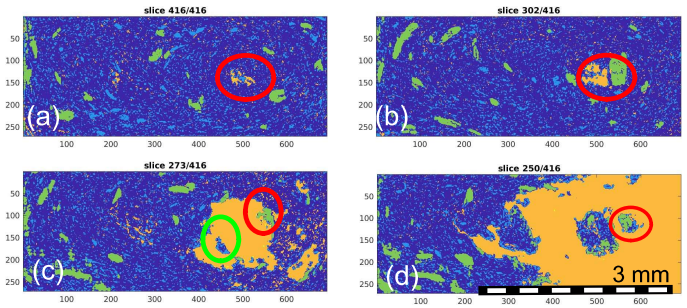

F92-40 top to bottom

In (a) it can be found again how aggregates seem to be surrounded by the fracture voids, indicator on how these are usually the part of the sample where the adhesion lack is made the most evident, either because its surroundings fail before and the fiber holds the longer, or because the fiber disattached from the matrix material the first. Anyhow, this evidence makes sense as aggregations are just fibers whose surface area in volume ratio are the smallest, meaning that the load they hold is the highest and the area to get attach to the material is the smallest. This also coincides with the founding that higher aspect ratio fibers work better in composite

On the other hand, it is interesting to watch how the right aggregate breaks apart from an inner pore that it had and it grows (b) and (c).

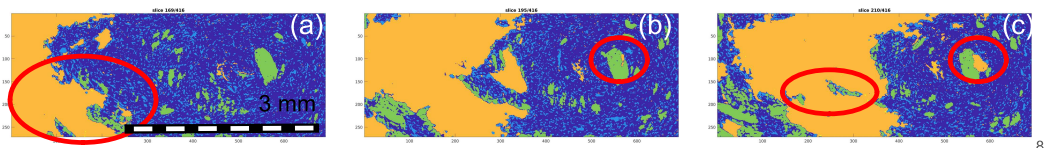

F92-40 font to back

Looking at the differences between the premortem sample and the postmortem in the same slice (c), there does not seem to be a big difference on the size of the pores apart from a big increase on them.

In figure (d) it can be seen an straight cut from the big aggregate in the lower part of the sample, making a new faliure from adhesion. However in (b) can be found an individual fiber that belonged to the inner part of the aggregate and broke appart. It seems that when aggregates are long enough, these seem to adhere sufficiently good to the matrix (good aspect ratio).

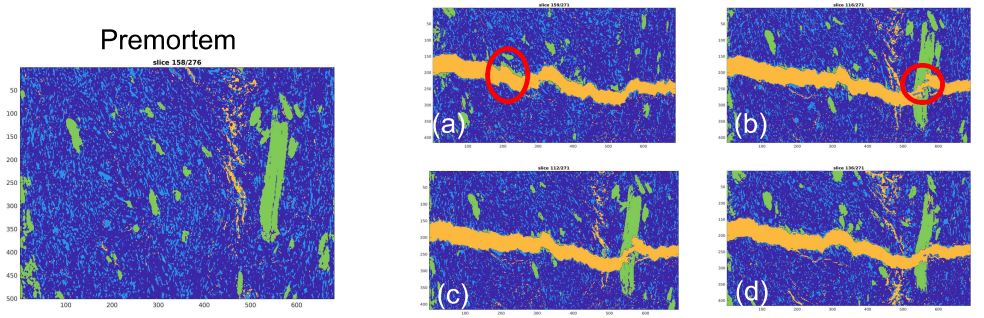

F92-40 font to back

A good indicative on how the fiber matrix interaction is, could be to analyze a fracture on a sample that was composed of many fibers with different aspect ratios. By making the sample fail at the middle of these fibers it could be identified the minimum aspect ratio needed for the fiber to break apart.

On (a) from the previous slide, it can be identified another straight cut on the samples. This fracture surface can be identified composed by the frontier between two different fibers: an aggregate on top, and a fiber on the bottom. This could come either from a group of fibers that due to being together were not as exposed to the surface treatment as the others, or from a fiber next to an aggregate where the matrix between them failed.

Ref-40

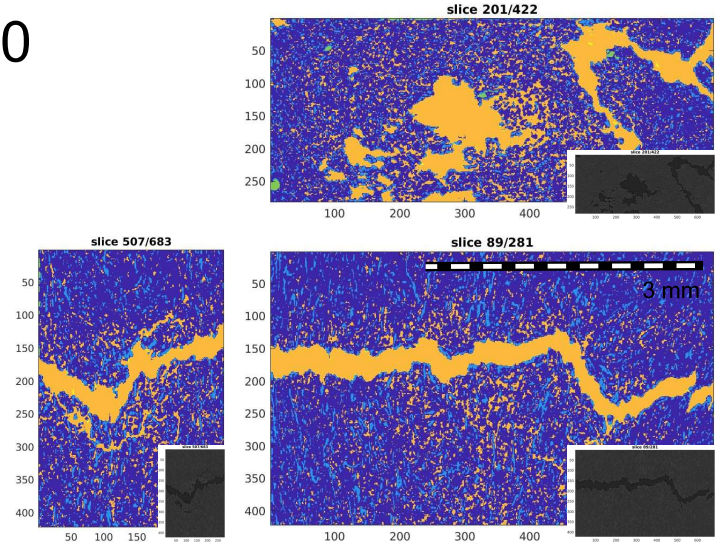

Ref-40 bottom to top

Artifacts or shell marks?

On the Figures below it can be seen some ring marks centered on the sample. This ring marks only appear on the bottom part of the sample and are concentric to each other. One could think that these are some ring artefacts caused by a defect in some scintillator pixels, but there are many reasons that differ from that thought:

The tomograph machine is relatively new, which makes improbable for the scintillator to be already broken and even more in many different voxels (different radius for the marks are found).

Also, the samples were scanned in batches of three and unless this sample was the one placed in the center, there would not be a reason for the marks to be centered in the middle part of the sample.

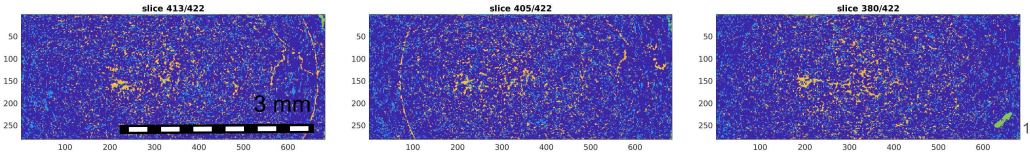

Ref-40 bottom to top

Artifacts or shell marks?

Other reasons that creates doubt on the nature of this circular void is that no similar shape has been found in other samples.

On the other hand, if the nature of these marks come from the sample and not from the tomography, we could be looking at some beach marks (also known as clamshells), a characteristic shape found in samples which failed because of fatigue. This mark comes as a result of a cyclic crack propagation from a tension-relaxation cycle. Although this could be caused some discontinuous loading in the tensile test machine, this would not explain why the voids do not increase with size but just keep such an small size.

Another possible explanation could be caused by the uniform loading in the sample that makes that all sections separated from the center sample are subjected to the same stress, and so the material should fail at the same time. However, because of the nature of the sample and the fact that in real life this usually never happens, it is thought that it is more probable for these marks to be caused by some imaging error

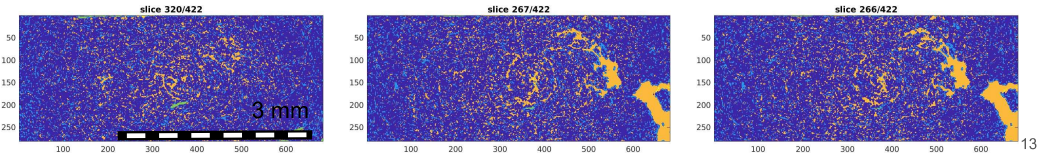

Ref-40

The big amount of aislated fibers found between the samples (left pictures) indicates that there are a lot of small fibers that did not break but tore apart from the matrix, being this one one of the ones with the worst adhesive properties found yet. On the other hand on both sides slices it can be found a high concentration of porosity in the samples. And in the centered picture it can be seen how the fracture happened in a similar way to the orientation of the fibers, similar to the plastic flow when filling the mould.

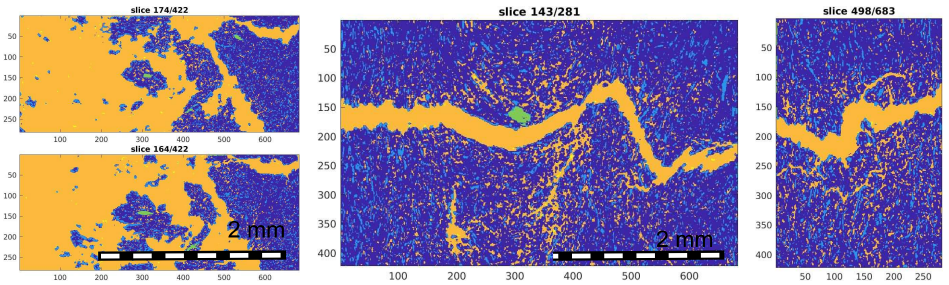

Six-40

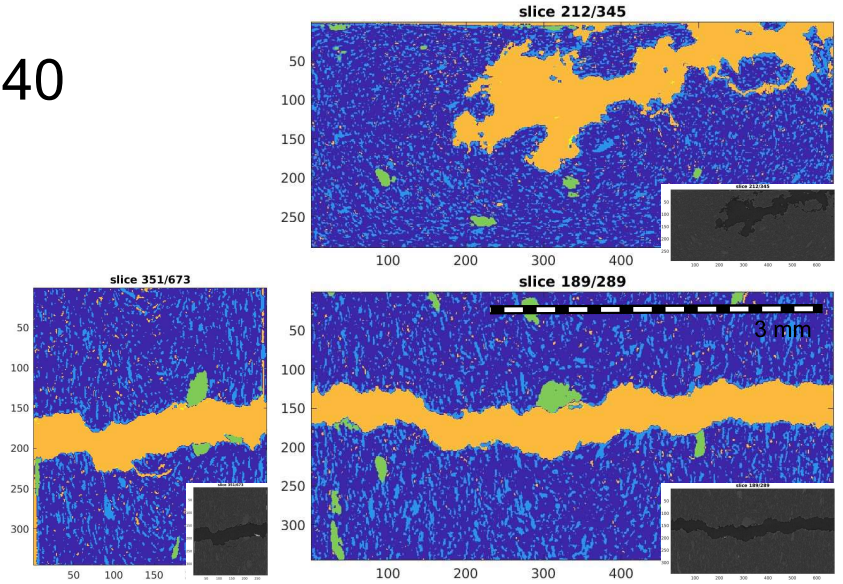

Six-40 top view

From the fracture it can be seen how there are less small groups of fibers that are presented in the fracture area, and the ones that are found are of a bigger size than the reference sample.
On figure (c), it is shown the fiber orientation in oval shapes concentric to the center of the sample. This may influence on the fracture shape that the voids appear in (d), following a similar pattern that this ovals.

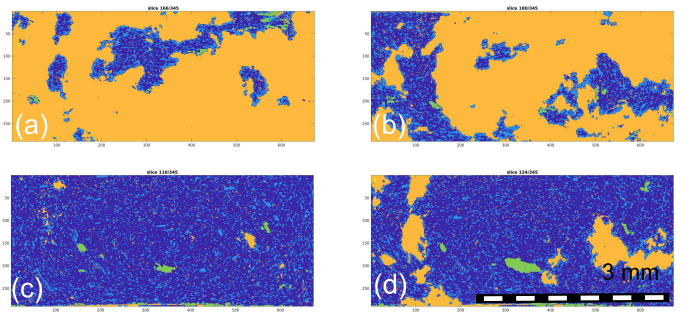

Six-40 side views

On this image, an aggregate with a planar shape is broken by the fracture, indicating the adhesion worked properly here. However in Figure (a) it seems that fracture happens following a similar pattern perpendicular to the fiber alignment in some places, meaning again some fiber/matrix adhesion dalure.
Moreover, On Figure (c) it is seen a fiber standing alone in the sample.

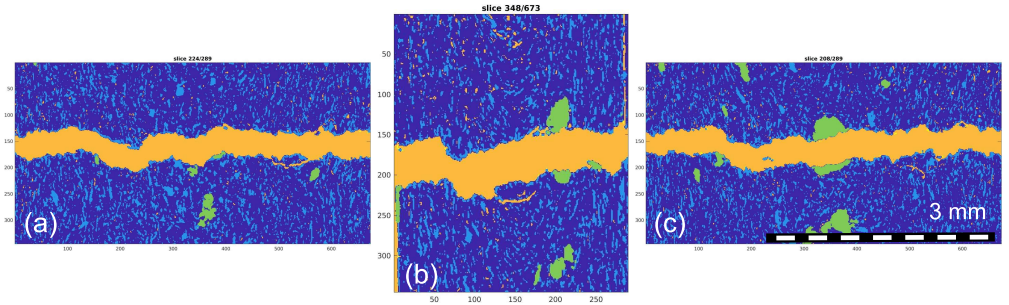

F92-20

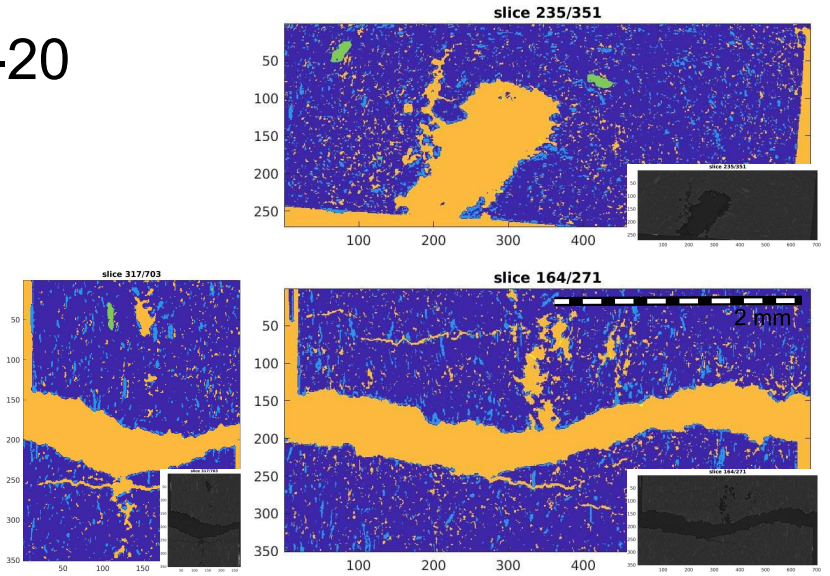

F92-20 top view

This sample is characteristic for its reduced amount of fibers, which can be easily identified by just taking a look at this phase in the pictures. Fibers are not only less common to be spotted but aggregates are not found to be as big as in other samples and more voids are seen in the middle of the sample.
Also not many individual fibers seem to be spotted on the matrix, similar to F92-40. Although some fibers are still seen.

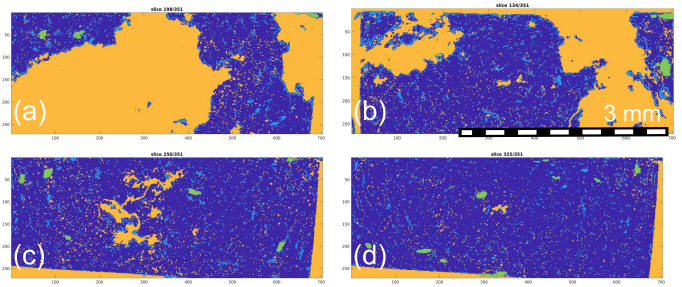

F92-20 side views

It is seen a great number of transversal cracks in the sample that are not in contact with the fractured area. This material broke in a more ductile way than the previous ones, which is in accordance with with the fact that is the one with the least amount of fibers, meaning that it should behave more similarly to a polymer.
On figure (b) an aggregate of small size is seen cleanly separated from the matrix, although it is a very small one which means that its surface area was not big enough to hold it. Also, similar to other samples, horizontally aligned fibers act as cracks propagators as it can be seen in (d)

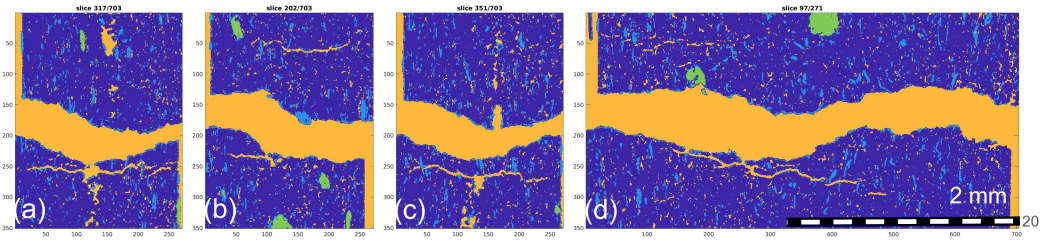

Top view adhesion comparison

To compare the fiber/matrix adhesion, it is used a visual analysis explained previously where an snapshot is taken to the top view of the tomography in the height where the fracture is visible but the surface of the sample pieces are near. Those fibers that failed to adhere to the matrix and did not break will be shown as individual fibers.

And as most of the fibers are aligned with the sample orientation (as seen in the orientation analysis from the first shipment samples) this will be a good indicative on which fibers adhered better to the matrix

Top view adhesion comparison